Order Number 9507295

A study of the link between cloud microphysics and climate change

Hu, Yong-Xiang, Ph.D.

University of Alaska Fairbanks, 1994

U·M·I
300 N. Zeeb Rd.
Ann Arbor, MI 48106

A Study of the Link between Cloud Microphysics and Climate Change

A

THESIS

Presented to the Faculty

of the University of Alaska Fairbanks

in Partial Fulfillment of the Requirements

for the Degree of

DOCTOR OF PHILOSOPHY

By

Yong-Xiang Hu, B.S., M.S.

Fairbanks, Alaska

May 1994

A study of the Link between Cloud Microphysics and Climate Change

by

Yong-Xiang Hu

RECOMMENDED:

Dr. David Musgrave

Dr. Manfred Rees

Dr. Glenn E. Shaw

Dr. Shee-Chee Tsay

Dr. Brenton Watkins

Dr. Knut Stamnes, Chairman, Advisory Committee

Dr. John Morack, Head, Physics Department

APPROVED:

Dr. Paul Reichardt, Dean, College of Natural Sciences

Dr. Joe Kan, Dean of the Graduate School

May 3, 1994

Date

Abstract

This thesis is concerned with the link between cloud microphysical properties and the climate.

The climate- related cloud radiative properties (fluxes and heating rates) are determined by the second and the third moments of the cloud droplet size distribution. The detailed distribution of the cloud droplet size is difficult to observe and unneccessary to obtain for climate purposes.

An accurate parameterization of cloud optical properties suitable for climate models is developed. This parameterization has been widely adopted in the atmospheric modeling community.

A new radiative-convective model has been developed and used for studying cloud-climate interactions. The radiative transfer method adopted in the model is accurate and numerically stable. The energy balance at the Earth's surface is treated in a self-consistent manner which avoids artificial tuning. The cloud radiative properties are accurately incorporated and are suitable for sensitivity studies of cloud-radiation-climate interactions.

A sensitivity study of the role of cloud microphysical properties in the climate system is performed by studying the impact of cloud radiative forcing on the equilibrium state temperature. The cloud droplet size is found to be an important variable in the climate system. A climate sensitivity study is performed to highlight the important role of the cloud absorption.

An adjoint radiative transfer method is developed for use in cloudy and aerosol-loaded atmospheres. The physical meaning of the adjoint radiative properties are discussed. This adjoint method allows for rapid computation of the impact of the changes in atmospheric state (including cloud properties, aerosol properties and temperature profile) on the radiative energy budget and the radiative heating rates

of the atmosphere. It is therefore expected to be useful in global climate modeling and the remote sensing of the atmosphere and the Earth from space.

Based on the above studies, a preliminary study of the atmospheric irreversibility is performed to elucidate the connection between cloud microphysical properties and the macrophysical direction of global climate. The globally averaged climate processes are irreveresible: the long-term variation of the atmospheric motion tends to approach the radiative energy balance; the convective instability prevents the pure radiative equilibrium in the troposphere; the latent heat release enhances the convective motion. The conditionally variational principle (the climate version of Glansdorf - Prigogine universal criteria for convective instability) which describes the macrophysical character of the climate system is established.

The radiative properties of clouds in the climate system are governed by the irreversibility of the global atmosphere as a whole. The role of clouds in the climate system is to change the distribution of the net radiative cooling of the atmosphere so that the heat released at each layer by the moist convective motion is balanced by the net radiative cooling.

Contents

List of Figures

List of Tables

Acknowledgments

I would like to give my most sincere thanks to Dr. Knut Stamnes for the support, encouragement and guidance; Drs. David Musgrave, Fred Rees, Glenn Shaw, S-C. Tsay, Brenton Warkins, Kolf Jayaweera and L.-C. Lee for stimulating discussions, criticism and suggestions; Dr. Qilong Min and Qiang Ji for constructive arguements and helps; everybody of our group (Drs. A. Kylling, J. Slusser, V. Fulyushkin, Elena, T. Zhang, fellow students Jin, Jun, Han, Fun, North, Jennifer, Rune, Eric, Jill, Kyle, Mary, Scott, computer wizards ... forgive me if I forgot anybody) for cooperations and competition for resources (such as Knut and our computers); Department of Energy for financial support; Geophysical Institute library for supplying the best spiritual food to survive those endless and longly weekends; God for keeping me believe: tomorrow will be better.

Chapter 1

Introduction

The ultimate energy source of the atmospheric motion is the radiation from the sun. As the global annual average, the net incoming shortwave radiation is balanced by the outgoing longwave radiation at the top of the atmosphere. Within the atmosphere, the pure radiative equilibrium is convectively unstable: the pure radiative equilibrium temperature gradients at the lower atmospheric layers are too large. The convective motion brings moisture from the surface of the Earth to the relatively cooler atmosphere, forms the clouds and generates the rain. The latent heat released as a result of the condensation enhances the convection.

The clouds, on the other hand, redistribute the radiative energy and alter the atmospheric motion field. The clouds reflect part of the solar energy back to space and thus cool the whole Earth and atmosphere system (the so - called cloud albedo effect). The clouds can also act as a greenhouse: absorb part of the longwave radiation from the Earth's surface, re-emit about half of the absorbed energy back to the Earth's surface and thus warm the Earth's surface and the lower atmosphere (the so - called cloud greenhouse effect).

The combination of the cloud albedo effect and the cloud greenhouse effect acting together slightly cools the Earth's surface and the lower atmosphere (Ra-

manathan et al., 1989).

Cloud formation, dissipation and their radiative effects constitute the largest uncertainty in global climate modeling. The major differences among the available climate models are due to the differences in the cloud radiation parameterizations (Cess et al, 1992).

The radiative properties of clouds depend on their jeight and morphology, as well as microphysics. The cloud morphology include individual cloud shape, horizontal and vertical extent, cloud fraction and cloud overlap. The cloud microphysical properties includes particle (liquid or solid) size distribution, cloud water or ice amount and the statistical variation in time and space of the parameters. The shortwave optical properties of different types of water clouds with equivalent cloud droplet radii between $5\mu m$ to $16\mu m$ may be parameterized as a linear function of cloud liquid water path and cloud equivalent radius. In current climate models, cloud equivalent radius is frequently assumed to be $10\mu m$ to simplify the cloud radiation calculations.

The greenhouse effect of the CO_2 concentration doubling is about 4 W/m^2 in radiative heating of the lower atmosphere and the surface of the Earth. A slight variation of the cloud microphysical properties leads to effects comparable to the CO_2 doubling impact on the greenhouse effect. To assess the climate effect of CO_2 concentration doubling, more accurate cloud radiation calculations are needed. This need inspired the research reported in this thesis.

It is important to establish which physical properties of clouds are important to the climate system and relate the global climatology of these properties to their impact on radiation. In the first four chapters of this thesis, a quantitative investigation is undertaken of the sensitivity of the climate system to the changes in cloud drop size, or, the importance of cloud microphysical properties.

In Chapter 2, the optical properties of water clouds are discussed. Based on

electromagnetic theory of optical properties of different size distributions, we find that it is sufficient to relate the cloud optical properties to only the second and the third moments of the size distribution. An accurate parameterization of cloud radiative properties is established based on this.

In Chapter 3, a one dimensional radiative - convective model is developed which incorporates the new cloud parameterization scheme. Unlike most radiative - convective models, which have some difficulty treating the lower surface boundary, this model has a more physically sound and numerically stable scheme for the treatment of the energy exchange at the lower boundary.

In Chapter 4, the sensitivities of the cloud radiative forcing to the changes in cloud droplet size, cloud water amount and cloud height are examined. It is shown that a slight change in cloud droplet size can cause a significant change in cloud solar radiative forcing for regular clouds. For optically thin clouds, the infrared radiation is also very sensitive to changes in the cloud equivalent radius.

The sensitivity of the climate equilibrium temperature profile to changes in cloud equivalent radius is also discussed in Chapter 4. Compared to the existing climate, a 10% increase in cloud equivalent radius, or a 15% decrease of cloud water amount could increase the Earth's surface temperature by about 2^0C, which is about the same effect as doubling the CO_2 concentration in the model.

The radiative transfer calculations consume most of the computing time in climate models. In Chapter 5, the adjoint method for radiative transfer is developed to speed up the computations of radiative fluxes and heating rates. The idea of the adjoint radiative transfer method is similar to the Green's function method. Instead of repeatedly solving the radiative transfer equations, the adjoint method solves the adjoint equation of radiative transfer once and for all. The radiative properties for different atmospheric conditions are then obtained by simple integration of the radiative source functions corresponding to those conditions.

The cloud radiative effect is the most important adjustment of the climate system. On the other hand, clouds form as a result of the atmospheric general circulation, which is driven by the radiative heating of the relatively warm regions (such as the surface of the Earth and the Tropics) and the net radiative cooling of the cold regions (such as the atmosphere and the polar regions). The mechanisms which control the interaction between the cloud microphyscial processes and the climate macrophysical behavior are not yet well understood. In Chapter 6, an entropy approach to the climate system is introduced based on atmospheric irreversibility concepts to provide a theoretical framework for advancing our understanding of the basic behavior of the climate system. The one dimensional radiative - convective model has been used to explore the consequences of this approach, which allows us to treat the whole climate system as a single entity and thus provide a better understanding of the interaction between different processes that acting together determine the evolution of the climate system. This approach also facilitates the study of feedback mechanisms in the climate system.

Chapter 2

Parameterization of the Cloud Radiative Properties

2.1 Introduction

Clouds influence the climate by changing the radiative properties such as the shortwave albedo, infrared emission and absorption. The cloud optical and hence radiative properties depend on cloud drop size distribution and/or cloud liquid water content (Paltridge 1974, Platt 1976). Cloud microphysical properties and morphology are expected to change with climate. Changes in the climate system affect clouds in several ways. The atmosphere is expected to contain more water vapour for a warmer ocean surface (Raval and Ramanathan 1989), which may lead to a higher liquid water content of clouds. It has been hypothesized that dimethylsulfate production in the ocean may be an important source of cloud condensation

[0] This chapter is based on material previously published as Y.X. Hu and K. Stamnes, An accurate parameterizationof radiative properties of warm cloud suitable for climate models , *Journal of Climate, 17*, 611-624, 1993.

nuclei over the remote oceans which may affect cloud microphysics (Charlson *et al.*, 1987). The increasing industrial pollution, aircraft contrails and shipstack effluents also provide more cloud condensation nuclei which may change the cloud drop size distribution. Such changes of cloud properties will cause changes in cloud radiative properties and the resulting feedbacks may be comparable in size with the effect of a doubling of CO_2.

Experimental data have been used to make some advances in the study of climate feedback processes between cloud water content and temperature (Somerville and Remer 1984; Platt and Harshvardhan, 1988). Changes in cloud liquid water content and dropsize distribution will most likely occur independent of each other (Slingo, 1989). To investigate the effect of cloud microphysical processes on climate, it is therefore desirable to separate the dependence of cloud optical properties on droplet size distribution and liquid water content. To assess the impact of cloud-radiation-climate interactions and feedback mechanisms, we must know the relationship between cloud microphysical processes and cloud radiative properties. Given the droplet size distribution, the important optical parameters, such as volume extinction coefficient, single scattering albedo and asymmetry factor, of eight types of clouds have been determined from Mie theory (Stephens, 1979). Such calculations are, however, extremly time-consuming and consequently impractical for use in climate models. It is therefore desirable to devise parameterizations in which the optical properties of water clouds are determined by a few moments of the size distribution.

The equivalent radius of the droplet distribution is a well defined quantity and it is possible to relate volume extinction coefficient directly to liquid water content and equivalent radius of cloud droplets (Paltridge and Platt, 1976). For spherical cloud droplets, the liquid water content and the equivalent radius are the most important cloud microphysical parameters related to radiative properties (Slingo,

1989).

For shortwave radiation, Slingo and Schrecker (1982) developed a simple parameterization of single scattering albedo and asymmetry factor as a linear function of equivalent radius in the droplet size range from 4.2 μm to 16.6 μm. For a larger range of drop sizes, Ackerman and Stephens (1987) found a good nonlinear fitting of the single scattering albedo in terms of equivalent radius for the solar and near infrared spectral region. For longwave radiation, Tsay *et al.* (1989) performed a linear parameterization for equivalent radii between 4μm and 12μm appropriate for arctic stratus clouds. In this size range the linear relations between optical properties and equivalent radius constitute a good parameterization.

To simulate the process of cloud-radiation-climate interaction accurately and reliably in large scale models, it is neccessary to have an adequate parameterization for a wider range of cloud drop sizes and for the entire solar and terrestrial wavelength ranges. The purpose of this study is to provide such a parameterization from which cloud heating and cooling rates may be reliably and efficiently computed.

The new parameterization of the radiative properties of water clouds presented here is based on cloud optical properties computed from Mie theory for both solar and terrestrial spectra and for cloud equivalent radii in the range 2.5 - 60 μm. It is found that cloud optical properties depend mainly on equivalent radius throughout the solar and terrestrial spectrum and are insensitive to the details of the droplet size distribution, such as shape, skewness, width and modality (single or bimodal). This suggests that in cloud models, aimed at predicting the evolution of cloud microphysics with climate change and conversely the impact of cloud microphysics on climate evolution, it is sufficient to determine the third and the second moments of the size distribution (the ratio of which determines the equivalent radius). It also implies that measurements of the cloud liquid water content and the extinction

coefficient are sufficient to determine cloud optical properties experimentally (i.e. measuring the complete droplet size distribution is not required). Based on the detailed calculations, the optical properties are parameterized as a function of cloud liquid water path and equivalent cloud droplet radius by using a nonlinear least square fitting. The parameterization is performed separately for the range of radii 2.5μm - 12μm, 12μm - 30μm and 30μm - 60μm respectively. Cloud heating and cooling rates are computed from this parameterization by using a comprehensive radiation model. Comparison with similar results obtained from exact Mie scattering calculations shows that our parameterization yields very accurate results and that it is several thousand times faster. This parameterization separates the dependence of cloud optical properties on droplet size and liquid water content, and is suitable for inclusion into climate models.

2.2 Parameterization of Cloud Optical Properties

2.2.1 The Dependence of Cloud Optical Properties on Equivalent Radius

The cloud optical properties needed for radiative transfer calculations in climate models are the volume extinction coefficient β_{ext}, the single scattering albedo ω, and the asymmetry factor g. Assuming spherical particles we have calculated these optical properties from so-called Mie theory (*cf.* *e.g.* Van de Hulst, 1957; Bohren and Huffmann, 1983) from the known index of refraction of water (Palmer and Williams, 1974; Downing and Williams, 1975; Hale and Querry, 1973). The extinction and scattering coefficients are

$$\beta_{ext} = \int_0^\infty n(r) r^2 Q_{ext}(r)\, dr \tag{2.1}$$

$$\beta_{sca} = \int_0^\infty n(r) r^2 Q_{sca}(r)\, dr \tag{2.2}$$

where r is droplet radius, n(r) is the cloud droplet size distribution, Q_{ext} is the extinction efficiency, and Q_{sca} is the scattering efficiency. Q_{ext} and Q_{sca} are computed by Mie theory for a number of radii r spanning the droplet sizes of interest and then perform the neccessary integrations over the size distribution to determine β_{ext} and β_{sca} from Equation 2.1 and 2.2. The single scattering albedo ω and the asymmetry factor are:

$$\omega = \frac{\beta_{sca}}{\beta_{ext}} \tag{2.3}$$

$$g = \frac{1}{2}\int_{-1}^{1} p(\mu)\mu\, d\mu \tag{2.4}$$

where μ is the cosine of the scattering angle, and $p(\mu)$ is the phase function.

Given the droplet size distribution n(r), the equivalent radius is defined as the ratio of the third to the second moment of the size distribution

$$r_e = \int_0^\infty n(r) r^3\, dr \Big/ \int_0^\infty n(r) r^2\, dr. \tag{2.5}$$

For shortwave radiation, the volume extincton coefficient β_{ext} has a very weak dependence on wavelength (Slingo and Schrecker, 1982). It is directly related to the liquid water content and the equivalent radius as follows

$$\beta_{ext} \approx 3LWC/2r_e \tag{2.6}$$

where LWC is the liquid water content of the cloud. This is a good approximation when the *size parameter* $2\pi r/\lambda$ is large (Paltridge and Platt, 1976; Stephens, 1978)

so that the extinction efficiency factor asymptotes to 2. It is in general inadequate for longwave radiation. As already noted, because it is too time consuming to do the exact calculation, it is desirable to parameterize also the dependence of the single scattering albedo and the asymmetry factor of cloud droplets in terms of equivalent radius and to extend this parameterization to longwave radiation. We use the generalized gamma distribution to represent the cloud droplet size distribution,

$$n(r) = \frac{N_0}{\Gamma(\gamma) r_m} (\frac{r}{r_m})^{\gamma-1} exp(-r/r_m) \tag{2.7}$$

where N_0 is the total (volume) number concentration, Γ is the gamma function, r_m is a characteristic radius of the distribution which represents its skewness, and γ is a constant which defines the shape of the distribution such that large values of γ correspond to broad distributions (*cf.* Tsay and Stephens, 1990, Stephens *et al.*, 1991 for details).

Substituting Equation 2.7 into 2.5, for a bi-modal size distribution, $n(r) = (1-c)n_1(r) + cn_2(r)$, we find that the equivalent radius of the cloud droplet r_e can be expressed as

$$r_e = \frac{(1-c)(\gamma_1+2)(\gamma_1+1)\gamma_1 r_{m1}^3 + c(\gamma_2+2)(\gamma_2+1)\gamma_2 r_{m2}^3}{(1-c)(\gamma_1+1)\gamma_1 r_{m1}^2 + c(\gamma_2+1)\gamma_2 r_{m2}^2} \tag{2.8}$$

where $n_1(r)$ and $n_2(r)$ denote the concentrations of the two modes and c is the fraction of droplets belonging to the second mode (denoted by subscript 2).

For a single mode [$c = 0$, $n(r) = n_1(r)$] this reduces to

$$r_e = (\gamma + 2) r_m \tag{2.9}$$

Different types of clouds have different total number concentrations, mode radii and shapes of size distributions (Stephens, 1979) and thus different radiative prop-

erties. The success of a parameterization in terms of a single parameter such as the equivalent radius depends to a large extent on how sensitive this parameterization is to changes in shape, skewness, modality (single or bi-modal), and total number concentration of the size distribution (which is related to the liquid water content). To investigate this issue we computed cloud optical properties for a wide variety of different size distributions obtained by changing the shape, the skewness, the modality and the total number concentration while keeping the equivalent radius fixed. Thus, for a fixed equivalent radius we computed the optical properties for distributions with entirely different shapes (γ varying from 2 to 18), different total number concentrations (varying from $100cm^{-3}$ to $200cm^{-3}$) and different numbers of modes (single and bi-modal). The skewnesses of the size distributions were also changed so as to keep the equivalent radius constant. For the example given in Figure 2.1 the equivalent radius is 20 μm. The computed optical properties for the distributions given in Figure 2.1 are provided in Figure 2.2. The top panel shows the ratio β/LWC (the extinction coefficient divided by the liquid water content). The differences of these ratios for different Γ distributions in Figure 2.1 are within 1-2% of their magnitudes for most wavelengths and never exceeds 6%. For the single scattering albedo ω and the asymmetry factor g the differences are even smaller. Use of different values for the equivalent radius yields results similar to those depicted in Figure 2.2 for illustration purposes.

A comparison of the optical properties of clouds with the same equivalent radius but different types of distributions (lognormal distribution versus generalized gamma distribution) with entirely different widths (Figure 2.3) indicates that for most wavelengths the differences are less than 8 percent. Figure 2.2 and Figure 2.3 show that distributions with entirely different shapes, skewnesses, modalities, widths and number concentrations, but with the same equivalent radius yield essentially identical cloud optical properties throughout the entire solar and terres-

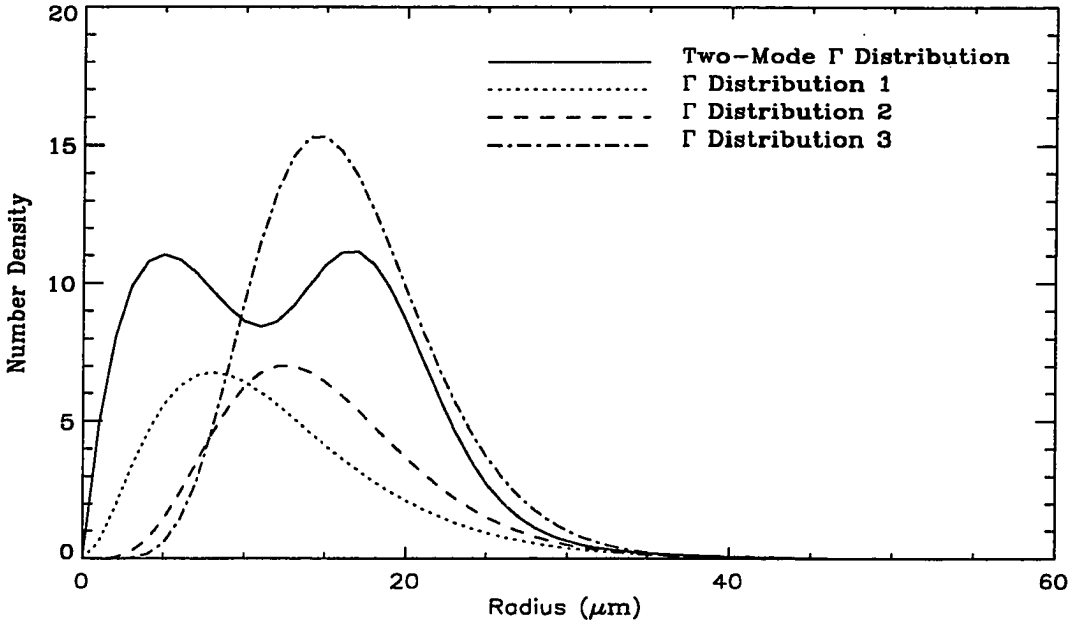

Figure 2.1 Gamma distributions for the same equivalent radius (r_e = 20 micron) with different shape and skewness of the size distribution (single mode and double mode) and total number concentration of cloud droplets. These different shapes were used to compute the optical properties in Figure 2.2.

trial spectrum. This finding is in agreement with expectations on physical grounds for large size parameters ($2\pi r/\lambda$), where the extinction efficiency factor asymptotes to 2 (solar radiation), but it is not so obvious for small size parameters (terrestrial radiation). Thus, for most wavelengths the perturbations of cloud optical and, hence, radiative properties obtained by changing the shape, the skewness and modality of the cloud droplet distribution for a given cloud liquid water content and equivalent radius are negligible compared with those resulting from changes in the equivalent radius and liquid water content. Consequently, there appears to be a definite dependence of cloud optical properties on equivalent radius and liquid water content which are insensitive to details of the size distribution such as modality, shape, width and skewness throughout the solar and thermal infrared spectral ranges (0.25 - 100 μm).

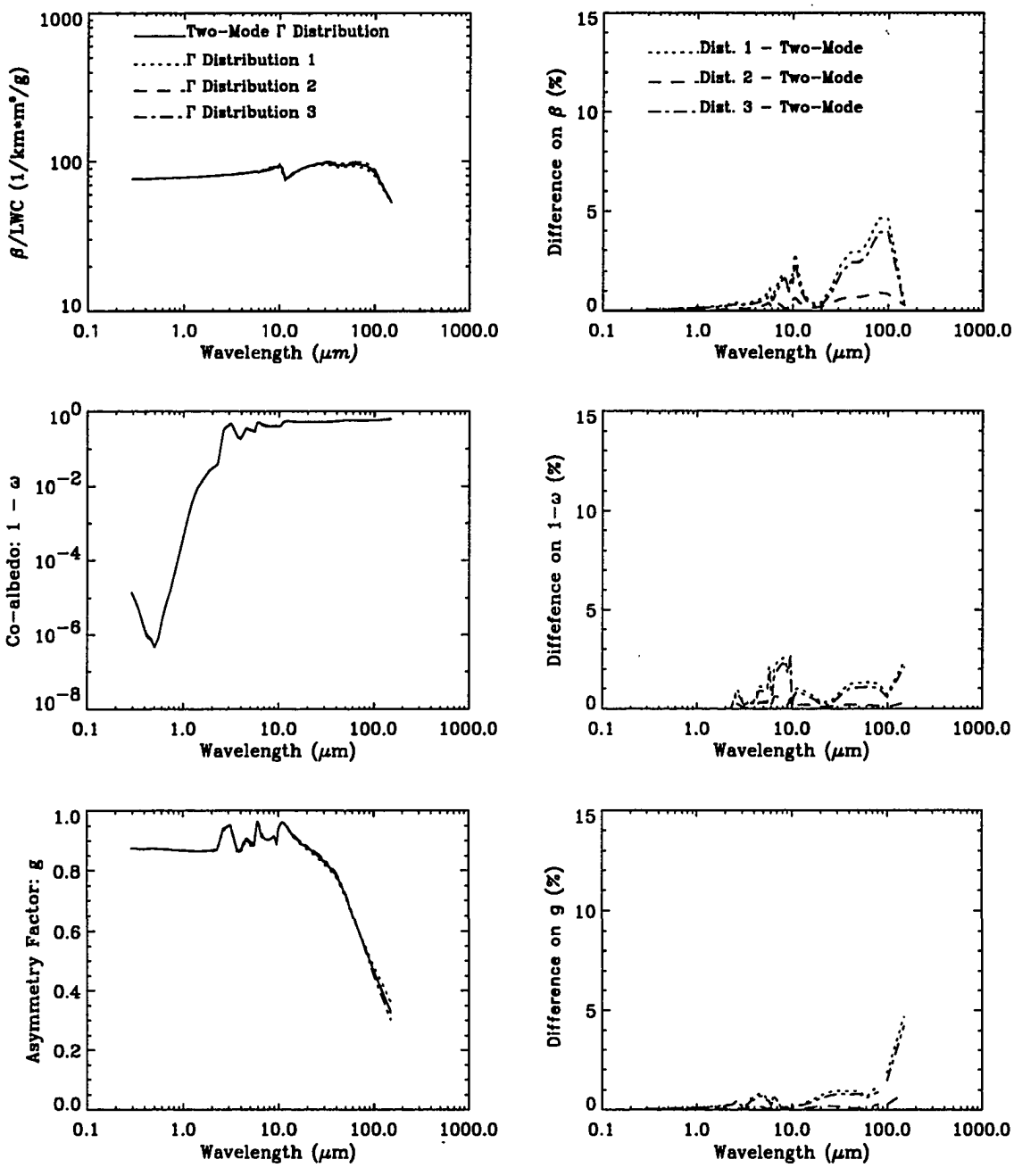

Figure 2.2 Comparison of optical properties obtained by Mie calculations for the different size distributions in Figure 2.1 having the same cloud equivalent radius.

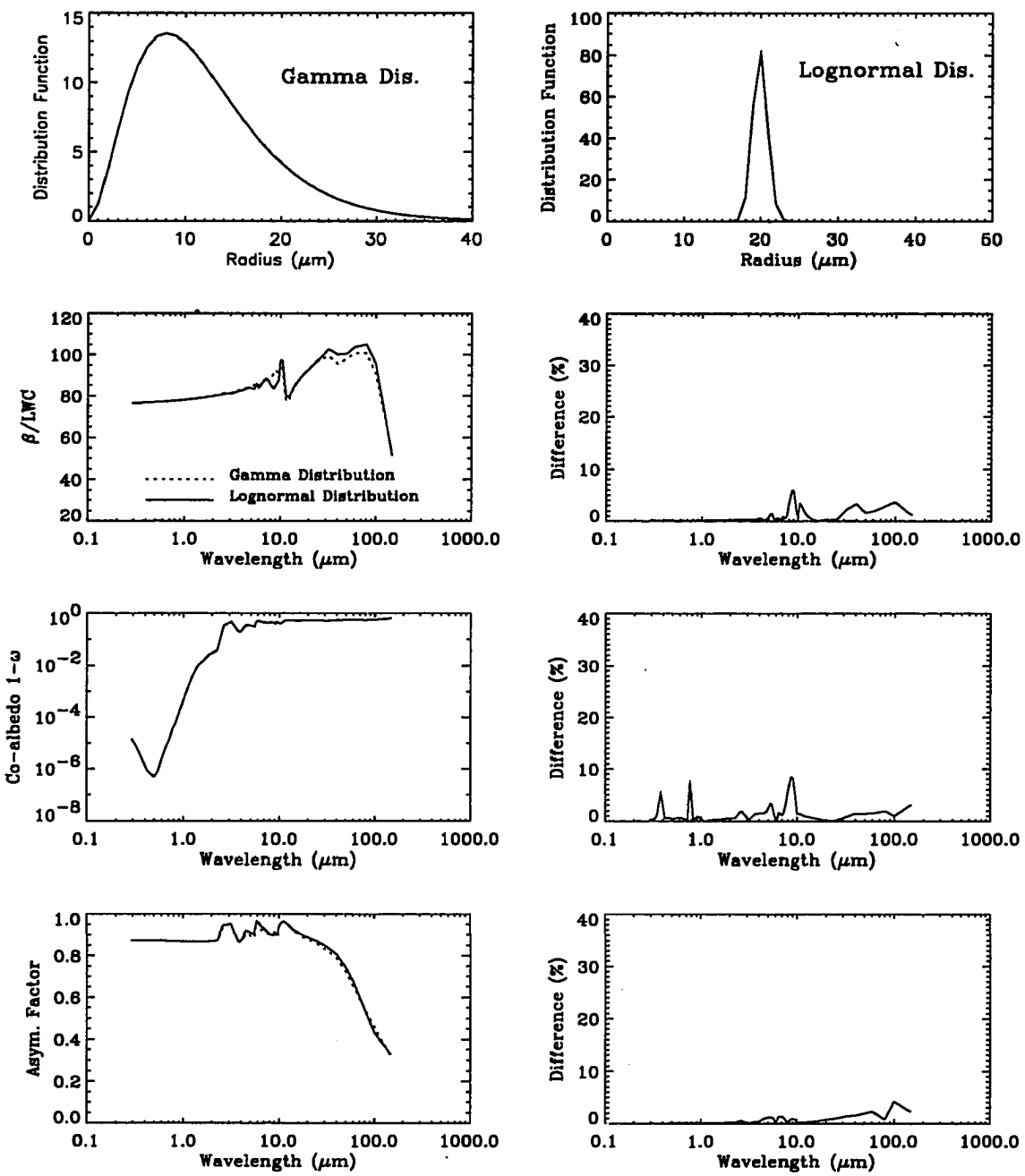

Figure 2.3 Comparison of optical properties obtained by Mie calculations for two different size distributions (Γ distribution and Lognormal distribution) with the same cloud equivalent radius, but with very different widths..

2.2.2 The Parameterization of Optical Properties as a Function of Equivalent Radius

For each wavelength, by changing the shape (γ), skewness (r_m) of the size distribution, and the total number concentration of the cloud droplets in Equation 2.7, we generated a group of "data" relating the optical properties to cloud liquid water content and equivalent radius for a variety of cloud droplet size distributions with equivalent radii ranging from 2.5 μm to 60 μm. In the small size range, for example from 4 μm to 16 μm, it is reasonable to fit the function relating shortwave optical properties (volume extinction coefficient β_{ext}, single scattering albedo ω, asymmetry factor g) and equivalent radius linearly as follows (Slingo and Schrecker, 1982):

$$\beta_{ext}/LWC = a + b/r_e \tag{2.10}$$

$$\omega = c + dr_e \tag{2.11}$$

$$g = e + fr_e \quad . \tag{2.12}$$

Tsay *et al.* (1989) fitted both longwave and shortwave radiative properties of arctic stratus clouds using a linear parameterization (Equations 2.10 through 2.12) for equivalent radii ranging from 4 μm to 12 μm. For larger drop sizes, a linear fitting will no longer be accurate because the curves for the single scattering albedo and asymmetry factor deviate substantially from a straight line.

To make the fit more accurate, a nonlinear fitting procedure is needed. Ackerman and Stephens (1987) used the following form to parameterize the droplet absorption for solar wavelengths:

$$1 - \omega = ck^{-1}r_e^p \tag{2.13}$$

where ω is the single scattering albedo, c and p are constants, and k is the absorption coefficient. We will extend this type of parameterization to apply for the entire shortwave and longwave regions. Thus, we adopt the following form for the extinction coefficient β, the scattering albedo ω and the asymmetry factor g for both solar and terrestrial wavelengths

$$\beta_{ext}/LWC = a_1 r_e^{b_1} + c_1 \tag{2.14}$$

$$1 - \omega = a_2 r_e^{b_2} + c_2 \tag{2.15}$$

$$g = a_3 r_e^{b_3} + c_3 \tag{2.16}$$

where LWC is the liquid water content of the cloud, and $1 - \omega$ is the co-albedo. In our parameterization we have taken the equivalent radius, r_e, to be in units of micrometers (μm) and we have chosen the other units such that Equation 2.14 should be multiplied by the liquid water content in units of grams per cubic meter (gm^{-3}) to yield the extinction coefficient in units per meter (m^{-1}).

All of the coefficients a_i, b_i, c_i (i=1,2,3) in Eqns 2.14 - 2.16 are constants for a given wavelength. Using the least square method, we may determine these coefficients. It is possible to fit one function for the whole range (2.5μm to 60μm), but this is less accurate than employing a separate fit in the following three radii ranges

1) small size, 2.5μm to 12μm

2) medium size, 12μm to 30μm

3) large size, 30μm to 60μm.

$\lambda(\mu m)$	a_1	b_1	c_1	a_1	b_1	c_1	a_1	b_1	c_1
0.290	1.63(3)	-1.03(0)	7.66(-1)	1.63(3)	-1.03(0)	9.90(-1)	9.40(2)	-8.06(-1)	-1.01(1)
0.314	1.67(3)	-1.04(0)	3.83(0)	1.61(3)	-1.02(0)	5.44(-1)	9.41(2)	-8.06(-1)	-1.01(1)
0.344	1.67(3)	-1.04(0)	3.49(0)	1.62(3)	-1.02(0)	6.34(-1)	9.42(2)	-8.06(-1)	-1.02(1)
0.379	1.68(3)	-1.05(0)	4.26(0)	1.64(3)	-1.03(0)	8.33(-1)	9.48(2)	-8.08(-1)	-1.01(1)
0.419	1.70(3)	-1.05(0)	4.49(0)	1.64(3)	-1.02(0)	6.44(-1)	9.54(2)	-8.10(-1)	-9.99(0)
0.459	1.72(3)	-1.06(0)	4.99(0)	1.65(3)	-1.03(0)	7.23(-1)	9.55(2)	-8.10(-1)	-1.00(1)
0.499	1.73(3)	-1.06(0)	5.13(0)	1.66(3)	-1.03(0)	8.13(-1)	9.62(2)	-8.12(-1)	-9.95(0)
0.544	1.75(3)	-1.07(0)	5.95(0)	1.67(3)	-1.03(0)	8.73(-1)	9.63(2)	-8.12(-1)	-9.98(0)
0.603	1.76(3)	-1.06(0)	5.01(0)	1.68(3)	-1.03(0)	9.28(-1)	9.70(2)	-8.14(-1)	-9.91(0)
0.664	1.79(3)	-1.07(0)	5.98(0)	1.69(3)	-1.03(0)	9.89(-1)	9.76(2)	-8.16(-1)	-9.84(0)
0.719	1.81(3)	-1.08(0)	6.85(0)	1.70(3)	-1.04(0)	1.04(0)	9.78(2)	-8.16(-1)	-9.89(0)
0.766	1.84(3)	-1.09(0)	8.81(0)	1.71(3)	-1.04(0)	1.01(0)	9.84(2)	-8.18(-1)	-9.79(0)
0.821	1.86(3)	-1.09(0)	8.61(0)	1.73(3)	-1.04(0)	1.16(0)	9.91(2)	-8.20(-1)	-9.74(0)
0.929	1.87(3)	-1.09(0)	8.41(0)	1.74(3)	-1.04(0)	1.19(0)	9.99(2)	-8.22(-1)	-9.69(0)
1.046	1.91(3)	-1.10(0)	7.51(0)	1.77(3)	-1.05(0)	1.46(0)	1.01(3)	-8.24(-1)	-9.65(0)
1.142	1.94(3)	-1.11(0)	1.01(1)	1.78(3)	-1.05(0)	1.32(0)	1.01(3)	-8.26(-1)	-9.61(0)
1.232	1.96(3)	-1.11(0)	9.29(0)	1.80(3)	-1.05(0)	1.50(0)	1.03(3)	-8.30(-1)	-9.44(0)
1.393	1.98(3)	-1.11(0)	7.61(0)	1.83(3)	-1.06(0)	1.63(0)	1.04(3)	-8.32(-1)	-9.40(0)
1.587	2.01(3)	-1.11(0)	8.80(0)	1.87(3)	-1.06(0)	1.93(0)	1.05(3)	-8.36(-1)	-9.31(0)
1.855	2.15(3)	-1.15(0)	1.42(1)	1.91(3)	-1.07(0)	1.96(0)	1.07(3)	-8.40(-1)	-9.22(0)
2.247	3.26(3)	-1.46(0)	5.42(1)	1.99(3)	-1.08(0)	2.54(0)	1.09(3)	-8.46(-1)	-9.08(0)
2.618	4.56(3)	-1.61(0)	5.74(1)	2.05(3)	-1.09(0)	2.66(0)	1.12(3)	-8.52(-1)	-8.94(0)
3.145	2.71(3)	-1.27(0)	2.35(1)	2.02(3)	-1.08(0)	2.24(0)	1.12(3)	-8.52(-1)	-8.99(0)
3.690	5.29(3)	-1.73(0)	7.34(1)	2.17(3)	-1.10(0)	3.01(0)	1.17(3)	-8.64(-1)	-8.67(0)
R_e :	2.5	to 12.5	μm	12.5	to 30	μm	30	to 60	μm

Table 2.1 The coefficients a_2, b_2, c_2 of (ar^b+c) as a function of wavelength $\lambda(\mu m)$ for the fitting of the *extinction coefficient* in the solar region. Note that a (b) in the table means a$\times 10^b$.

We first choose 24 bands in the visible and near infrared part of the spectrum (0.3 - 4.0 μm) and 50 bands in the infrared (terrestrial) spectrum (4.0 - 150.0 μm). These band intervals are the same as those used by Slingo (1982, 1989) and Tsay *et al.* (1989) to perform the parameterizations. The coefficients a_i, b_i, c_i (i=1,2,3) for the fitting in the shortwave region are listed in Tables 2.1 - 2.3 .

Tables 2.4 - 2.6 give the corresponding values for the longwave region. For the small and medium droplet sizes, the index b_1 of the volume extinction coefficient is close to -1.0 in the shortwave region implying that the liquid water path is proportional to r_e^{-1}. But in the longwave region the extinction coefficient deviates from this simple form. The upper panels of Figure 2.4 and Figure 2.5 show the deviation of the fitting from the exact value. The differences between the fitting

$\lambda(\mu m)$	a_2	b_2	c_2	a_2	b_2	c_2	a_2	b_2	c_2
R_e :	2.5	to 12.5	μm	12.5	to 30	μm	30	to 60	μm
0.290	1.42(-6)	7.66(-1)	-1.02(-6)	9.00(-7)	9.42(-1)	-9.60(-7)	3.14(-6)	6.88(-1)	-1.16(-5)
0.314	-2.33(-5)	-2.32(-1)	1.95(-5)	5.08(-7)	9.88(-1)	5.97(-7)	2.18(-6)	6.90(-1)	-7.64(-6)
0.344	-2.03(-5)	-1.52(0)	4.01(-6)	3.68(-7)	9.22(-1)	-4.01(-8)	7.50(-7)	7.82(-1)	-2.36(-6)
0.379	1.43(-7)	9.52(-1)	-2.31(-8)	3.94(-7)	7.06(-1)	-7.93(-7)	3.42(-7)	7.64(-1)	-1.07(-6)
0.419	2.57(-8)	1.21(0)	1.01(-7)	1.67(-7)	7.12(-1)	-3.65(-7)	1.35(-7)	7.78(-1)	-3.94(-7)
0.459	2.10(-8)	1.13(0)	5.59(-8)	2.75(-7)	5.16(-1)	-6.04(-7)	6.85(-8)	8.22(-1)	-1.44(-7)
0.499	3.72(-9)	1.60(0)	1.07(-7)	2.77(-8)	9.74(-1)	-1.07(-8)	2.25(-7)	5.48(-1)	-7.05(-7)
0.544	1.82(-8)	1.21(0)	6.89(-8)	3.23(-8)	1.01(0)	4.62(-8)	9.12(-8)	7.94(-1)	-3.12(-7)
0.603	2.70(-7)	7.34(-1)	-2.43(-7)	1.19(-7)	9.76(-1)	6.76(-8)	3.32(-7)	7.62(-1)	-1.09(-6)
0.664	5.47(-7)	8.14(-1)	-1.41(-7)	5.91(-7)	8.46(-1)	-9.34(-7)	8.34(-7)	7.78(-1)	-2.25(-6)
0.719	9.95(-7)	8.56(-1)	-4.37(-7)	1.88(-7)	1.32(0)	3.08(-6)	2.03(-5)	3.32(-1)	-4.32(-5)
0.766	5.93(-7)	1.26(0)	1.69(-6)	4.52(-6)	6.72(-1)	-8.03(-6)	6.16(-6)	6.52(-1)	-2.04(-5)
0.821	8.03(-7)	1.44(0)	5.04(-6)	3.79(-5)	3.82(-1)	-6.22(-5)	6.09(-6)	7.88(-1)	-1.23(-5)
0.929	7.42(-6)	1.05(0)	5.08(-6)	1.58(-5)	8.30(-1)	-1.64(-5)	3.08(-5)	7.12(-1)	-9.82(-5)
1.046	2.36(-4)	4.10(-1)	-2.69(-4)	2.82(-5)	1.00(0)	4.65(-5)	1.50(-4)	6.60(-1)	-5.20(-4)
1.142	1.59(-4)	7.86(-1)	-1.33(-4)	8.54(-5)	9.62(-1)	5.50(-5)	3.58(-4)	6.70(-1)	-1.21(-3)
1.232	3.11(-4)	8.20(-1)	-2.17(-4)	2.27(-4)	9.14(-1)	-3.57(-5)	7.03(-4)	6.90(-1)	-2.34(-3)
1.393	1.01(-3)	7.16(-1)	-9.84(-4)	4.62(-4)	9.44(-1)	1.57(-4)	1.97(-3)	6.50(-1)	-6.45(-3)
1.587	1.38(-3)	7.90(-1)	-1.29(-3)	7.25(-4)	9.58(-1)	7.05(-4)	3.65(-3)	6.28(-1)	-1.15(-2)
1.855	4.00(-3)	6.88(-1)	-4.48(-3)	2.10(-3)	8.66(-1)	-4.43(-4)	1.32(-2)	5.06(-1)	-3.44(-2)
2.247	1.25(-2)	6.02(-1)	-1.62(-2)	5.81(-3)	8.08(-1)	-3.69(-3)	4.81(-2)	4.08(-1)	-1.06(-1)
2.618	2.00(0)	4.60(-2)	-2.06(0)	5.92(-1)	1.06(-1)	-5.89(-1)	-1.13(0)	-1.34(-1)	9.75(-1)
3.145	-1.22(0)	-1.90(0)	4.93(-1)	-9.00(-5)	1.40(0)	4.85(-1)	2.17(-1)	-7.48(-1)	4.57(-1)
3.690	-5.94(-1)	-5.24(-1)	4.22(-1)	-2.76(0)	-4.00(-2)	2.76(0)	-1.17(0)	-5.40(-1)	5.37(-1)

Table 2.2 The coefficients a_2, b_2, c_2 of (ar^b+c) as a function of wavelength $\lambda(\mu m)$ for the fitting of the *co-albedo* in the solar region. .

and Mie calculation are within 3 percent and much smaller for most of wavelength. The fittings in the visible region have a higher accuracy than the fittings in the solar near infrared and the terrestrial infrared region. In the visible region the fittings for the extinction coefficients are almost identical to the exact Mie calculations. The fittings for larger droplets are more accurate than the fittings for smaller droplets.

The middle panels of Figure 2.4 and Figure 2.5 show the accuracy of the fittings for single scattering albedo. The differences between the Mie calculation and the parameterization are within a few percent and never exceed 6 percent. The lower panels of Figure 2.4 and Figure 2.5 show the accuracy of the fittings for the asymmetry factor. The differences between parameterization and Mie calculation are smaller than 3%.

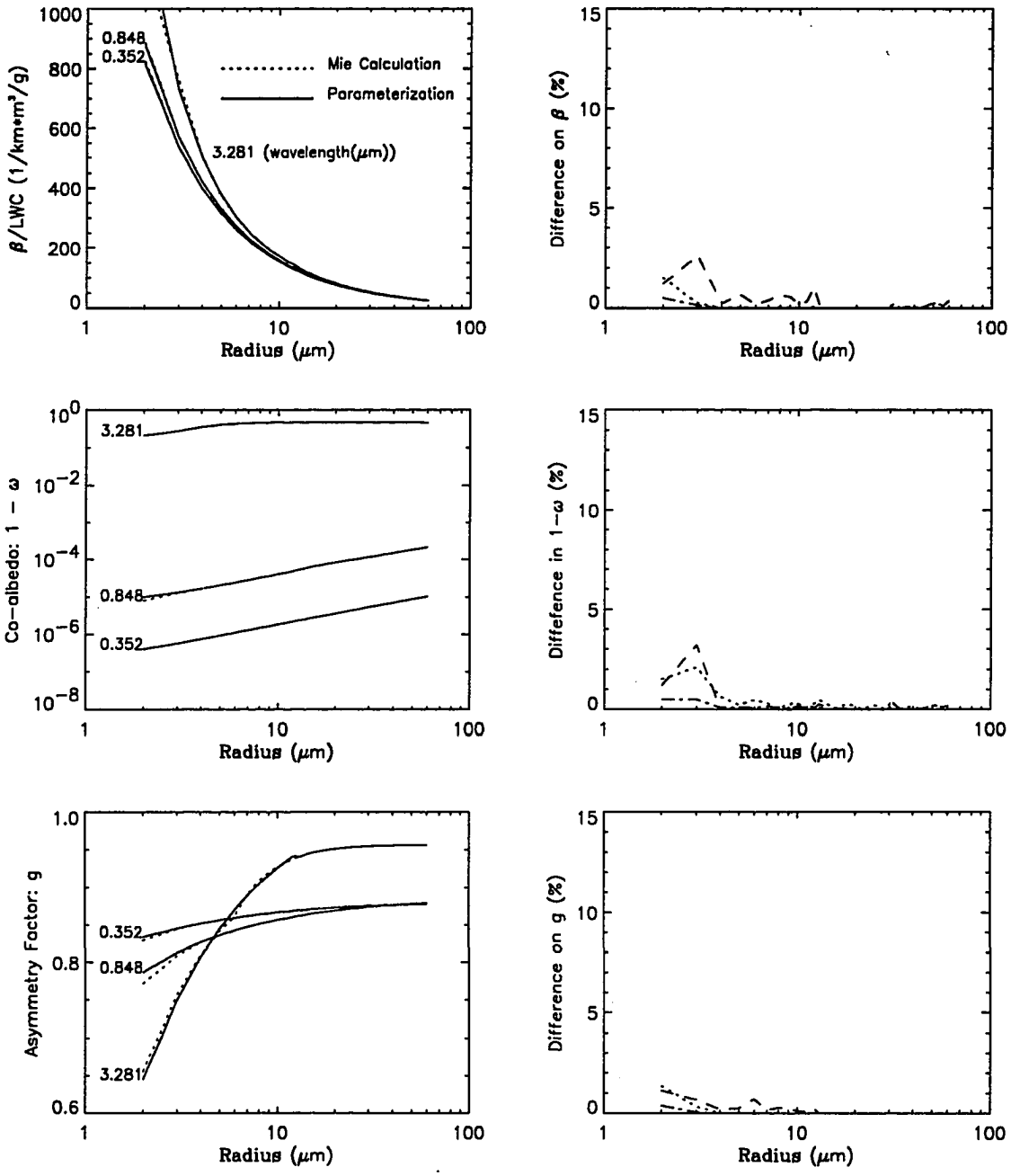

Figure 2.4 Volume extinction coefficient (divided by liquid water content), co-albedo and asymmetry factor as functions of equivalent radius for wavelengths 0.352, 0.848 and 3.281 μm from the Mie calculation and the parameterization and the differences between the results of the parameterization and the Mie calculation.

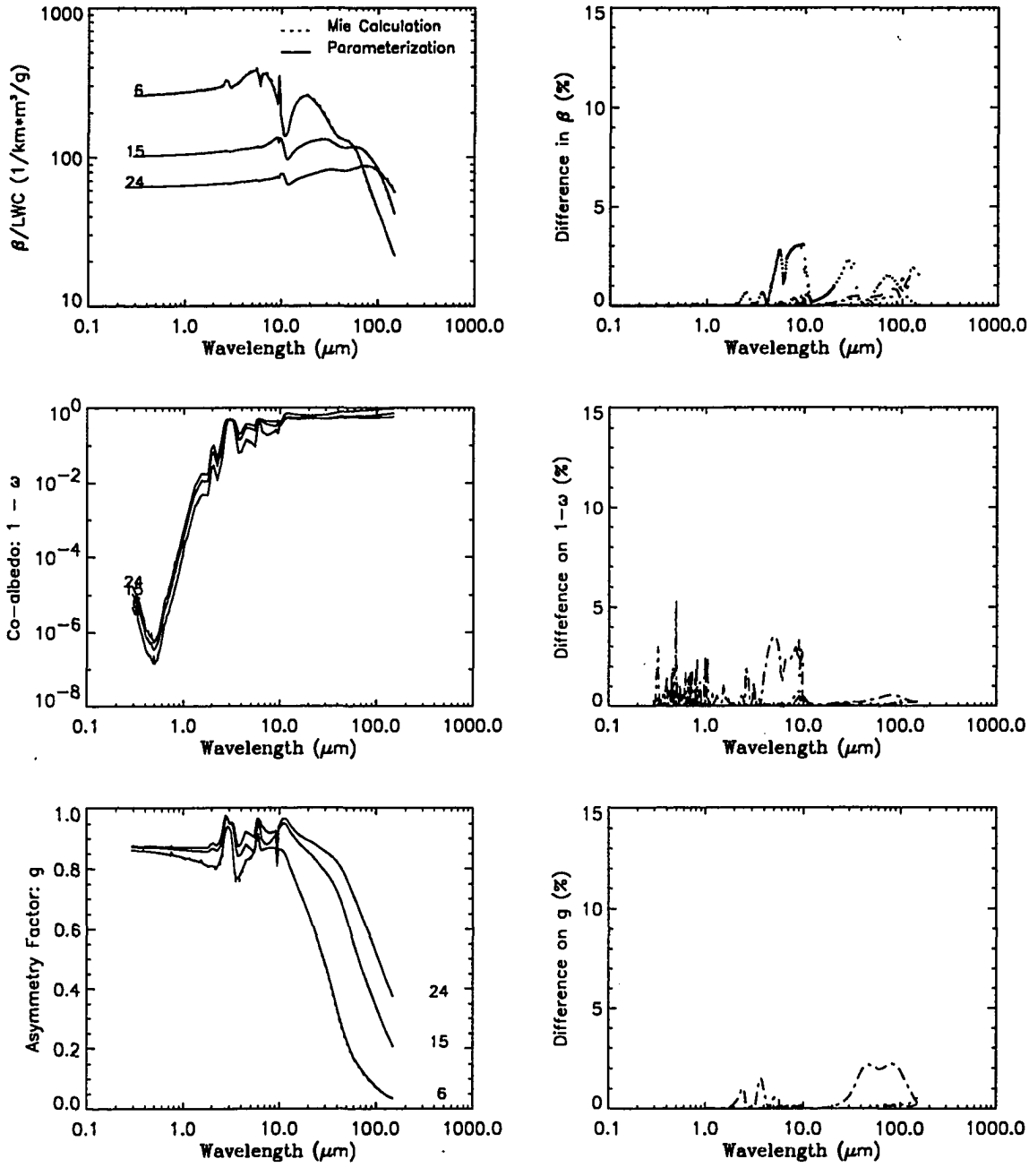

Figure 2.5 Volume extinction coefficient (divided by liquid water content) , co-albedo and asymmetry factor as functions of wavelengths for equivalent radius 6, 15 and 24 μm from the Mie calculation and the parameterization and the differences between the results of the parameterization and the Mie calculation.

$\lambda(\mu m)$	a_3	b_3	c_3	a_3	b_3	c_3	a_3	b_3	c_3
R_e :	2.5	to 12.5	μm	12.5	to 30	μm	30	to 60	μm
0.290	1.11(-1)	9.40(-2)	7.30(-1)	-3.15(-1)	-1.47(0)	8.78(-1)	-9.92(-2)	-9.08(-1)	8.80(-1)
0.314	-8.06(-2)	-7.62(-1)	8.83(-1)	-8.43(-2)	-8.06(-1)	8.82(-1)	-1.30(-1)	-9.86(-1)	8.81(-1)
0.344	-8.29(-2)	-6.88(-1)	8.84(-1)	-9.08(-2)	-8.06(-1)	8.81(-1)	-1.50(-1)	-1.01(0)	8.80(-1)
0.379	-6.75(-2)	-6.12(-1)	8.82(-1)	-1.63(-1)	-1.02(0)	8.81(-1)	-2.64(-1)	-1.18(0)	8.80(-1)
0.419	-9.98(-2)	-8.00(-1)	8.82(-1)	-1.02(-1)	-7.80(-1)	8.83(-1)	-1.77(-1)	-1.01(0)	8.82(-1)
0.459	-1.09(-1)	-7.24(-1)	8.86(-1)	-1.11(-1)	-7.88(-1)	8.84(-1)	-1.77(-1)	-9.80(-1)	8.83(-1)
0.499	-1.15(-1)	-7.56(-1)	8.85(-1)	-1.09(-1)	-7.48(-1)	8.85(-1)	-1.84(-1)	-9.66(-1)	8.83(-1)
0.544	-1.24(-1)	-7.82(-1)	8.85(-1)	-1.20(-1)	-7.48(-1)	8.86(-1)	-2.07(-1)	-9.84(-1)	8.84(-1)
0.603	-1.24(-1)	-6.02(-1)	8.94(-1)	-1.33(-1)	-7.66(-1)	8.86(-1)	-2.05(-1)	-9.52(-1)	8.84(-1)
0.664	-1.37(-1)	-6.76(-1)	8.90(-1)	-1.55(-1)	-8.16(-1)	8.85(-1)	-2.03(-1)	-9.20(-1)	8.84(-1)
0.719	-1.41(-1)	-6.94(-1)	8.89(-1)	-1.57(-1)	-7.82(-1)	8.86(-1)	-2.14(-1)	-9.16(-1)	8.85(-1)
0.766	-2.31(-1)	-1.23(0)	8.75(-1)	-1.15(-1)	-6.28(-1)	8.89(-1)	-2.55(-1)	-9.74(-1)	8.84(-1)
0.821	-1.71(-1)	-8.26(-1)	8.83(-1)	-1.67(-1)	-7.44(-1)	8.88(-1)	-2.58(-1)	-9.36(-1)	8.85(-1)
0.929	-1.86(-1)	-8.24(-1)	8.84(-1)	-1.74(-1)	-7.24(-1)	8.88(-1)	-2.89(-1)	-9.42(-1)	8.85(-1)
1.046	-2.13(-1)	-8.00(-1)	8.87(-1)	-2.12(-1)	-7.82(-1)	8.88(-1)	-2.74(-1)	-8.86(-1)	8.87(-1)
1.142	-3.14(-1)	-1.20(0)	8.71(-1)	-2.08(-1)	-7.10(-1)	8.91(-1)	-2.84(-1)	-8.62(-1)	8.88(-1)
1.232	-3.74(-1)	-1.25(0)	8.71(-1)	-2.06(-1)	-6.68(-1)	8.94(-1)	-2.84(-1)	-8.16(-1)	8.90(-1)
1.393	-4.61(-1)	-1.31(0)	8.71(-1)	-2.19(-1)	-6.34(-1)	8.99(-1)	-2.31(-1)	-6.54(-1)	8.98(-1)
1.587	-5.82(-1)	-1.39(0)	8.70(-1)	-2.38(-1)	-5.96(-1)	9.06(-1)	-2.20(-1)	-5.34(-1)	9.10(-1)
1.855	-3.58(-1)	-6.40(-1)	9.25(-1)	-2.51(-1)	-5.02(-1)	9.23(-1)	-2.31(-1)	-4.10(-1)	9.35(-1)
2.247	5.98(-3)	1.10(0)	7.66(-1)	-3.01(-1)	-4.30(-1)	9.58(-1)	-2.94(-1)	-2.68(-1)	1.01(0)
2.618	4.06(-8)	5.44(0)	8.61(-1)	-6.56(-1)	-8.78(-1)	9.63(-1)	-3.87(-1)	-5.70(-1)	9.86(-1)
3.145	-2.85(-1)	-6.56(-1)	1.01(0)	-3.20(0)	-2.16(0)	9.65(-1)	-1.65(0)	-1.94(0)	9.65(-1)
3.690	1.80(-3)	1.67(0)	7.56(-1)	-6.08(-1)	-6.50(-1)	9.87(-1)	-8.86(-1)	-8.10(-1)	9.76(-1)

Table 2.3 The coefficients a_3, b_3, c_3 of (ar^b+c) as a function of wavelength $\lambda(\mu m)$ for the fitting of the *asymmetry factor* in the solar region. .

We also computed the optical properties with a finer spectral resolution by dividing each of the bands above into 4 bands (24×4 bands for wavelengths between 0.3 - 4.0 μm and 50×4 bands for wavelengths between 4.0 - 150.0 μm) and repeated the parameterization. The differences between this parameterization and the Mie calculation have similar magnitudes as (slightly smaller than) those for the 24 and 50 band spectral resolution. As demonstrated in Figures 2.2, 2.3 and 2.5, the cloud optical properties depend strongly on wavelength in the near infrared and atmospheric window regions. Therefore the cloud radiative properties will be more accurate with a higher spectral resolution in these particular regions.

$\lambda(\mu m)$	a_1	b_1	c_1	a_1	b_1	c_1	a_1	b_1	c_1
R_e :	2.5	to 12.5	μm	12.5	to 30	μm	30	to 60	μm
3.900	6.40(3)	-1.79(0)	7.03(1)	2.24(3)	-1.11(0)	3.32(0)	1.20(3)	-8.70(-1)	-8.51(0)
4.100	5.42(3)	-1.63(0)	4.78(1)	2.26(3)	-1.12(0)	3.29(0)	1.22(3)	-8.74(-1)	-8.38(0)
4.300	4.30(3)	-1.42(0)	1.52(1)	2.28(3)	-1.12(0)	3.16(0)	1.23(3)	-8.76(-1)	-8.35(0)
4.500	3.32(3)	-1.19(0)	-3.31(1)	2.28(3)	-1.11(0)	2.91(0)	1.24(3)	-8.78(-1)	-8.32(0)
4.700	2.69(3)	-9.84(-1)	-9.66(1)	2.28(3)	-1.11(0)	2.66(0)	1.26(3)	-8.82(-1)	-8.19(0)
4.900	2.29(3)	-7.86(-1)	-1.89(2)	2.28(3)	-1.11(0)	2.42(0)	1.27(3)	-8.84(-1)	-8.16(0)
5.100	2.03(3)	-5.46(-1)	-3.88(2)	2.28(3)	-1.11(0)	2.19(0)	1.28(3)	-8.88(-1)	-8.03(0)
5.300	2.52(3)	-2.26(-1)	-1.30(3)	2.30(3)	-1.11(0)	2.25(0)	1.30(3)	-8.92(-1)	-7.90(0)
5.400	-4.31(4)	8.00(-3)	4.41(4)	2.34(3)	-1.12(0)	2.60(0)	1.31(3)	-8.94(-1)	-7.86(0)
5.500	-1.10(3)	2.04(-1)	1.96(3)	2.41(3)	-1.13(0)	3.47(0)	1.31(3)	-8.94(-1)	-7.90(0)
5.700	-2.61(2)	4.58(-1)	9.55(2)	2.76(3)	-1.19(0)	6.82(0)	1.32(3)	-8.96(-1)	-7.82(0)
5.900	-1.84(2)	5.00(-1)	7.83(2)	3.12(3)	-1.24(0)	9.51(0)	1.30(3)	-8.92(-1)	-7.94(0)
6.000	-4.93(2)	2.70(-1)	1.11(3)	2.92(3)	-1.22(0)	8.24(0)	1.27(3)	-8.84(-1)	-8.20(0)
6.100	-3.15(4)	8.00(-3)	3.23(4)	2.74(3)	-1.19(0)	6.86(0)	1.28(3)	-8.86(-1)	-8.14(0)
6.200	1.95(3)	-2.50(-1)	-9.02(2)	2.61(3)	-1.16(0)	5.49(0)	1.30(3)	-8.90(-1)	-8.04(0)
6.300	2.41(3)	-1.86(-1)	-1.38(3)	2.62(3)	-1.16(0)	5.36(0)	1.32(3)	-8.94(-1)	-7.92(0)
6.500	-1.14(3)	1.86(-1)	1.95(3)	2.76(3)	-1.18(0)	6.34(0)	1.35(3)	-9.00(-1)	-7.76(0)
6.700	-1.87(2)	5.32(-1)	8.45(2)	3.03(3)	-1.22(0)	8.35(0)	1.37(3)	-9.04(-1)	-7.66(0)
7.000	-4.36(1)	9.24(-1)	5.82(2)	3.56(3)	-1.29(0)	1.16(1)	1.39(3)	-9.08(-1)	-7.56(0)
7.100	-1.76(1)	1.20(0)	4.99(2)	4.06(3)	-1.34(0)	1.40(1)	1.40(3)	-9.10(-1)	-7.52(0)
7.300	-7.13(0)	1.49(0)	4.43(2)	4.74(3)	-1.40(0)	1.65(1)	1.41(3)	-9.12(-1)	-7.48(0)
7.600	-1.97(0)	1.91(0)	3.87(2)	5.98(3)	-1.49(0)	1.96(1)	1.42(3)	-9.14(-1)	-7.47(0)
8.000	-2.89(-1)	2.57(0)	3.35(2)	8.00(3)	-1.60(0)	2.25(1)	1.44(3)	-9.16(-1)	-7.48(0)
8.600	-1.29(-2)	3.65(0)	2.84(2)	9.63(3)	-1.66(0)	2.26(1)	1.46(3)	-9.20(-1)	-7.42(0)
9.000	-2.60(-4)	5.06(0)	2.48(2)	8.53(3)	-1.59(0)	1.83(1)	1.50(3)	-9.28(-1)	-7.15(0)
9.600	-7.62(-2)	3.00(0)	3.02(2)	7.52(3)	-1.55(0)	1.91(1)	1.52(3)	-9.30(-1)	-7.13(0)
10.000	-9.91(-6)	6.00(0)	1.95(2)	2.37(3)	-1.02(0)	-1.69(1)	1.96(3)	-1.02(0)	-3.73(0)
10.500	-5.91(4)	-6.00(0)	1.55(2)	8.17(2)	-4.24(-1)	-1.35(2)	2.45(3)	-1.09(0)	-1.57(0)
11.000	-3.88(-5)	5.24(0)	1.40(2)	7.94(2)	-1.48(-1)	-4.23(2)	1.68(3)	-9.66(-1)	-5.84(0)
11.500	-1.79(0)	1.36(0)	1.66(2)	5.38(2)	-2.88(-1)	-1.48(2)	9.77(2)	-7.88(-1)	-1.28(1)
12.500	-8.34(1)	4.12(-1)	3.51(2)	7.11(2)	-6.06(-1)	-3.72(1)	8.92(2)	-7.62(-1)	-1.35(1)
13.500	-4.90(2)	1.66(-1)	8.69(2)	1.07(3)	-7.94(-1)	-1.73(1)	1.03(3)	-8.08(-1)	-1.15(1)
14.000	-7.78(2)	1.28(-1)	1.20(3)	1.28(3)	-8.62(-1)	-1.27(1)	1.13(3)	-8.36(-1)	-1.05(1)
14.500	-7.47(2)	1.38(-1)	1.19(3)	1.40(3)	-8.94(-1)	-1.08(1)	1.19(3)	-8.50(-1)	-1.01(1)
15.000	-6.18(2)	1.64(-1)	1.07(3)	1.50(3)	-9.18(-1)	-9.58(0)	1.24(3)	-8.62(-1)	-9.66(0)
15.500	-4.56(2)	2.08(-1)	9.07(2)	1.59(3)	-9.38(-1)	-8.61(0)	1.28(3)	-8.72(-1)	-9.37(0)
16.500	-2.83(2)	2.90(-1)	7.28(2)	1.73(3)	-9.66(-1)	-7.26(0)	1.35(3)	-8.86(-1)	-8.97(0)
17.000	-1.82(2)	3.78(-1)	6.15(2)	1.82(3)	-9.82(-1)	-6.67(0)	1.40(3)	-8.96(-1)	-8.67(0)
17.500	-1.23(2)	4.66(-1)	5.41(2)	1.89(3)	-9.94(-1)	-6.18(0)	1.44(3)	-9.04(-1)	-8.42(0)
18.000	-7.98(1)	5.70(-1)	4.81(2)	1.95(3)	-1.00(0)	-6.07(0)	1.47(3)	-9.10(-1)	-8.28(0)
19.000	-3.52(1)	7.86(-1)	4.02(2)	2.02(3)	-1.01(0)	-6.14(0)	1.53(3)	-9.20(-1)	-8.01(0)
20.000	-9.86(0)	1.16(0)	3.30(2)	2.03(3)	-1.00(0)	-7.63(0)	1.61(3)	-9.34(-1)	-7.58(0)
25.000	-1.22(-1)	2.61(0)	2.37(2)	1.69(3)	-8.92(-1)	-2.02(1)	1.81(3)	-9.66(-1)	-6.71(0)
32.000	-7.27(-6)	6.00(0)	1.76(2)	9.38(2)	-5.44(-1)	-8.44(1)	2.13(3)	-1.01(0)	-5.72(0)
40.000	-2.93(4)	-5.18(0)	1.44(2)	1.19(3)	-9.20(-2)	-8.08(2)	1.86(3)	-9.52(-1)	-8.68(0)
50.000	-3.93(3)	-3.69(0)	1.35(2)	-7.38(2)	8.00(-2)	1.03(3)	1.52(3)	-8.72(-1)	-1.30(1)
60.000	-4.00(2)	-1.60(0)	1.39(2)	-9.44(1)	3.06(-1)	3.34(2)	1.54(3)	-8.62(-1)	-1.45(1)
80.000	8.63(1)	2.92(-1)	-6.76(1)	-4.07(-1)	1.48(0)	1.32(2)	1.36(3)	-7.90(-1)	-2.17(1)
100.000	1.71(0)	1.36(0)	2.87(1)	-1.90(-7)	5.41(0)	8.89(1)	6.85(2)	-4.68(-1)	-6.75(1)
150.000	3.93(-2)	2.35(0)	1.90(1)	-4.49(3)	-1.84(0)	7.12(1)	-2.26(-1)	1.29(0)	8.10(1)

Table 2.4 The coefficients a_1, b_1, c_1 of (ar^b+c) as a function of wavelength $\lambda(\mu m)$ for the fitting of the *extinction coefficient* in the terrestrial region .

$\lambda(\mu m)$	a_2	b_2	c_2	a_2	b_2	c_2	a_2	b_2	c_2
R_e :	2.5	to 12.5	μm	12.5	to 30	μm	30	to 60	μm
3.900	1.69(-1)	2.84(-1)	-2.17(-1)	6.57(-2)	4.66(-1)	-8.47(-2)	-1.68(0)	-1.64(-1)	1.20(0)
4.100	1.40(-1)	3.60(-1)	-1.90(-1)	1.44(-1)	3.40(-1)	-1.86(-1)	-1.55(0)	-3.58(-1)	7.30(-1)
4.300	1.50(-1)	4.04(-1)	-2.07(-1)	1.29(0)	8.80(-2)	-1.41(0)	-2.84(0)	-7.66(-1)	5.42(-1)
4.500	1.40(-1)	4.70(-1)	-1.93(-1)	-1.27(0)	-2.24(-1)	9.81(-1)	-8.65(0)	-1.29(0)	4.93(-1)
4.700	7.89(-2)	6.28(-1)	-1.08(-1)	-1.19(0)	-2.94(-1)	8.33(-1)	-1.15(1)	-1.41(0)	4.90(-1)
4.900	3.83(-2)	8.28(-1)	-4.42(-2)	-1.27(0)	-2.34(-1)	9.60(-1)	-8.50(0)	-1.28(0)	4.96(-1)
5.100	1.77(-2)	1.06(0)	-3.46(-3)	-1.39(0)	-1.92(-1)	1.10(0)	-6.49(0)	-1.16(0)	5.03(-1)
5.300	6.96(-3)	1.36(0)	2.61(-2)	-1.48(0)	-1.74(-1)	1.19(0)	-5.09(0)	-1.04(0)	5.13(-1)
5.400	3.68(-3)	1.57(0)	3.91(-2)	-1.50(0)	-1.74(-1)	1.19(0)	-4.41(0)	-9.76(-1)	5.20(-1)
5.500	2.29(-3)	1.73(0)	4.96(-2)	-1.35(0)	-2.30(-1)	9.83(-1)	-4.50(0)	-9.88(-1)	5.19(-1)
5.700	1.92(-3)	1.87(0)	1.16(-1)	-3.34(0)	-1.14(0)	5.09(-1)	-4.19(1)	-2.02(0)	4.82(-1)
5.900	9.32(-4)	2.07(0)	2.70(-1)	-1.59(3)	-3.99(0)	4.93(-1)	-1.15(-4)	1.15(0)	4.97(-1)
6.000	1.32(-4)	2.61(0)	3.96(-1)	-6.31(4)	-6.00(0)	5.02(-1)	3.19(-1)	-6.20(-1)	4.59(-1)
6.100	2.13(-3)	1.62(0)	3.72(-1)	-1.05(-11)	6.00(0)	5.02(-1)	4.34(-1)	-7.44(-1)	4.61(-1)
6.200	3.83(-2)	7.74(-1)	2.31(-1)	-6.06(-10)	4.87(0)	5.00(-1)	4.03(-1)	-7.22(-1)	4.57(-1)
6.300	3.56(-2)	8.60(-1)	1.74(-1)	-6.27(4)	-6.00(0)	4.93(-1)	1.82(-1)	-3.40(-1)	4.33(-1)
6.500	7.68(-3)	1.41(0)	1.63(-1)	-9.39(1)	-2.84(0)	4.87(-1)	-1.93(-12)	5.20(0)	4.82(-1)
6.700	2.28(-3)	1.83(0)	1.59(-1)	-2.36(1)	-2.12(0)	4.90(-1)	-6.01(6)	-6.00(0)	4.80(-1)
7.000	6.59(-4)	2.26(0)	1.67(-1)	-1.95(1)	-1.96(0)	4.91(-1)	-2.54(4)	-4.21(0)	4.80(-1)
7.100	2.80(-4)	2.56(0)	1.69(-1)	-1.79(1)	-1.87(0)	4.92(-1)	-2.77(3)	-3.47(0)	4.81(-1)
7.300	1.13(-4)	2.87(0)	1.72(-1)	-1.78(1)	-1.83(0)	4.93(-1)	-9.06(2)	-3.09(0)	4.82(-1)
7.600	2.67(-5)	3.38(0)	1.82(-1)	-2.00(1)	-1.84(0)	4.95(-1)	-5.94(2)	-2.93(0)	4.83(-1)
8.000	1.96(-6)	4.33(0)	1.96(-1)	-1.97(1)	-1.79(0)	5.01(-1)	-5.23(2)	-2.87(0)	4.85(-1)
8.600	1.91(-8)	6.00(0)	2.21(-1)	-1.40(1)	-1.59(0)	5.23(-1)	-1.45(3)	-3.18(0)	4.87(-1)
9.000	1.35(2)	-6.00(0)	2.47(-1)	-6.68(0)	-1.23(0)	5.66(-1)	-5.13(3)	-3.55(0)	4.89(-1)
9.600	2.69(-8)	5.93(0)	2.38(-1)	-1.55(1)	-1.69(0)	5.19(-1)	-4.70(4)	-4.33(0)	4.85(-1)
10.000	7.67(0)	-3.08(0)	2.96(-1)	-1.68(0)	-2.14(-1)	1.28(0)	-1.79(5)	-4.55(0)	4.96(-1)
10.500	1.70(0)	-1.50(0)	3.23(-1)	8.00(-3)	9.36(-1)	2.74(-1)	-6.31(4)	-4.19(0)	5.03(-1)
11.000	1.07(0)	-8.10(-1)	3.27(-1)	3.01(-8)	4.04(0)	4.57(-1)	-1.82(4)	-3.99(0)	5.05(-1)
11.500	9.80(-1)	-4.36(-1)	2.31(-1)	4.73(1)	-2.67(0)	5.07(-1)	-3.52(-4)	9.38(-1)	5.21(-1)
12.500	9.43(-1)	-3.90(-1)	2.32(-1)	1.96(0)	-1.16(0)	4.82(-1)	8.68(-1)	-8.10(-1)	4.64(-1)
13.500	8.57(-1)	-5.22(-1)	3.42(-1)	1.09(0)	-8.90(-1)	4.58(-1)	1.05(0)	-8.48(-1)	4.52(-1)
14.000	8.38(-1)	-6.18(-1)	3.88(-1)	8.47(-1)	-7.82(-1)	4.47(-1)	9.69(-1)	-8.14(-1)	4.45(-1)
14.500	8.36(-1)	-6.76(-1)	4.08(-1)	7.25(-1)	-7.08(-1)	4.39(-1)	9.26(-1)	-7.92(-1)	4.42(-1)
15.000	8.41(-1)	-7.32(-1)	4.25(-1)	6.30(-1)	-6.34(-1)	4.31(-1)	8.83(-1)	-7.68(-1)	4.39(-1)
15.500	8.53(-1)	-7.86(-1)	4.38(-1)	5.55(-1)	-5.60(-1)	4.21(-1)	8.43(-1)	-7.44(-1)	4.36(-1)
16.500	8.82(-1)	-8.72(-1)	4.55(-1)	4.70(-1)	-4.34(-1)	3.95(-1)	7.97(-1)	-7.12(-1)	4.32(-1)
17.000	9.18(-1)	-9.46(-1)	4.66(-1)	4.34(-1)	-3.24(-1)	3.59(-1)	7.58(-1)	-6.84(-1)	4.29(-1)
17.500	9.54(-1)	-1.01(0)	4.73(-1)	4.48(-1)	-2.24(-1)	2.94(-1)	7.25(-1)	-6.60(-1)	4.27(-1)
18.000	1.00(0)	-1.07(0)	4.80(-1)	6.34(-1)	-1.06(-1)	6.19(-2)	6.95(-1)	-6.36(-1)	4.24(-1)
19.000	1.10(0)	-1.17(0)	4.86(-1)	-2.97(-1)	1.08(-1)	9.35(-1)	6.35(-1)	-5.86(-1)	4.19(-1)
20.000	1.22(0)	-1.25(0)	4.88(-1)	-2.33(-2)	4.34(-1)	6.10(-1)	5.41(-1)	-4.94(-1)	4.08(-1)
25.000	1.39(0)	-1.23(0)	4.71(-1)	-8.04(-4)	1.05(0)	5.44(-1)	5.33(-1)	-1.28(-1)	1.71(-1)
32.000	1.38(0)	-9.68(-1)	4.13(-1)	6.00(4)	-6.00(0)	5.21(-1)	-1.42(-3)	8.88(-1)	5.51(-1)
40.000	1.27(0)	-5.24(-1)	2.35(-1)	1.18(2)	-3.02(0)	5.23(-1)	-2.62(-4)	1.22(0)	5.44(-1)
50.000	1.92(0)	-1.90(-1)	-5.67(-1)	9.23(0)	-1.75(0)	5.15(-1)	-9.94(-2)	2.04(-1)	7.38(-1)
60.000	-1.05(1)	2.40(-2)	1.18(1)	9.92(0)	-1.74(0)	5.15(-1)	-1.26(-1)	1.86(-1)	7.78(-1)
80.000	-3.03(-1)	4.12(-1)	1.49(0)	4.12(1)	-2.28(0)	5.18(-1)	-4.56(-4)	1.09(0)	5.54(-1)
100.000	-3.95(-2)	9.70(-1)	1.12(0)	3.91(1)	-2.12(0)	5.02(-1)	1.16(-1)	-3.16(-1)	4.91(-1)
150.000	-1.37(-3)	2.03(0)	1.01(0)	1.06(1)	-1.31(0)	4.12(-1)	1.62(7)	-6.00(0)	5.13(-1)

Table 2.5 The coefficients a_2, b_2, c_2 of (ar^b+c) as a function of wavelength $\lambda(\mu m)$ for the fitting of the *co-albedo* in the terrestrial region .

$\lambda(\mu m)$	a_3	b_3	c_3	a_3	b_3	c_3	a_3	b_3	c_3
R_e :	2.5	to 12.5	μm	12.5	to 30	μm	30	to 60	μm
3.900	3.90(-8)	5.68(0)	7.74(-1)	-6.01(-1)	-4.78(-1)	1.01(0)	-6.42(-1)	-4.50(-1)	1.03(0)
4.100	1.25(-8)	6.00(0)	7.88(-1)	-8.16(-1)	-6.62(-1)	9.86(-1)	-8.09(-1)	-5.84(-1)	1.01(0)
4.300	9.54(-9)	6.00(0)	8.04(-1)	-1.23(0)	-8.54(-1)	9.84(-1)	-1.50(0)	-8.82(-1)	9.91(-1)
4.500	7.39(-9)	6.00(0)	8.21(-1)	-1.94(0)	-1.07(0)	9.84(-1)	-3.76(0)	-1.28(0)	9.81(-1)
4.700	1.75(1)	-4.88(0)	8.27(-1)	-2.34(0)	-1.13(0)	9.84(-1)	-4.67(0)	-1.36(0)	9.80(-1)
4.900	1.72(0)	-3.05(0)	8.24(-1)	-2.36(0)	-1.11(0)	9.84(-1)	-3.80(0)	-1.27(0)	9.82(-1)
5.100	2.80(-1)	-1.51(0)	8.17(-1)	-2.20(0)	-1.06(0)	9.88(-1)	-3.20(0)	-1.19(0)	9.84(-1)
5.300	-6.52(-1)	4.00(-2)	1.55(0)	-1.77(0)	-9.28(-1)	1.00(0)	-2.82(0)	-1.13(0)	9.87(-1)
5.400	-4.16(-3)	9.86(-1)	8.76(-1)	-1.41(0)	-7.94(-1)	1.02(0)	-2.68(0)	-1.10(0)	9.88(-1)
5.500	-4.37(-4)	1.76(0)	8.67(-1)	-1.15(0)	-6.66(-1)	1.05(0)	-2.99(0)	-1.14(0)	9.88(-1)
5.700	-5.23(1)	-6.00(0)	8.75(-1)	-1.14(0)	-7.46(-1)	1.04(0)	-1.64(1)	-1.86(0)	9.78(-1)
5.900	-9.70(-1)	-2.10(0)	9.23(-1)	-1.75(0)	-1.24(0)	9.93(-1)	-7.22(1)	-2.64(0)	9.76(-1)
6.000	-5.59(-1)	-1.36(0)	9.59(-1)	-2.36(0)	-1.63(0)	9.79(-1)	-7.59(0)	-2.13(0)	9.75(-1)
6.100	-4.23(-1)	-1.04(0)	9.67(-1)	-5.93(0)	-2.02(0)	9.73(-1)	-3.65(0)	-1.92(0)	9.72(-1)
6.200	-3.36(-1)	-4.00(-1)	1.05(0)	-1.78(1)	-2.39(0)	9.67(-1)	-3.95(0)	-1.94(0)	9.68(-1)
6.300	-3.84(-1)	-2.18(-1)	1.13(0)	-1.79(1)	-2.26(0)	9.69(-1)	-1.63(1)	-2.30(0)	9.67(-1)
6.500	-6.21(-1)	-1.90(0)	8.83(-1)	-5.65(0)	-1.59(0)	9.82(-1)	-7.50(1)	-2.55(0)	9.69(-1)
6.700	-1.88(1)	-4.55(0)	8.67(-1)	-2.49(0)	-1.14(0)	1.00(0)	-8.29(1)	-2.46(0)	9.71(-1)
7.000	-4.02(1)	-5.00(0)	8.69(-1)	-1.15(0)	-7.08(-1)	1.05(0)	-7.77(1)	-2.38(0)	9.72(-1)
7.100	-4.01(1)	-4.93(0)	8.71(-1)	-8.21(-1)	-4.06(-1)	1.15(0)	-7.41(1)	-2.33(0)	9.73(-1)
7.300	-2.79(1)	-4.58(0)	8.74(-1)	-1.43(0)	-8.80(-2)	2.01(0)	-7.32(1)	-2.29(0)	9.74(-1)
7.600	-1.34(1)	-3.92(0)	8.80(-1)	9.07(-2)	3.50(-1)	6.46(-1)	-8.13(1)	-2.30(0)	9.75(-1)
8.000	-6.30(0)	-3.21(0)	8.89(-1)	3.98(-3)	9.94(-1)	8.26(-1)	-9.01(1)	-2.30(0)	9.76(-1)
8.600	-3.17(0)	-2.50(0)	9.05(-1)	1.09(-4)	1.88(0)	8.78(-1)	-9.10(1)	-2.28(0)	9.78(-1)
9.000	-2.30(0)	-2.11(0)	9.20(-1)	4.55(-6)	2.68(0)	9.00(-1)	-6.16(1)	-2.15(0)	9.81(-1)
9.600	-3.24(0)	-2.44(0)	8.84(-1)	8.45(-3)	8.12(-1)	8.04(-1)	-1.01(2)	-2.33(0)	9.72(-1)
10.000	-1.84(0)	-1.71(0)	9.47(-1)	8.52(-5)	1.74(0)	9.17(-1)	-7.45(0)	-1.53(0)	9.88(-1)
10.500	-1.76(0)	-1.55(0)	9.72(-1)	-2.24(-1)	-5.46(-1)	9.94(-1)	-7.39(-1)	-8.40(-1)	1.00(0)
11.000	-1.85(0)	-1.50(0)	9.82(-1)	-1.16(0)	-1.33(0)	9.82(-1)	-4.65(-1)	-8.54(-1)	9.94(-1)
11.500	-2.02(0)	-1.50(0)	9.84(-1)	-1.78(0)	-1.46(0)	9.83(-1)	-1.27(0)	-1.31(0)	9.86(-1)
12.500	-2.24(0)	-1.50(0)	9.75(-1)	-2.12(0)	-1.48(0)	9.74(-1)	-2.06(0)	-1.46(0)	9.75(-1)
13.500	-2.40(0)	-1.48(0)	9.63(-1)	-2.30(0)	-1.48(0)	9.61(-1)	-2.32(0)	-1.47(0)	9.61(-1)
14.000	-2.46(0)	-1.46(0)	9.57(-1)	-2.41(0)	-1.47(0)	9.54(-1)	-2.51(0)	-1.48(0)	9.54(-1)
14.500	-2.51(0)	-1.44(0)	9.54(-1)	-2.51(0)	-1.47(0)	9.50(-1)	-2.69(0)	-1.48(0)	9.50(-1)
15.000	-2.53(0)	-1.42(0)	9.52(-1)	-2.62(0)	-1.46(0)	9.46(-1)	-2.89(0)	-1.49(0)	9.46(-1)
15.500	-2.56(0)	-1.40(0)	9.51(-1)	-2.73(0)	-1.46(0)	9.43(-1)	-3.10(0)	-1.50(0)	9.43(-1)
16.500	-2.57(0)	-1.35(0)	9.51(-1)	-2.92(0)	-1.46(0)	9.39(-1)	-3.49(0)	-1.52(0)	9.39(-1)
17.000	-2.58(0)	-1.32(0)	9.52(-1)	-3.06(0)	-1.45(0)	9.37(-1)	-3.84(0)	-1.53(0)	9.36(-1)
17.500	-2.57(0)	-1.29(0)	9.53(-1)	-3.16(0)	-1.44(0)	9.36(-1)	-4.15(0)	-1.54(0)	9.34(-1)
18.000	-2.56(0)	-1.26(0)	9.55(-1)	-3.25(0)	-1.44(0)	9.35(-1)	-4.53(0)	-1.56(0)	9.33(-1)
19.000	-2.53(0)	-1.21(0)	9.61(-1)	-3.36(0)	-1.42(0)	9.35(-1)	-5.26(0)	-1.58(0)	9.32(-1)
20.000	-2.51(0)	-1.15(0)	9.71(-1)	-3.39(0)	-1.37(0)	9.37(-1)	-6.63(0)	-1.62(0)	9.31(-1)
25.000	-2.38(0)	-9.36(-1)	1.03(0)	-3.29(0)	-1.24(0)	9.44(-1)	-1.20(1)	-1.71(0)	9.30(-1)
32.000	-2.27(0)	-5.48(-1)	1.32(0)	-3.79(0)	-1.16(0)	9.49(-1)	-1.57(1)	-1.67(0)	9.31(-1)
40.000	-7.79(1)	-6.00(-3)	7.75(1)	-6.69(0)	-1.29(0)	9.38(-1)	-1.24(1)	-1.50(0)	9.32(-1)
50.000	2.73(-1)	5.40(-1)	-4.70(-1)	-8.99(0)	-1.29(0)	9.31(-1)	-1.59(1)	-1.49(0)	9.17(-1)
60.000	7.07(-2)	8.84(-1)	-1.65(-1)	-7.52(0)	-1.10(0)	9.47(-1)	-2.02(1)	-1.48(0)	9.00(-1)
80.000	2.47(-2)	1.15(0)	-7.20(-2)	-4.07(0)	-6.80(-1)	1.10(0)	-1.66(1)	-1.29(0)	9.02(-1)
100.000	7.53(-3)	1.48(0)	-2.62(-2)	-3.12(0)	-2.98(-1)	1.75(0)	-1.07(1)	-1.03(0)	9.32(-1)
150.000	9.87(-4)	1.99(0)	-6.72(-4)	1.89(1)	1.80(-2)	-1.97(1)	-4.38(0)	-5.46(-1)	1.14(0)

Table 2.6 The coefficients a_3, b_3, c_3 of (ar^b+c) as a function of wavelength $\lambda(\mu m)$ for the fitting of the *asymmetry factor* in the terrestrial region .

2.3 Accuracy of Radiative Fluxes, Heating and Cooling Rates

In order for the paramerization to be useful for climate studies, it is important that it accurately predicts the cloud forcing, which is usually defined as the difference in radiative fluxes and/or heating rates between an atmosphere with clouds and the clear sky case.

Using the comprehensive multiple scattering code developed by Stamnes *et al.* (1988) and the cloud-atmosphere radiation model of Tsay *et al.* (1989), we have compared the cloud forcing (both heating rates and fluxes) obtained from our present parameterization (both for regular and higher spectral resolution) of cloud optical properties with that resulting from the exact Mie calculations, as well as from the linear parameterization valid for equivalent radii between 4 and 12 μm (Tsay *et al.*, 1989).

The lower panel of Figure 2.6 shows the net solar fluxes (cloud forcing) obtained from Mie calculations and from the three kinds of parameterizations, as well as the clear-sky atmosphere. The cloud layer is placed at an altitude between 5 km and 5.1 km (549 mb to 554 mb) with an equivalent radius of 8.00 μm and liquid water content of 0.1 g/m^3. We used a solar zenith angle of 45^o in this calculation. The difference between net fluxes obtained from our present parameterizations and from the Mie calculation are less than 0.5 W/m^2, which is much less than 1% of the cloud forcing and the new parameterization is significantly more accurate than the linear parameterization. The differences of cloud forcings in heating rates between the parameterization and exact Mie computation are less then 2% of the total solar cloud forcing.

For infrared radiation (Figure 2.7), the differences of radiative fluxes calculated

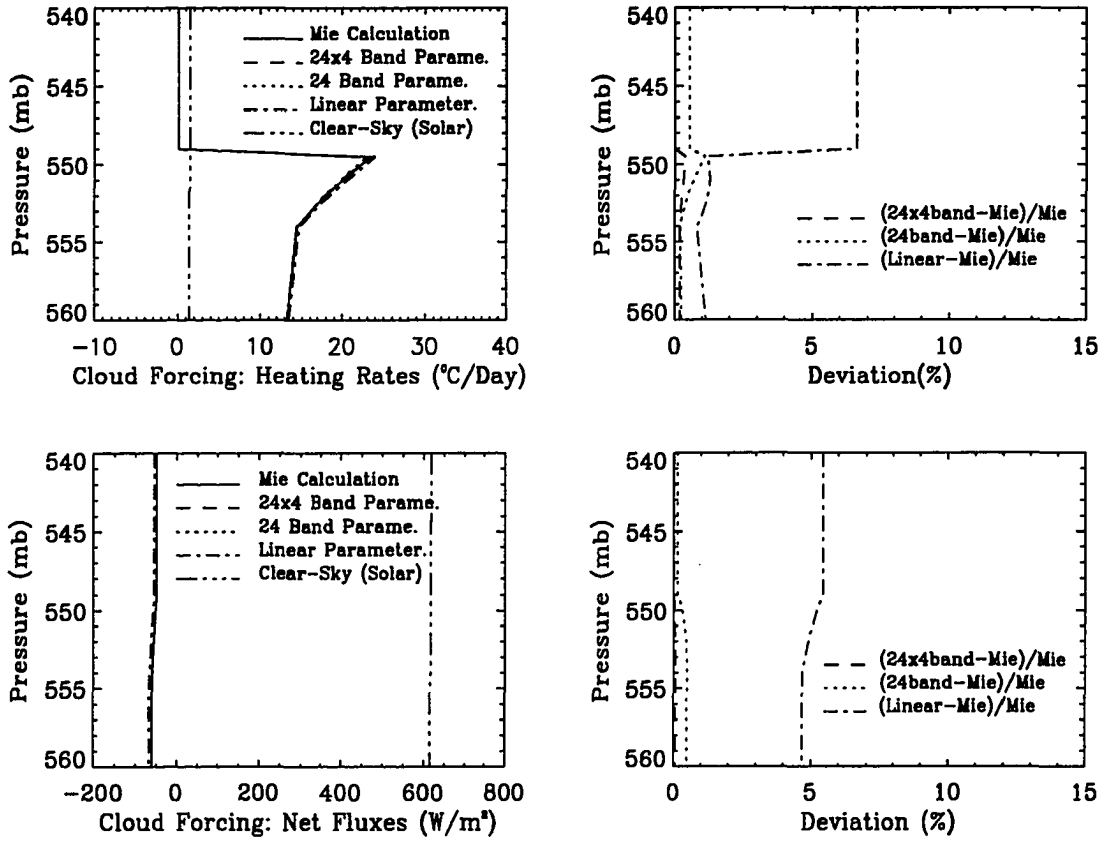

Figure 2.6 The left panels are the heating rates and the net fluxes due to cloud forcing (cloudy sky - clear sky) for solar radiation as a function of pressure in the atmosphere, using the different cloud parameterizations for cloud effective radius of 8 μm. The solid curve is from the Mie calculation and the dashed curve (indistinguishable from the solid curve) is for our new parameterization with 24 × 4 bands. The dotted curve is for our new parameterization with 24 bands. The chain-dotted curve is for the linear parameterization. The clear sky background radiation is also given. The right panels show the differences between the parameterizations and the Mie calculation.

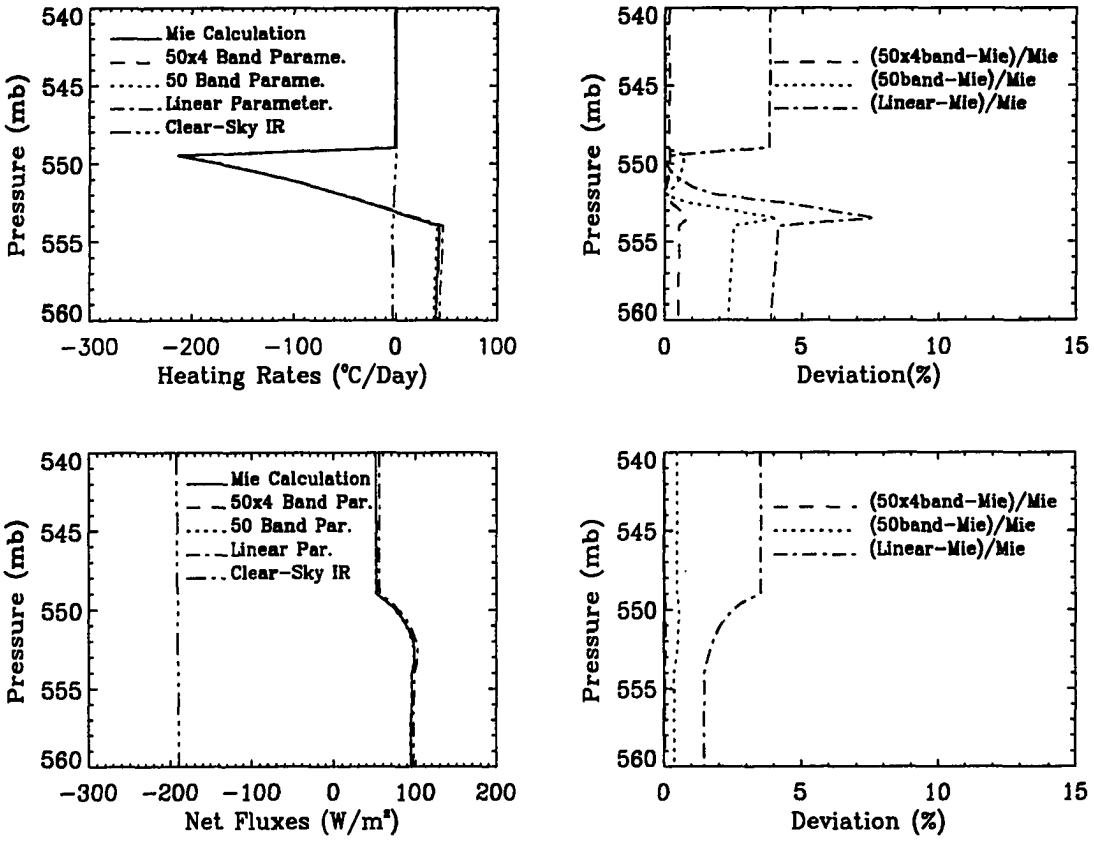

Figure 2.7 The left panels are the heating rates and the net fluxes due to cloud forcing (cloudy sky - clear sky) for terrestrial radiation as a function of pressure in the atmosphere, with the different cloud parameterizations for cloud effective radius of 8 μm. The solid curve is from the Mie calculation and the dashed curve (indistinguishable from the solid curve) is for our new parameterization with 50 × 4 bands. The dotted curve is for our new parameterization with 50 bands. The chain-dotted curve is for the cloud parameterization by Tsay *et al.* The clear sky background radiation is also given. The right panels show the differences between the parameterizations and the Mie calculation..

from the present parameterizations and the Mie calculation are less than 1%. The error for the cooling rates is within 4% of the total terrestrial cloud forcing.

The accuracy of the cloud forcing from the parameterization using the coarser spectral resolution (24 bands in solar and 50 in infrared) is not as good as that obtained from the parameterization using the 4-times higher resolution. From Figure 2.6 and Figure 2.7, the differences of the cloud forcing between the Mie calculation and the parameterization with the regular spectral resolution are about 5 times larger than those obtained with the 4-times higher resolution. From Figure 2.6 and Figure 2.7, it is also clear that the accuracy of the present parameterization with the coarser resolution is much better than the accuracy obtained with the linear parameterization.

2.4 Summary of the Chapter

A new parameterization of water cloud optical properties has been presented. This parameterization is valid for equivalent radii in the range from 2.5 μm to 60 μm and pertains to shortwave as well as longwave radiation. The parameterization yields very accurate heating and cooling rates. For the study of the feedback mechanism of cloud microphysics and climate, this parameterization will be reliable.

We find that there is a unique relation between cloud radiative properties and the equivalent radius in both the shortwave and the longwave regions. This relationship is insensitive to the the details of the drop size distribution, such as shape, width and skewness. Moreover, single-mode and bi-modal distributions with the same equivalent radius yield essentially identical optical properties. Although our results are based on the use of the generalized gamma distribution, we expect the parameterization to be generally valid and to mimic the radiative properties of actual cloud droplet distributions occurring in nature. In fact, calculations with

the lognormal distribution yielded results very similar to those for the generalized gamma distribution. This is in agreement with expectations on physical grounds for large size parameters for which the extinction efficiency asymptotes to 2. This unique dependence of cloud optical properties on equivalent radius has important theoretical and experimental implications. From a climate modeling point of view it implies that only the second and the third moments of the size distribution are required in cloud models designed to predict the evolution of cloud microphysics with climate change. Experimentally, it implies that it is not necessary to measure the full size distribution to obtain the optical properties of clouds. It is sufficient to measure only the liquid water content and the extinction coefficient at a few wavelength in the visible part of the spectrum.

The new parameterization is almost as accurate and more than thousands of times faster than "exact" Mie calculations. We expect that it might be feasible to parameterize the optical properties of various kinds of atmospheric aerosols and ice clouds using a procedure similar to the one described here. The separation of the dependence of radiative properties on cloud equivalent radius and liquid water content is an important aspect of our parameterization that is expected to be very useful for climate sensitivity studies involving cloud-radiation-climate interactions and feedback mechanisms.

Chapter 3

A New Radiative-Convective Model

This chapter describes a new one dimensional radiative-convective model. The aim of this model is to study the effect of clouds on climate. With a comprehensive radiative transfer model, an accurate parameterization of cloud optical properties and an improved lower boundary energy balance condition, this model is capable of simulating not only the temperature profile but also the radiative energy budget of the Earth on climate scale and their responses to the changes in solar constant, atmospheric composition (e. g., the CO_2 concentration) and clouds.

3.1 Introduction

The global, long term average temperature of the Earth's atmosphere should approach a radiative equilibrium. But because the absorption of solar radiation is very strong at the surface of the Earth, the temperature gradient of the lower atmosphere in such an equilibrium is large and the atmosphere becomes convectively unstable. The convection brings sensible heat and latent heat up through the at-

mosphere and warms the lower part of the atmosphere (troposphere). As a result, the radiative equilibrium can never be achieved: there will be a net radiative cooling in the atmosphere and a net radiative warming at the Earth's surface. Such a convective instability prevents the static radiative equilibrium and generates the general circulation, water vapor transfer, clouds and precipitation which, together, constitute our climate.

Unfortunately, we are still unable to understand quantitatively such a radiatively and convectively balanced state of the climate. The main problem are concerned with the fact that the evaporation, transport, condensation and precipitation processes are so complex that we have to 'tune' our cumulus convective models (e. g. Kuo, 1974; Arakawa and Shubert, 1974; Emanual, 1991) to match the observations; the scale of cloud microphysical processes is so small that we have to parameterize them before they can be incorporated into climate models. The climate modeling result is very sensitive to the way one treats the water cycle. Assessments of cloud-climate interaction can be made only after careful senstivity studies.

A simple model which treats both the radiative transfer and the convection simply and accurately has been developed to help us understand the physics involved. We use a comprehensive radiative transfer model developed by Stamnes et al. (1988) and Tsay et al. (1989) to calculate the radiative energy fluxes and heating rates. Accurate parameterizations of cloud optical properties (Hu and Stamnes, 1993; Fu and Liou, 1993) are used for the radiative transfer calculations involving clouds. We use the pseudoadiabatic lapse rate as the "critical" lapse rate for convective adjustment. At the Earth's surface, the net incoming solar radiation is larger than the net outgoing infrared radiation. The total net radiative heating at the surface will be balanced by the sensible heat exchange and latent heat release. The temperature profile, precipitable water, total evaporation rate

and the planetary albedo estimated from this model are very close to those of the real climate of the Earth.

3.2 Model Structure

The model simulates the equilibrium temperature profile of the atmosphere through time stepping. Given an arbitrary initial temperature profile, for each time step, the radiative transfer equation is solved to derive the radiative heating rates (calculated from mean radiative intensity or radiative flux divergence) of each layer; if the temperature between any two adjacent layers after the radiative effects is convectively unstable, a convective adjustment is performed. This time stepping is carried out until the differences of the temperature between adjacent time steps for each layer are very close to zero. In this equilibrium (or steady) state, the net outgoing longwave radiation must equal the net incoming solar radiation at the top of the atmosphere.

A flow chart of the model is available from Appendix A of the thesis.

3.3 Radiative Transfer Talculations

In radiative fluxes and heating rates calculations, we consider absorption by the major radiatively-active atmospheric gases including water vapor, carbon dioxide, ozone and oxygen, absorption and scattering by clouds and molecular scattering. We use the atmosphere gas compositions from the U.S. Standard Atmosphere tables. Clouds are prescribed by cloud top height, cloud thickness, cloud water amount (gram per square meter), and cloud equivalent radius. The atmosphere is divided into 24 layers in which absorption and scattering properties are taken to be constant within each layer. Clouds can be put in any layer as long as the water

amount and equivalent radius are defined. For the sake of computational stability in time stepping, the atmosphere is isothermal within each layer to prevent the oscillation of the heating rates resulted from accumulated errors in the linear-in-depth thermal emission. The global average surface albedo for the shortwave radiation is assumed to be 0.2.

To solve the radiative transfer equation, we reduce the integration over frequency to a series of monochromatic problems through the exponential sum fitting of transmissions (ESFT) technique (Tsay et al., 1989). The solar radiation spectrum between 0.28 micron and 4 micron is divided into 24 bands. The thermal infrared radiation spectrum between 4 micron and 150 micron is divided into 50 bands. The cloud optical properties are parameterized over each individual band (Hu and Stamnes, 1993). We adopt the discrete ordinate approximation of Stamnes et al. (1988) to solve each monochromatic radiative transfer problem. The surface albedo is fixed at 0.2 for all the solar radiation wavelengths.

3.4 Convective Adjustments and the Lower Boundary Condition

Unlike the radiative transfer calculations, the convective processes cannot easily be considered as a one-dimensional process and must be modeled by some empirical or semi-empirical method to be incorporated into the one-dimensional model. The empirical methods are generally divided into two types: the lapse-rate adjustment and the so-called "physical parameterization of convection".

The lapse-rate adjustment methods are widely used in one-dimensional models (Manabe and Strickler, 1964; Ramanathan and Coakley, 1978; Hummel and Kuhn, 1981). The idea is to adopt an externally specified lapse rate, such as

the observational lapse rate (6.5 K/km), the moist-adiabatic lapse rate and the phseudo-adiabatic lapse rate. The scheme effectively cools the surface and redistributes heat vertically, while requiring that the total "convective heating" induced by adjustment processes be equal to the net radiative deficit at the ground. The radiative-convective equilibrium temperatures at every atmospheric layer are balanced by radiative cooling and the "convective heating" implied by the adjustment of lapse rates.

The so-called "physical parameterization of convection" are also called cumulus convection schemes, such as the Kuo scheme (1965, 1974), the Arakawa - Shubert scheme (1974) and the Emanuel scheme (1991). Instead of using the convective instability criteria and total energy conservation as the convective adjustment, these schemes parameterize the different individual physical processes such as sensible heat exchange and latent heat exchange, adjusting the aerodynamic drag coefficient, entrainment and detrainment, precipitation rate (percentage of precipitation to the total condensation, surface wind speed) to match the observational cumulus convection processes. Although these schemes are similar in principle, there are some differences in the detailed physics.

The Kuo scheme assumes that cumulus convection occurring in deep layers of unstable stratification is maintained by moisture supply due to large-scale convergence and evaporation from the surface. It also assumes that cumulus cloud air dissolves into the large scale environment at the same rate as it is generated by the moisture supply. A large part of the moisture supplied into a cloud through its base and sides condenses during its ascent and the precipitation is responsible for the net convective heating of the column. A disposable parameter has been introduced to decide the precipitation rate.

The Arakawa - Schubert scheme divides convection into three types: middle-level convection, penetrative convection and low-level convection. Each cloud en-

trains environmental air through its bases and through its sides, and detrains cloud air at its upper level. The environment is modified by detrainment of moisture through the cloud top and compensating subsidence within the cloud, which warms and dries the atmosphere. An entrainment parameter has to be defined to determine the entrainment and detrainment. The Emanuel scheme assume that the fundamental entities in cumulus convection are sub-scale drafts rather than the clouds themselves. Convection occurs when the environment is unstable to a parcel in reversible adiabatic ascent from the surface. Vertical transports are accomplished by saturated updrafts, downdrafts, by a single unsaturated downdraft driven by evaporation of falling precipitation, and by compensating subsidence. The main closure parameters are precipitation efficiency, which is the fraction of the precipitation that falls through unsaturated air, and the rate of evaporation from the falling rain drops.

The above schemes approach the convection from a three dimensional point of view. The entrainment and detrainment requirement makes these schemes difficult to include in a one-dimensional model. It is very difficult to obtain the closure parameters within 1-D models if they are time dependent. These schemes are designed for the interaction of cloud microphysical processes and the synoptic scale motion, for which the role of the radiation is not a major concern.

From a one-dimensional point of view, the physics of the convection in the atmosphere is very simple: when an air parcel is lifted adiabatically by natural perturbation, its pressure will decrease. Then the temperature will decrease because some of the internal energy will be consumed by the expansion. If the temperature of the air parcel after expansion is still larger than the temperature of the environment, the density of the air mass will be smaller than that of the environment and the air parcel will move upward again. So the convection happens when the lapse rate is large enough. When the temperature of the air parcel de-

creases, some water vapor condenses. The latent heat release within the air parcel heats it. This makes convection easier to happen.

In the absence of diabatic forcing such as radiative heating and frictional damping, the upward motion of the air parcel satisfies the adiabatic equation

$$\Delta Q = C_p \Delta T - \frac{RT}{P}\Delta P - \frac{L_v RT}{P}\Delta r = 0 \tag{3.1}$$

where C_p is the heat capacity of the air, T is the temperaure, P is the pressure and L_v is the latent heat released from the water vapor condensation. R is the gas constant for the air and r is the water vapor mixing ratio.

Q can not serve as a potential function as it is not a total differential unless it is divided by temperature T.

$$\frac{\Delta Q}{T} = C_p \Delta(lnT) - R\Delta(lnP) - \frac{L_v R}{P}\Delta r. \tag{3.2}$$

The right side of the above equation is a total differential for the so-called 'pseudo-adiabatic' processes. Thus, a potential temperature Θ_{se} can be defined as

$$\Theta_{se} = T(\frac{P_0}{P})^{R/C_p} exp(\frac{L_v r}{C_p P}). \tag{3.3}$$

Consider two adjacent layers with temperature and pressure T_u, P_u for the upper layer and T_l, P_l for the lower layer. An air parcel is lifted from the lower layer to the upper layer. If the potential temperature $\Theta_{se,u} < \Theta_{se,l}$, the temperature of the air parcel will be larger then T_u and the convection will happen in these two layers until $\Theta_{se,u} = \Theta_{se,d}$. The total static energy $C_p T + L_v r + gz$ is conserved during the convection if the convection starts from a layer.

The lower atmosphere is always convectively unstable because the net radiative heating of the surface and the net radiative cooling of the atmosphere keep the Θ_{se} of the lower atmosphere smaller than the Θ_{se} of the surface. The convective

adjustment brings energy from the surface to the atmosphere until the Θ_{se} of the lower atmosphere and the surface are equal. After the convective adjustment, for the climate of the Earth, the convection starts from the lower surface and extends to the tropopause. The convectively adjusted temperature T of each layer in the troposphere can be calculated if the surface temperature T_0 is determined by solving the equation

$$T(\frac{P_0}{P})^{R/C_p}exp(\frac{L_v r}{C_p P}) = T_0 exp(\frac{L_v r}{C_P P_0}). \tag{3.4}$$

The calculation of the temperature profile for the convective adjustment can be reduced to determining the temperature at the Earth's surface where the radiative energy deficit should balance the convective heat exchange.

As a global average, the lower level horizontal convergence and divergence cancel each other and the energy for convection comes from the total net heating from the surface (Schneider 1972). The convective engergy flux (including both sensible and latent heat exchanges) and the radiative energy flux at the Earth's surface are balanced. This convective energy coming from the surface will heat the atmosphere and eventually cancel the net radiative cooling of the atmosphere at the radiative-convective equilibrium state.

The implied small-scale convective energy flux for each layer of the atmosphere at a given time step Q_c can be defined as (Lindzen 1982)

$$Q_c = \rho C_p \Delta P \frac{(T - T_r)}{\Delta t} \tag{3.5}$$

where ρ is the density of the air, T_r is the instantaneous temperature profile determined by radiation alone, and T is the temperature profile after the convective adjustment. T can be calculated if the surface temperature is known, and Δt is the size of the time step. Since it is stipulated in the adjustment process that

no temperature discontinuity should exist and that there is no heat exchange at the ground, the vertical integral of Q_c over the convective region in the whole troposphere ($\sum Q_c$) must balance the radiative deficit at the surface.

At each time step, the surface temperature can be calculated by solving the energy balance equation at the surface

$$\sum Q_c = F_{net} \tag{3.6}$$

where F_{net} is the net radiative flux at the surface. The temperature profile of the entire troposphere can be calculated from $\Theta_{se}(T, P) = \Theta_{se}(T_0, P_0)$.

3.5 Model Validation

Temperature profile, planetary albedo, globally averaged evaporation rate (or precipitation rate), column water vapor amount (or the so-called precipitable water), cloud solar radiative forcing and cloud infrared radiative forcing calculated from the model are compared with the available knowledge of climate. It is not difficult to simulate just the temperature profile by tuning the cloud height, water amount or equivalent radius. The temperature profiles are the only validated output from previous radiative - convective models. It is neccessary to check the model result for all the above variables.

3.5.1 Temperature Profile

Figure 3.1 and Figure 3.2 are examples of the time stepping of the temperature profile. We adopt the U.S. Standard Atmosphere green house gas composition here. Three cloud layers are included: a. high clouds with cloud top height at 7 km, cloud water amount about $3g/m^2$, cloud droplet equivalent radius $10\mu m$; b. mid-

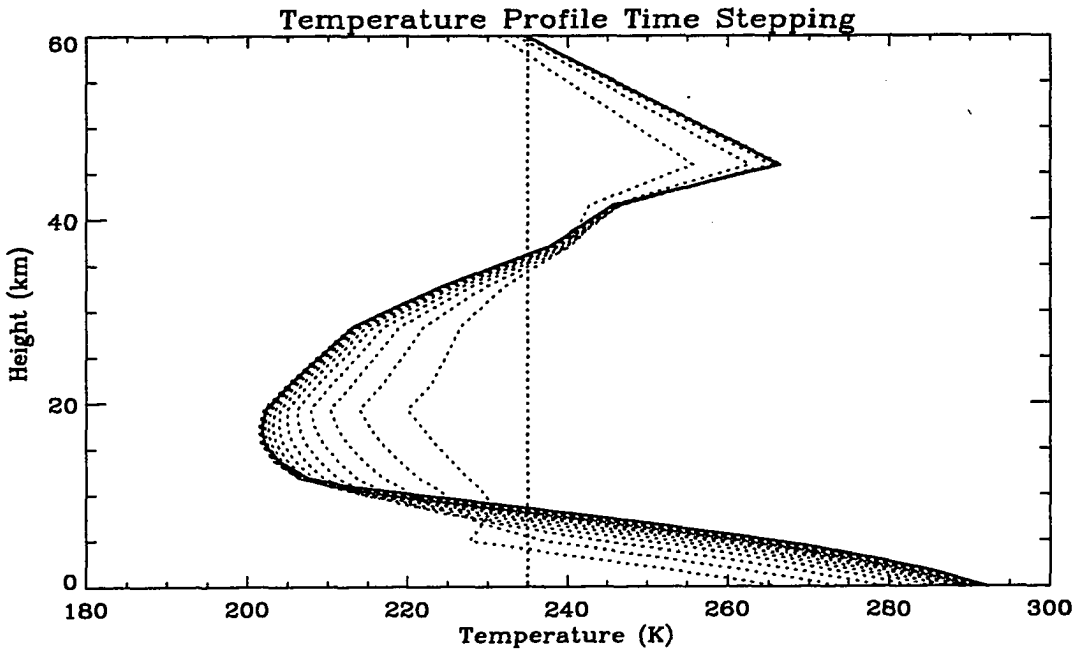

Figure 3.1 Time Stepping of Temperature Profiles I. The Initial temperature is 235K for every layer. The equilibrium state is the solid line.

level cloud with cloud top height at 4 km, cloud water amount about $8g/m^2$, cloud equivalent radius $7\mu m$; c. Low cloud with cloud top height at 2 km, cloud water amount about $10g/m^2$, cloud equivalent radius $7\mu m$. The initial temperatures of each layer for Figure 3.1 are 235K and the initial temperatures of each layer for Figure 3.2 are 280K. The equilibrium temperature profiles in Figure 3.1 and Figure 3.2 are the same. The model is not sensitive to the initial temperature profile.

Figure 3.3 is the comparison between the temperature profile calculated from the one dimesional radiative - convective model and the U.S. Standard atmosphere temperature profile. The two temperature profiles are close.

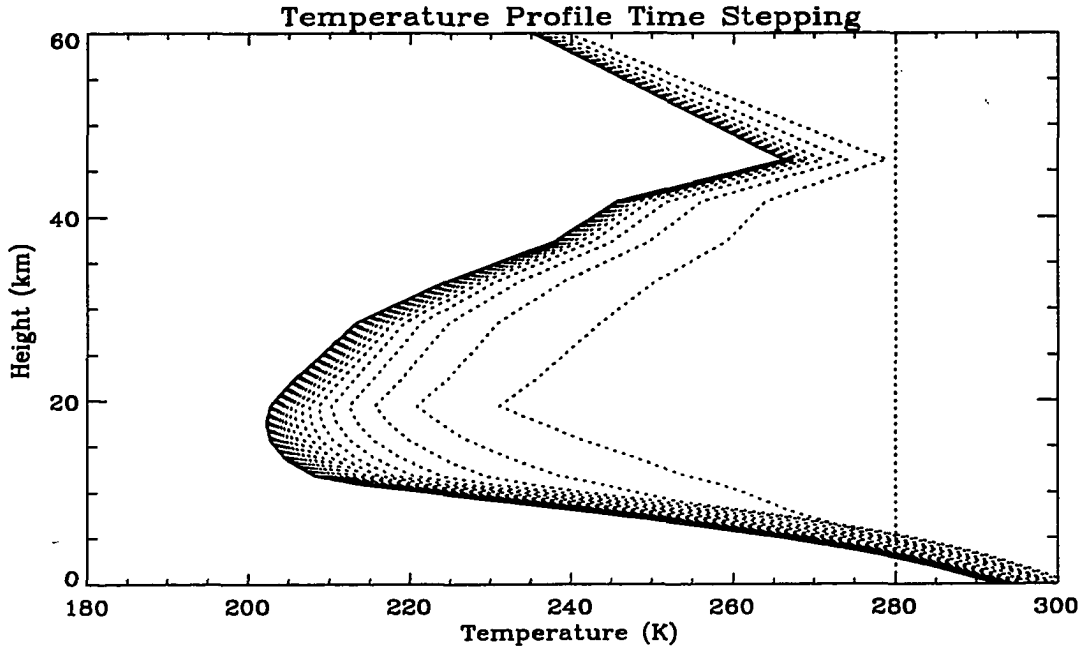

Figure 3.2 Time Stepping of Temperature Profiles II. The Initial temperature is 280K for every layer. The equilibrium state is the solid line.

3.5.2 The Radiative Fluxes and the Planetary Albedo

The net radiative fluxes for both the solar region and thermal infrared region at the equilibrium state are shown at Figure 3.4. The net outgoing thermal infrared radiation and the net incoming solar radiation at the top of the atmosphere are balanced. The annual global average net incoming solar radiation F_{net} is 239 W/m^2. This implies that the planetary albedo A_s is about 0.3

$$A_s = 1.0 - \frac{F_{net} \times 4\pi R^2}{1370 \times \pi R^2} \approx 0.3$$

For each level in the middle and upper atmosphere (12 kilometer and up), the incoming solar radiation and outgoing infrared radiation have the same magnitude. The heating of the atmosphere by solar radiation cancels the cooling from thermal infrared radiation for each layer above the tropopause. These layers are in radiative

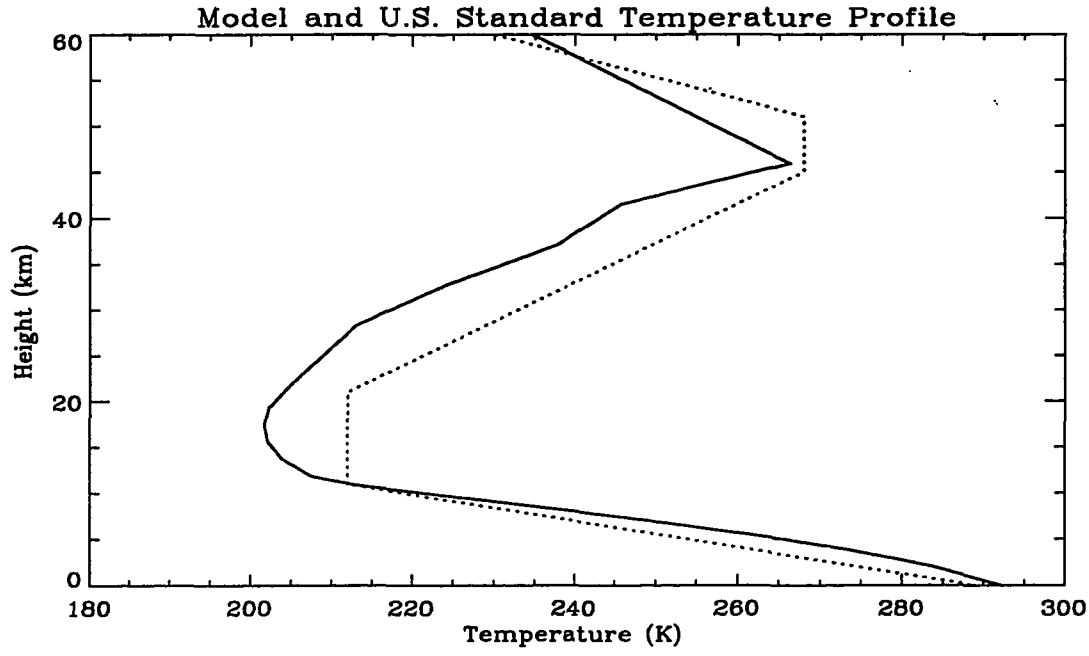

Figure 3.3 The comparison of the model output temperature profile (solid curve) with the U.S. Standard Atmosphere temperature profile (dotted curve). The small differences in the upper atmosphere are due to the model resolution.

equilibrium.

In the troposphere, the flux divergence of thermal infrared radiation is larger than flux convergence of solar radiation in each layer. These layers have a net radiative cooling effect. The atmosphere should move toward radiative equilibrium and the surface temperature should be higher if the convective instability did not exist. The convection prevents the surface temperature from getting too high, creates a net radiative heating at the ground and transports the excessive energy to the atmosphere through sensible and latent heat exchange, which balances the net radiative cooling of the lower atmosphere.

The net radiative fluxes at the ground (net downward solar radiation - net upward infrared radiation at the ground) is about 170 W/m^2. It equals the total convective fluxes (latent heat flux + sensible heat flux) as the excessive radiative

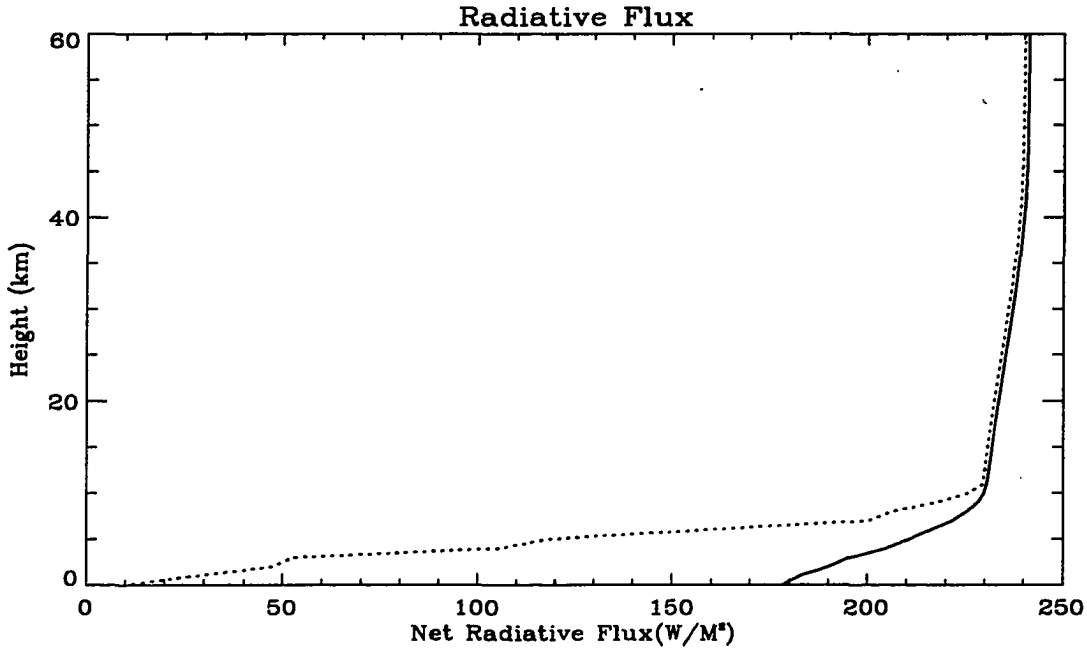

Figure 3.4 The net incoming solar fluxes (solid line) and the net outgoing thermal radiation fluxes (dashed line) in all levels at the equiblibrium state.

energy of the surface is transported to the troposphere by convection.

3.5.3 The Globally Averaged Precipitation Rate

The globally averaged precipitation rate can be estimated if the latent heat energy flux at the surface is available. The total convective fluxes (sensible heat + latent heat exchange at the surface) at the radiative-convective equilibrium state equals the net radiative flux at the surface. The latent heat flux F_l and sensible heat flux F_s are (Lindzen 1982)

$$F_l = C_D u_* L_v [q(T_*) - q(T(0))] \tag{3.7}$$

$$F_s = C_D u_* C_p [T_* - T(0)] \tag{3.8}$$

where C_D is the aerodynamic drag coefficient, u_* a 'gustiness' factor (Lindzen 1982), T(0) the air temperature at the ground, T_* the ground temperature and q the water vapor amount. $L_v \approx 2.45 \times 10^6 J/kg$, $C_p \approx 1006 J(kg)^{-1} K^{-1}$.

The ratio of latent heat and sensible heat is:

$$\begin{aligned} \frac{F_l}{F_s} &= \frac{L_v[q(T_*) - q(T(0))]}{\rho_{air} C_p[T_* - T(0)]} \\ &= \frac{L_v}{C_p} \frac{dr/dP}{dT/dP} \end{aligned} \tag{3.9}$$

where r is the water vapor mixing ratio in unit (kg/kg) and ρ_{air} is the density of the air at the ground.. As Θ_{se} is constant with the convection, $\frac{dr/dP}{dT/dP}$ at the surface can be calculated numerically. For a surface temperature around 290K, $\frac{dr/dP}{dT/dP} \approx 0.0004 K^{-1}$. This implies $\frac{F_l}{F_s} \approx 1$.

As we mentioned above, $F_l + F_s = 170 W/m^2$ from model calculation. So we can estimate that the latent heat exchange is about 85 W/m^2. This amount of energy will evaporate about $4.5 \times 10^{17} kg$ of water a year globally (or 1.07 m precipitation on average). Comparing this with the estimation of $4.24 \times 10^{17} kg$ (Peixoto and Oort 1992), we can conclude that the model estimation of evaporation rate is satisfactory.

3.6 Summary of the Chapter

1. A new one dimensional radiative - convective model is developed. This model incorporate a comprehensive radiative transfer model and an accurate parameterization of cloud optical properties. A simple and yet physically sound convective adjustment procedure has been developed to simulate the energy balance accurately.

2. The model yields a realistic estimate of the annual global average evaporation rate.

3. The temperature profile computed from the model matches the U.S. Standard atmosphere very well. At the same time, the planetary albedo and the evaporation rate estimated from the model results are reasonable.

Chapter 4

Sensitivity Study

4.1 Introduction

The imbalance of the net radiation (solar + terrestrial) is the ultimate driving force of the climate system. The climate of the Earth changes in response to variations in the radiatively-active substances of which the atmosphere - surface (land and ocean) system is composed. This includes changes in atmospheric gaseous composition and particle content (aerosol and clouds) as well as changes in land characteristics (e.g. vegetation and snow cover) and ocean thermal and optical properties (biological production and particles of organic or inorganic origin). Among the climate sensitive substances, water, including the liquid, solid and gas phases, has the biggest range of variation and the biggest potential impact on climate.

Clouds, which strongly impact climate through radiative energy redistribution via scattering and absorption of radiation, constitute the major source of uncertainty in global climate models (Mitchell, 1989; Ramanathan et al., 1989; Cess et al., 1990). There are two types of problems related to cloud - climate interactions. One of them is how to represent cloud radiative properties correctly in climate models assuming that cloud morphology and microphysical properties are given.

The other one is how to simulate the behaviour of clouds in a changing climate, or the feedback problem. Accurate computations of the radiative properties are required for studies of feedback mechanisms.

From a climate point of view, the cloud radiative properties are dependent on cloud morphology including cloud height and the the cloud optical properties which for water clouds are determined primarily by the cloud water amount and equivalent radius (cf. Chapter 2). The temperatures of the Earth's lower atmosphere and surface are sensitive to the radiative properties of clouds both for solar and terrestrial radiation. An increase of the cloud top height implies less outgoing infrared radiation and thus an increase in tropospheric temperature (Schneider, 1972; Wang, 1981; Wetherald and Manabe, 1988). An increase in cloud water amount leads to enhanced reflection of solar radiation and a cooling of the Earth's surface (Paltridge, 1980; Stephens and Webster, 1979; Charlock, 1982; Somerville and Remer, 1984; Roeckner et al., 1987). A decrease in the equivalent radius of the cloud droplet size distribution (with cloud liquid water fixed) also increases the cloud reflectivity and cools the Earth's surface (Twomey, 1978; Shaw, 1983; Charlson et al., 1987; Albrecht, 1989; Slingo, 1990; Wigley, 1991; Charlson et al., 1992; Shaw et al., 1992; Penner et al., 1992).

An inter-comparison of 19 different global climate models shows that the differences between model results stem mainly from climate induced changes of cloud radiative forcing (Cess et al., 1990). In current global climate models, the cloud equivalent radius is frequently assumed to be 10 μm. The attention of the climate modelers has been focused on the variations of the cloud water amount. Is the cloud drop size important at all? The first part of this chapter will provide a quantitative study of the sensitivity of the cloud equivalent radius, r_e, on the cloud radiative forcing.

Previous studies have demonstrated the importance of cloud optical properties

on climate by using radiative - convective models (Wang et al., 1981; Charlock, 1982; Somerville and Remer, 1984; Liou et al., 1985; Betts and Harshvardhan, 1987; Coakley et al., 1987; Albrecht, 1989; Mitchell et al., 1989; Platt, 1989). Most of these studies have focused on the importance of the cloud water amount, but have not paid much attension to cloud droplet size. The absorption by clouds is an important issue (Wiscombe, 1984; Ackerman and Stephens, 1987; Stephens and Tsay, 1990). For the same optical thickness, changes in equivalent radius affect the absorption. A new radiative - convective model has been developed (cf. Chapter 3) and will be applied here to study the relative importance of cloud droplet size by comparing its impact on climate with the impact of changes in other variables, such as greenhouse gases, the solar constant as well as the cloud height and water amount.

4.2 Cloud Radiative Forcing and Cloud Microphysical Properties

Cloud radiative forcing is defined as the difference of the net radiative fluxes between cloudy and clear sky at the top of the atmosphere (Ramanathan et al., 1989)

$$C = F_{cloudy} - F_{clear}. \tag{4.1}$$

where C is the cloud radiative forcing, F_{cloudy} and F_{clear} are the net radiative flux at the top of the atmosphere for cloudy and clear sky conditions, respectively.

Several studies suggest a simple linear relationship between the net solar radiation fluxes at the surface and at the top of the atmosphere (Ramanathan, 1987; Cess and Vulis, 1989; Cess, 1991; Chou, 1991). Climatology of solar radiative

forcing at the surface has been generated from satellite observations of the solar radiation at the top of the atmosphere using such a linear relation (Chertock et al., 1991; Li, 1993). While the appropriateness of the linear relation requires more study (Pinker and Tarpley, 1988; Schmetz, 1993), the cloud radiative forcing is still one of the most important indicators of the role of clouds in the climate system as it can be observed directly from space.

Using an atmospheric radiative transfer model (Stamnes et al., 1988; Tsay et al., 1989) with the new parameterizations of cloud optical properties (cf. Chapter 2), we study how the cloud radiative forcing depends on cloud height, cloud liquid water path and cloud equivalent radius in this chapter.

4.2.1 The Cloud Sensitivity Problem: Solar Radiation

4.2.1.1 Response of Cloud Forcing to Changes in Droplet Size for Fixed Liquid Water Path

The U.S. standard atmosphere has been used as the model inputs, such as atmospheric density, temperature and water vapor profiles. The sun is assumed to be overhead. The cloud radiative forcing C_{solar} is calculated from:

$$C_{solar} = \frac{\pi R_{Earth}^2}{4\pi R_{Earth}^2}(F_{cloudy} - F_{clear}) = \frac{1}{4}(F_{cloudy} - F_{clear}) \qquad (4.2)$$

where F is the net radiative flux at the top of the atmosphere. The reason for the coefficient $\frac{1}{4}$ is to simulate a global annual average.

The global shortwave cloud radiative forcing from the Earth Radiation Budget Experiment (ERBE) is $-44.5 W/m^2$ for the month of April 1985 (Ramanathan et al., 1989). The shortwave radiative forcing is large over mid- and high-latitude oceans with maximum values around $-150 W/m^2$ (Ramanathan et al., 1989; Harrison et al., 1990).

Figure 4.1 is an example of the computed radiative forcing for different cloud liquid water paths (5, 50 and 500 g/m^2). For clouds with liquid water paths around 50 g/m^2, the radiative forcing is very sensitive to the changes in the equivalent radius (Figure 4.2). A $1\mu m$ decrease in cloud equivalent radius generates up to $-15W/m^2$ more shortwave cloud radiative forcing.

A standard climate sensitivity study has been to consider the climate response to a 2% variation in the solar constant. Figure 4.3 shows that a 10% decrease in cloud equivalent radius will result in a $7-15\%$ increase in shortwave cloud radiative forcing. The changes in cloud radiative forcing are larger than $-5W/m^2$, which is similar to a 2% decrease in the solar constant (global average difference $0.02 \times 1373 \times 0.70 \times \frac{1}{4} \approx 4.5W/m^2$).

4.2.1.2 Response of Cloud Forcing to Changes in Cloud Equivalent Radius for Fixed Optical Thickness: the Cloud Absorption Problem

The general circulation is driven by the imbalance of the net surface radiative heating and the net atmospheric radiative cooling. The cloud absorption of solar radiation is an important part of the compensation to the longwave cooling of the atmosphere and thus affects the general circulation. The importance of the cloud absorption problem has been discussed in recent studies (Wiscombe, 1984; Stephens and Tsay, 1990).

To study the climate sensitivity to cloud absorption, we can look at the shortwave cloud radiative forcing as a function of cloud equivalent radius for fixed cloud optical thickness. As the asymmetry factors for different types of clouds do not vary significantly (g is always around 0.85), the differences in cloud forcing represents the climate effect of the changes in absorption (or the variations of single scattering albedo).

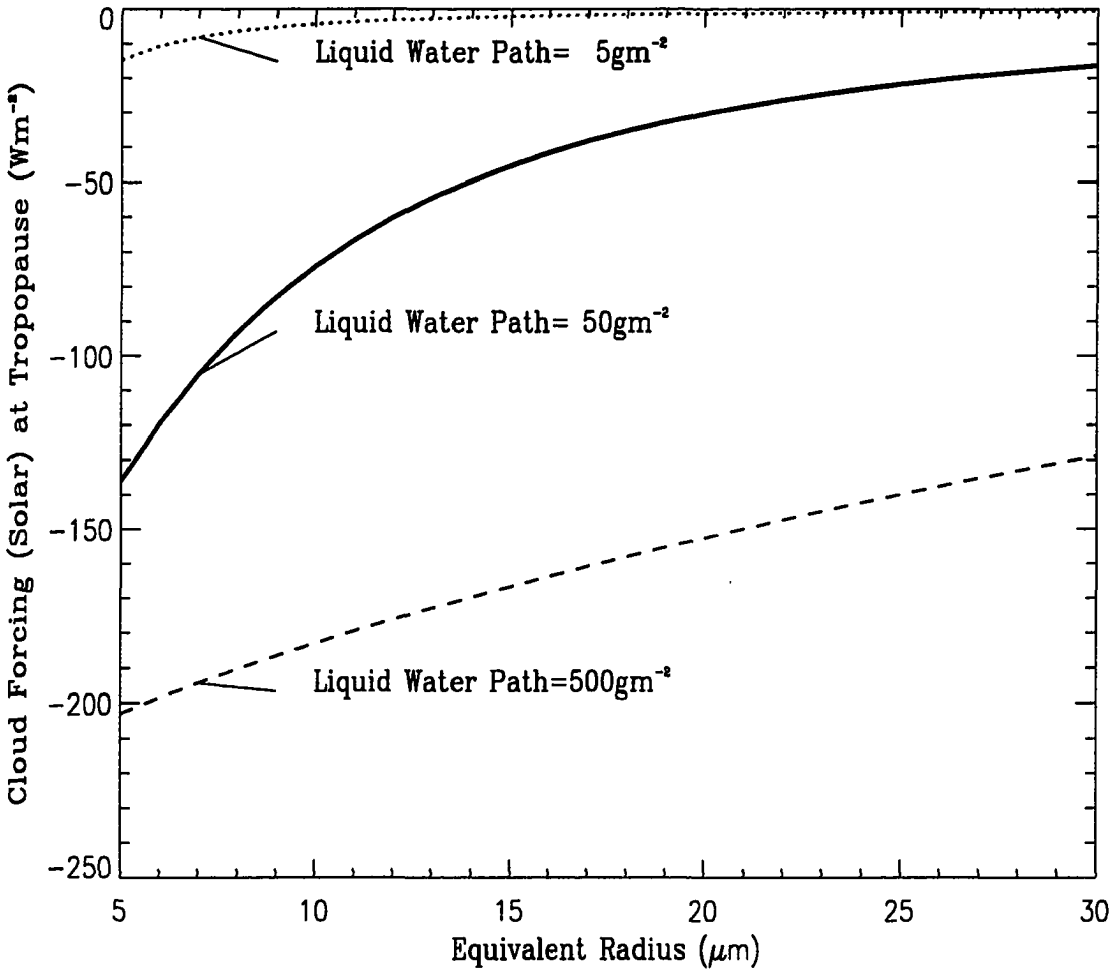

Figure 4.1 The shortwave cloud radiative forcing (global annual average) variations with equivalent radii of cloud droplet size distribution for thin (5 g/m^2), regular (50 g/m^2) and very thick clouds (500 g/m^2).

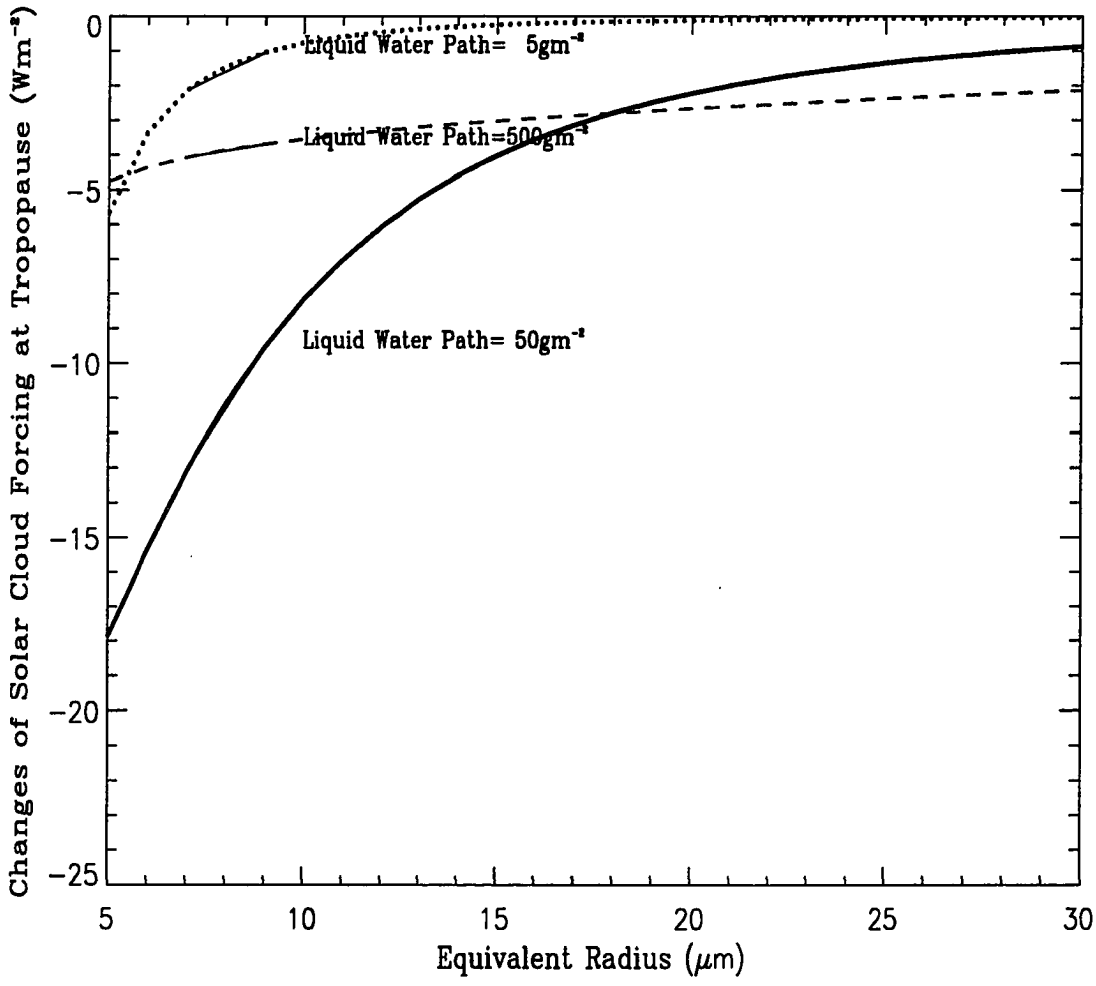

Figure 4.2 The changes of the shortwave cloud radiative forcing for a $1\mu m$ decrease in equivalent radius at different equivalent radii of cloud droplet size distribution for thin ($5\ g/m^2$), regular ($50\ g/m^2$) and very thick clouds ($500\ g/m^2$).

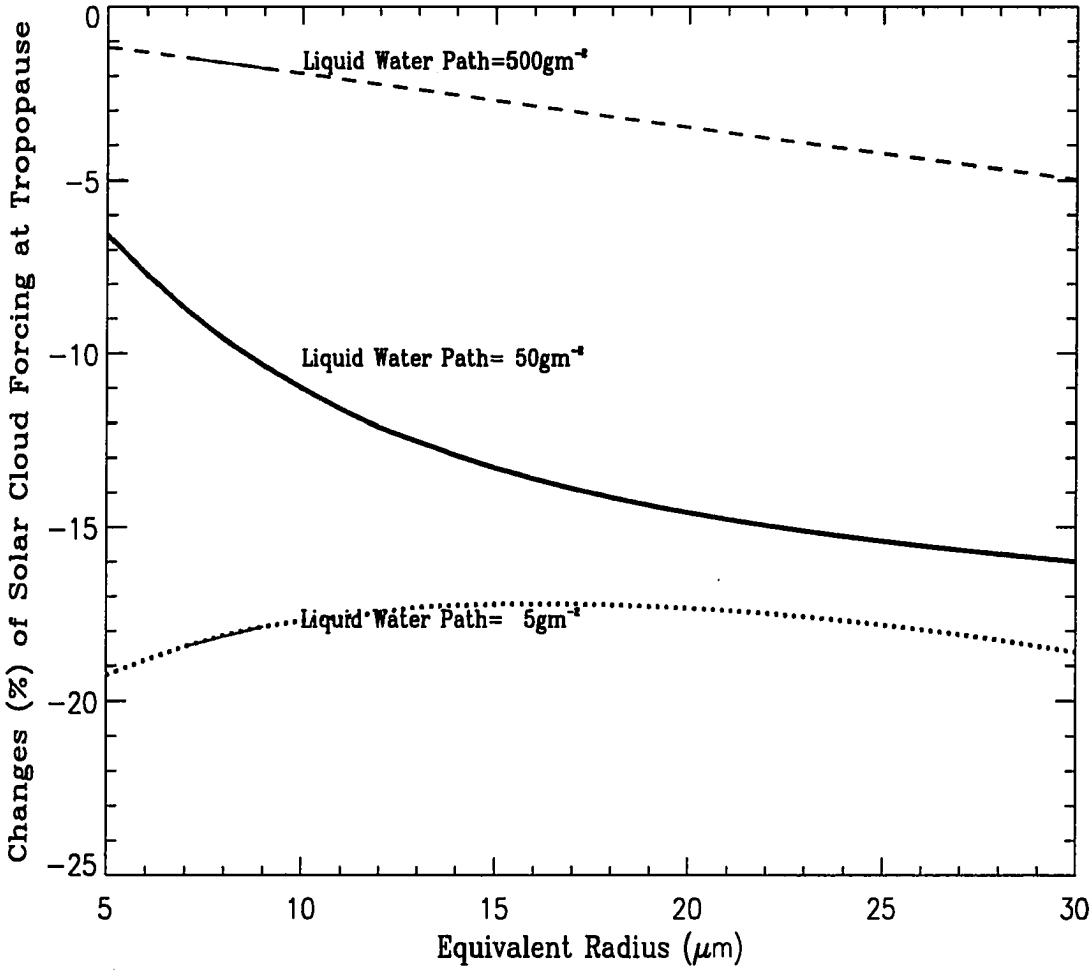

Figure 4.3 Percentage changes in shortwave cloud radiative forcing for a 10% decrease in equivalent radius at different equivalent droplet radii for thin (5 g/m^2), regular (50 g/m^2) and very thick clouds (500 g/m^2).

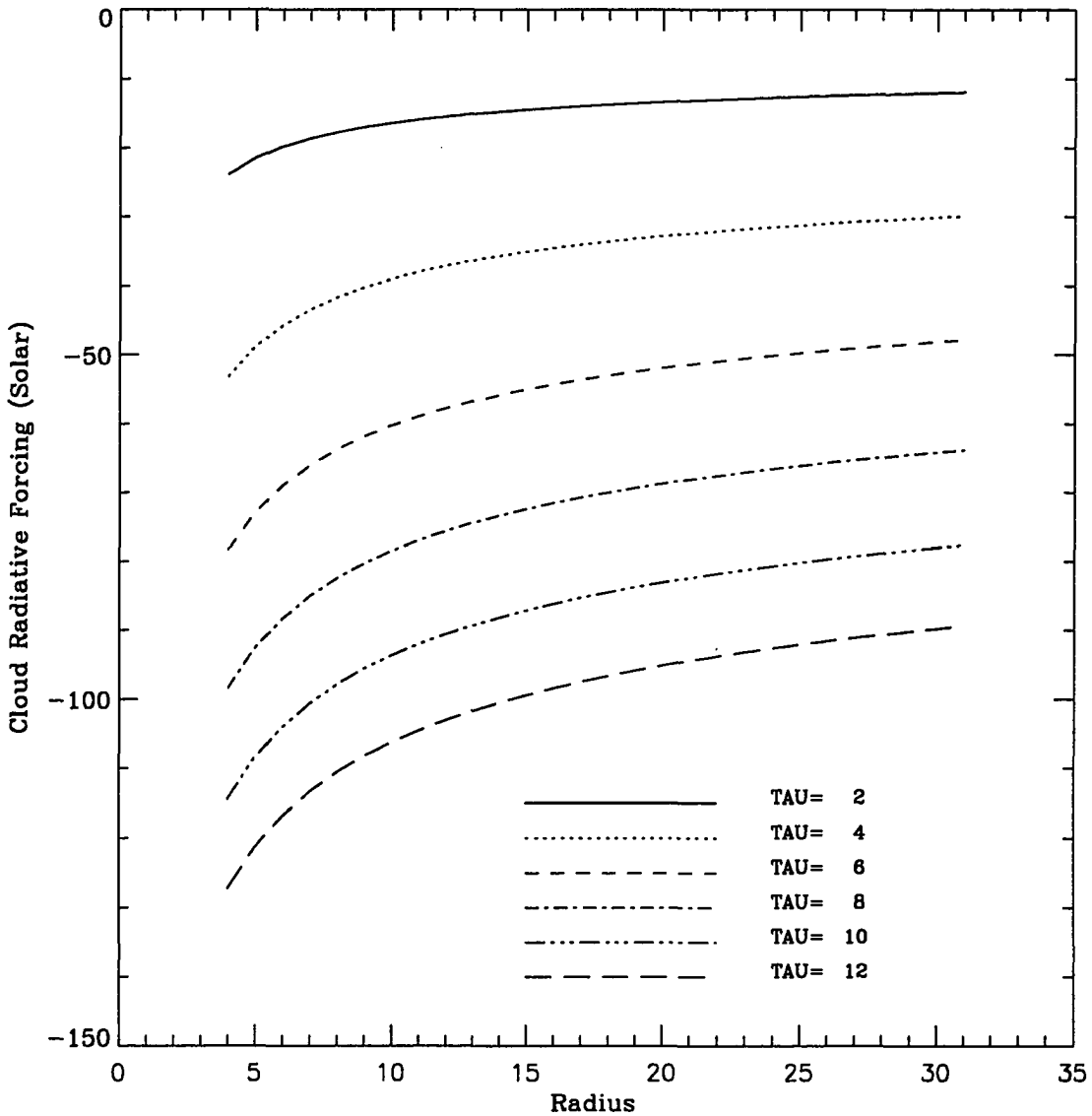

Figure 4.4 The shortwave cloud radiative forcing for different cloud equivalent radii for fixed cloud optical thickness.

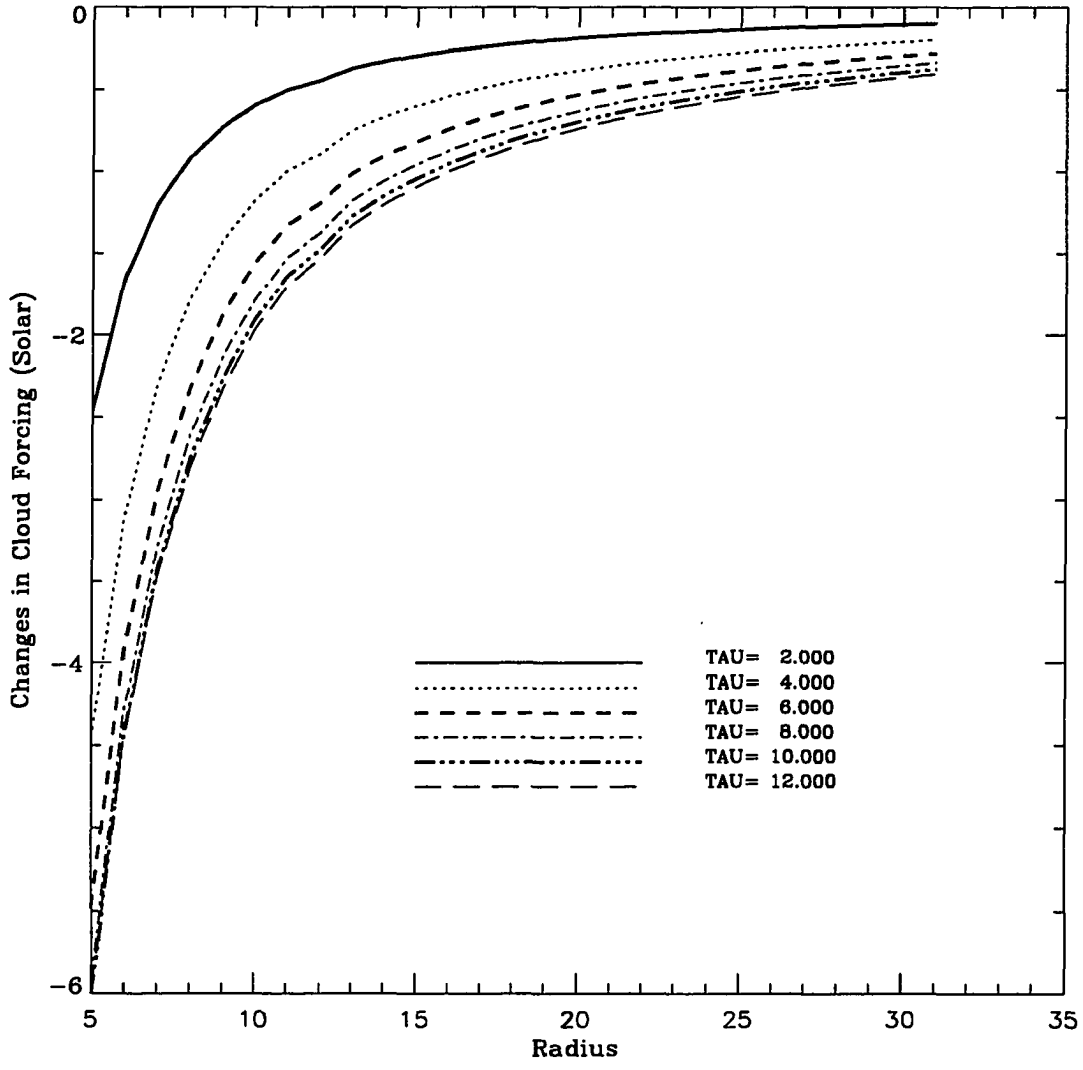

Figure 4.5 The changes of the shortwave cloud radiative forcing with a r_e decrease of $1\mu m$ for different cloud equivalent radii with fixed cloud optical thickness.

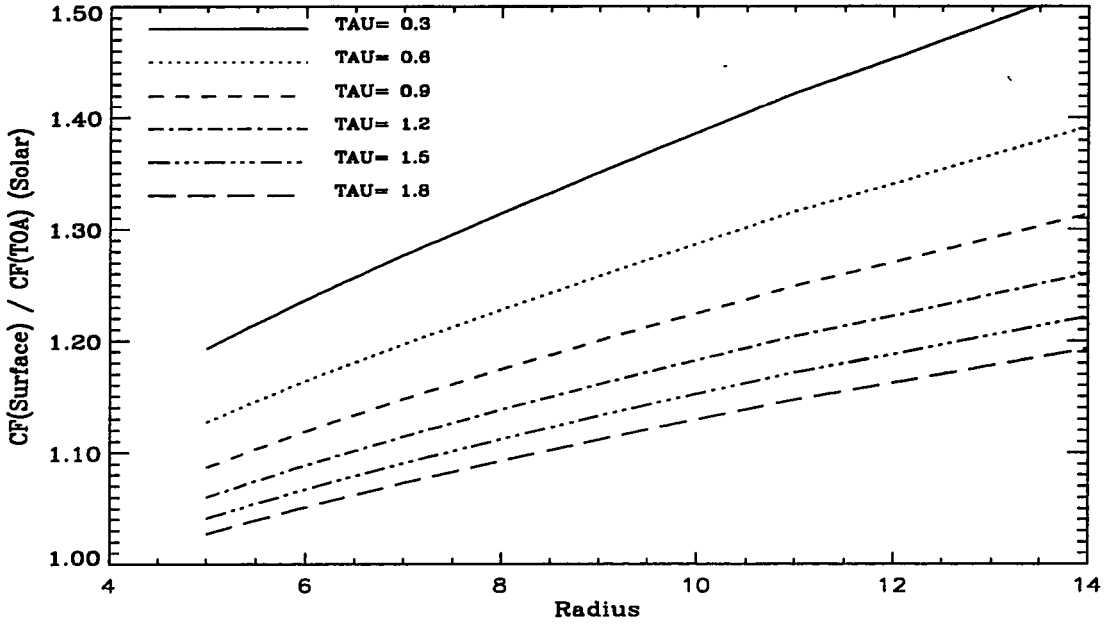

Figure 4.6 The shortwave cloud radiative forcing ratio between the surface and the top of the atmosphere for different equivalent radii with fixed cloud optical thickness (thin clouds).

Figures 4.4 and 4.5 show that for fixed cloud optical thickness, the shortwave radiative forcing changes a lot if the cloud equivalent radius varies. Here, the variation of the single scattering albedo is primarily responsible for the changes in the cloud forcing. Calculations (cf. Chapter 2) show that the single scattering albedo changes with cloud equivalent radius. The differences of the single scattering albedos between $r_e = 6\mu m$ and $r_e = 24\mu m$ are about one order of mangitude for all wavelengths (see Figure 2.5). Figure 4.4 shows that the difference in cloud radiative forcing caused by changes in droplet sizes (which impact single scattering albedo) can be as big as $25W/m^2$. In most climate models, the parameterization of shortwave cloud single scattering albedo is far from accurate. More research focusing on the cloud absorption problem (especially the shortwave absorption by the large drops) is needed.

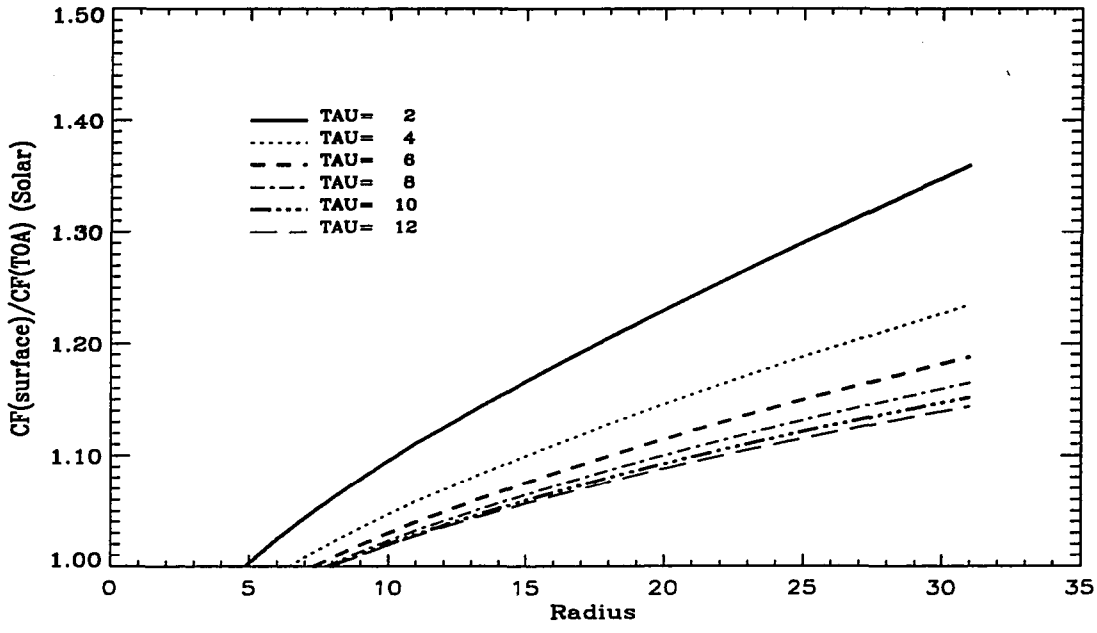

Figure 4.7 The shortwave cloud radiative forcing ratio between the surface and the top of the atmosphere for different equivalent radii with fixed cloud optical thickness (moderately thin clouds).

The cloud radiative forcing at the bottom of the atmosphere might be the most important component affecting the cloud - general circulation interaction. Figures 4.6, 4.7 and 4.8 show the relationship between the shortwave cloud radiative forcing at the bottom of the atmosphere and at the top of the atmosphere. Clearly, (1) this relationship is sensitive to cloud droplet size (regardless of optical thickness) and (2) unless the cloud is very thick, it is also very sensitive to cloud optical thickness.

4.2.2 The Cloud Sensitivity Study: Terrestrial Radiation

In most weather forcasting models, multiple scattering properties of the terrestrial radiation are not considered properly. In climate models, the thin clouds play a very important role in the energy redistribution processes. The radiative effects of

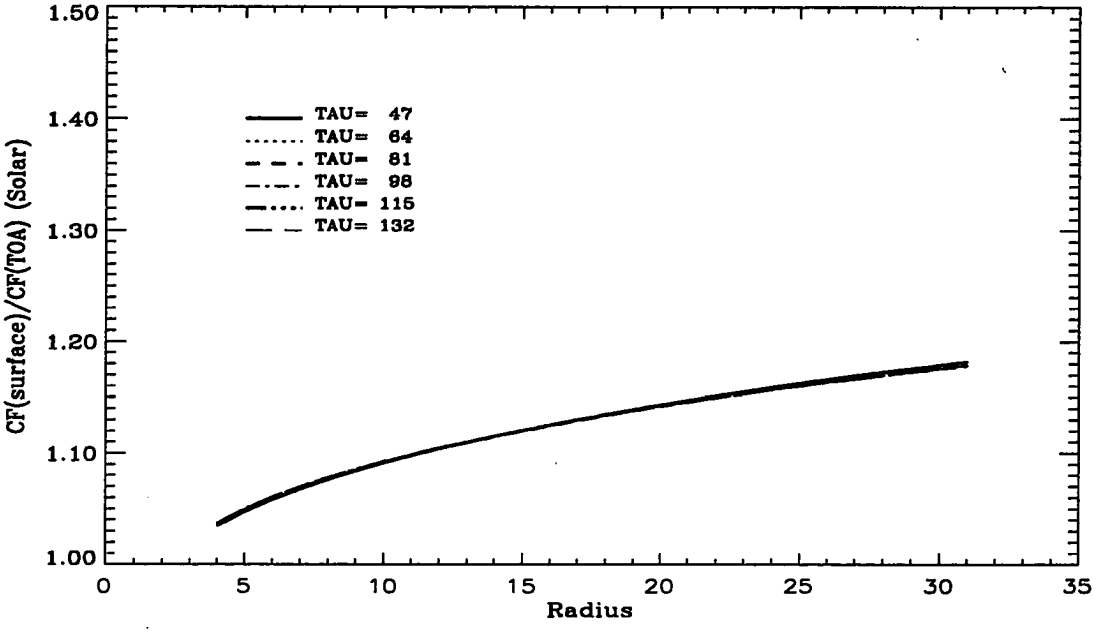

Figure 4.8 The shortwave cloud radiative forcing ratio between the surface and the top of the atmosphere for different equivalent radii with fixed cloud optical thickness (thick clouds).

the cirrus clouds might be one of the most important atmospheric 'thermostats' (Ramanathan and Collins, 1992).

An accurate and also simple parameterization of cloud optical properties such as extinction coefficient, single scattering albedo and asymmetry factor is needed in the radiative transfer calculations of the terrestrial radiation in climate models if the climate system is sensitive to the single scattering properties in the longwave radiation.

Figure 4.9 and 4.10 show that the longwave cloud radiative forcing are sensitive to the changes in cloud equivalent radius if the cloud is not too thick.

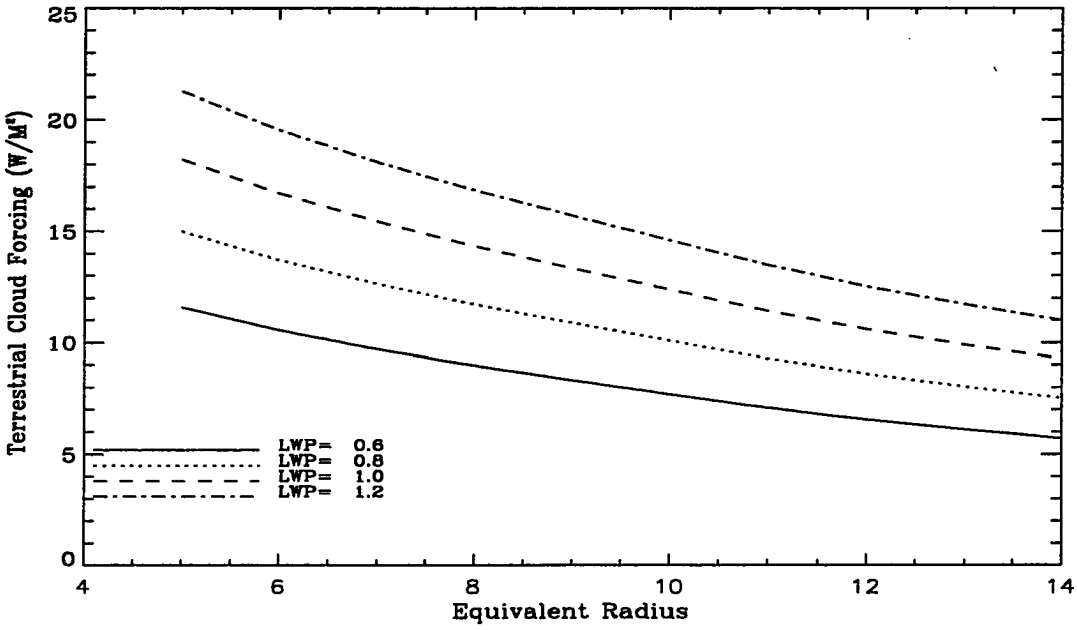

Figure 4.9 The longwave cloud radiative forcing at the top of the atmosphere for different equivalent radii with fixed cloud liquid water content (in g/m^2).

4.3 Equilibrium State Sensitivity Study

There are many feedback mechanisms within our climate system involving clouds and the hydrological cycle. Many studies demonstrated the importance of cloud water and height feedback in climate models (Wang et al., 1981; Charlock, 1982; Somerville and Remer, 1984; Betts and Harshvardhan, 1987; Coakley et al., 1987; Albrecht, 1989; Mitchell et al., 1989; Platt 1989). As a result of the increase in greenhouse gases, some studies show a slight positive cloud feedback (Wang et al., 1981; Liou et al., 1985), while other studies indicate large negative feedbacks (Paltridge, 1980; Somerville and Remer 1984; Mitchell et al., 1989). Cloud radiative forcing from ERBE indicates a slight positive feedback (Cess et al., 1992) by comparing the cloud radiative forcing variations in summer and winter. Most of the previous studies did not consider the variation in the cloud equivalent radius.

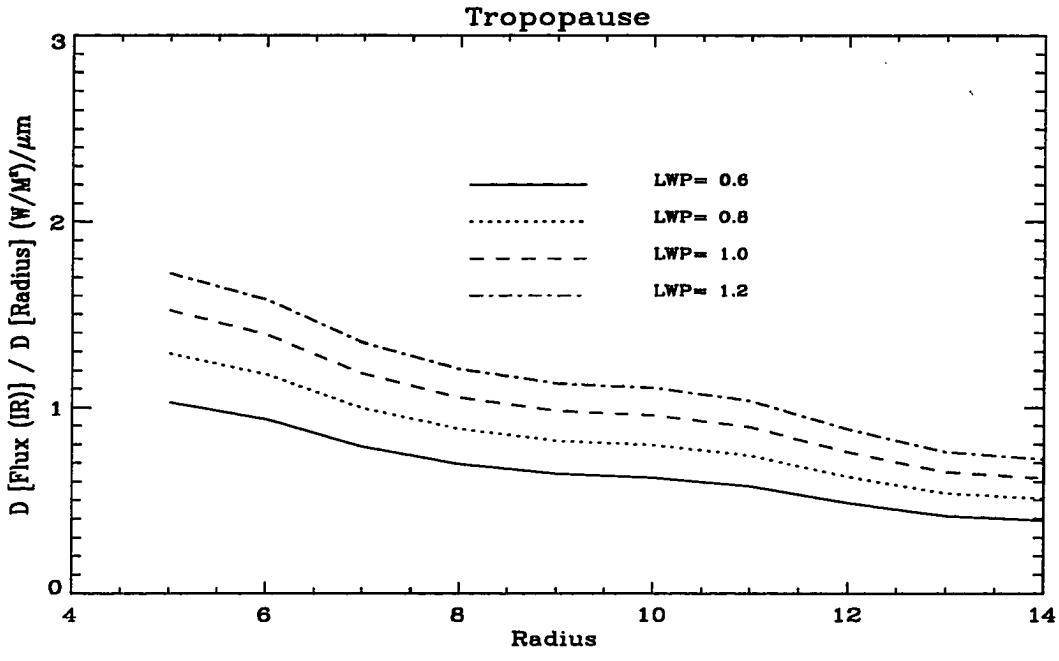

Figure 4.10 The change in longwave cloud radiative forcing caused by $1\mu m$ increase in equivalent radius for different equivalent radii with fixed cloud liquid water content (in g/m^2).

Clouds forming in a maritime enviornment are more likely to produce rain than clouds forming over the continents. Thus, the maritime clouds are less colloidally stable than their continental counterparts. In a nucleus-rich continental atmosphere, a given liquid water content must be distributed over numerous small droplets having small collection kernels or collection cross-section, which makes it difficult to produce rain. For a certain amount of cloud water, the bigger the cloud nucleus population, the smaller the cloud equivalent radius and the lesser is the likelihood for rain. The cloud amount and duration will increase as a result. This feedback process is a cooling mechanism in the atmosphere.

A quantitative sensitivity study of the equilibrium temperature profiles with changing cloud equivalent radii (with liquid water path fixed or with optical thickness fixed) is performed in this section.

4.3.1 Climate Sensitivity to the CO_2 Concentration Doubling or 2% Change in Solar Constant

The surface temperature changes by an amount ranging from 1.5 to 3^0C in current climate models as a result of carbon dioxide concentration doubling or a 2% increase in solar constant, depending on the treatment of clouds (Smith, 1990).

Based on the Radiative-Convective model developed for this study (cf. Chapter 3), the temperature increases by about 1.6^0C as a result of CO_2 concentration doubling (Figure 4.11), whereas the difference of a 2% changes in the solar constant causes a 1.5^0C change in surface temperature (Figure 4.12).

4.3.2 Climate Sensitivity to Cloud Water Path Variation and Cloud Droplet Size Variation

As the cloud optical thickness is very sensitive to the cloud droplet size ($\tau_{solar} \propto LWC/r_e$), the shortwave radiation is very sensitive to this parameter. The equilibrium states of the one dimensional radiative - convective model with different cloud liquid water contents and equivalent radii show that the temperature profiles are very sensitive to the cloud microphysical properties (Figure 4.13). A 15% decrease in the cloud liquid water path or a 10% increase in the cloud equivalent radius will increase the surface temperature by about 1.6^0C, the same as that resulting from CO_2 concentration doubling.

The sensitivity calculations with the radiative - convective model suggest that the cloud equivalent radius should not be artificially assigned in climate models. Better understanding of the variations of r_e in a changing climate is needed for the correct predictions of climate change.

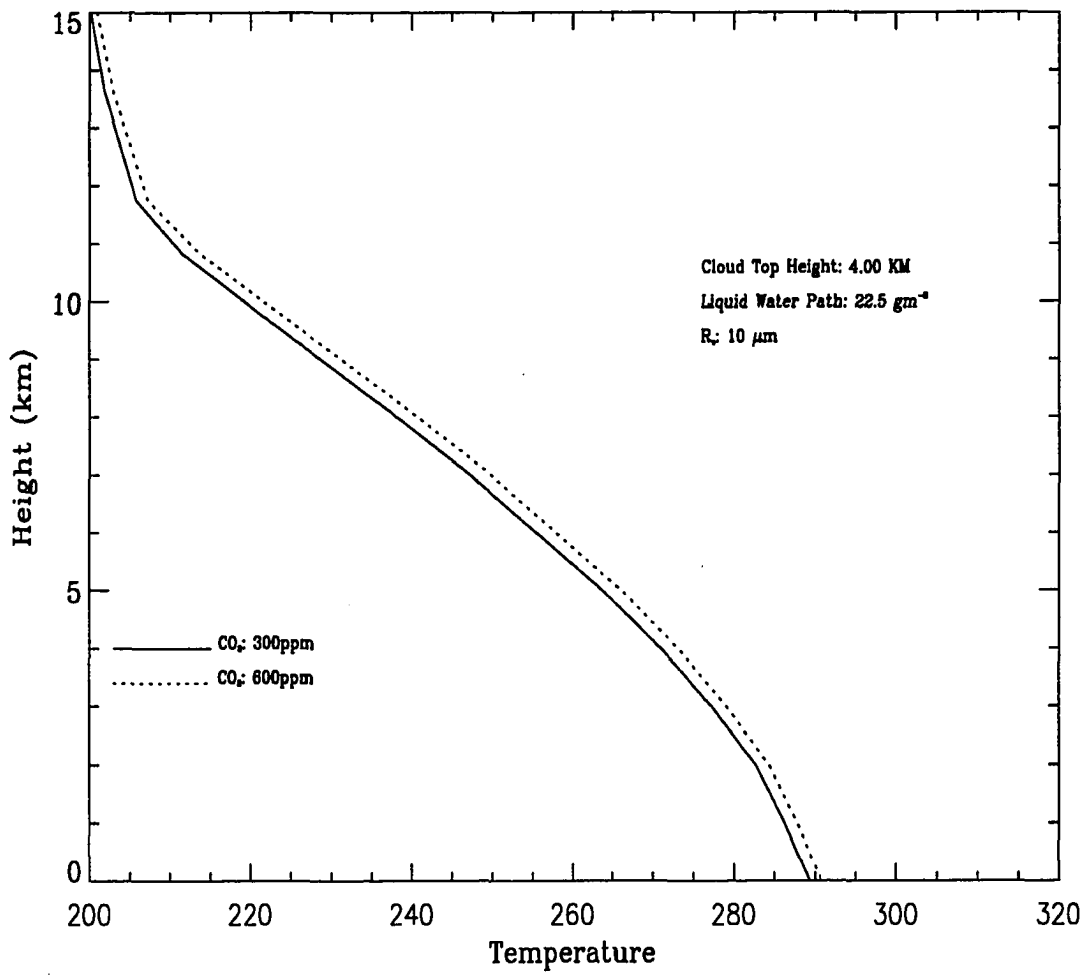

Figure 4.11 The equilibrium of temperature profiles for different CO_2 concentrations: 300 unit per million or 600 unit per million..

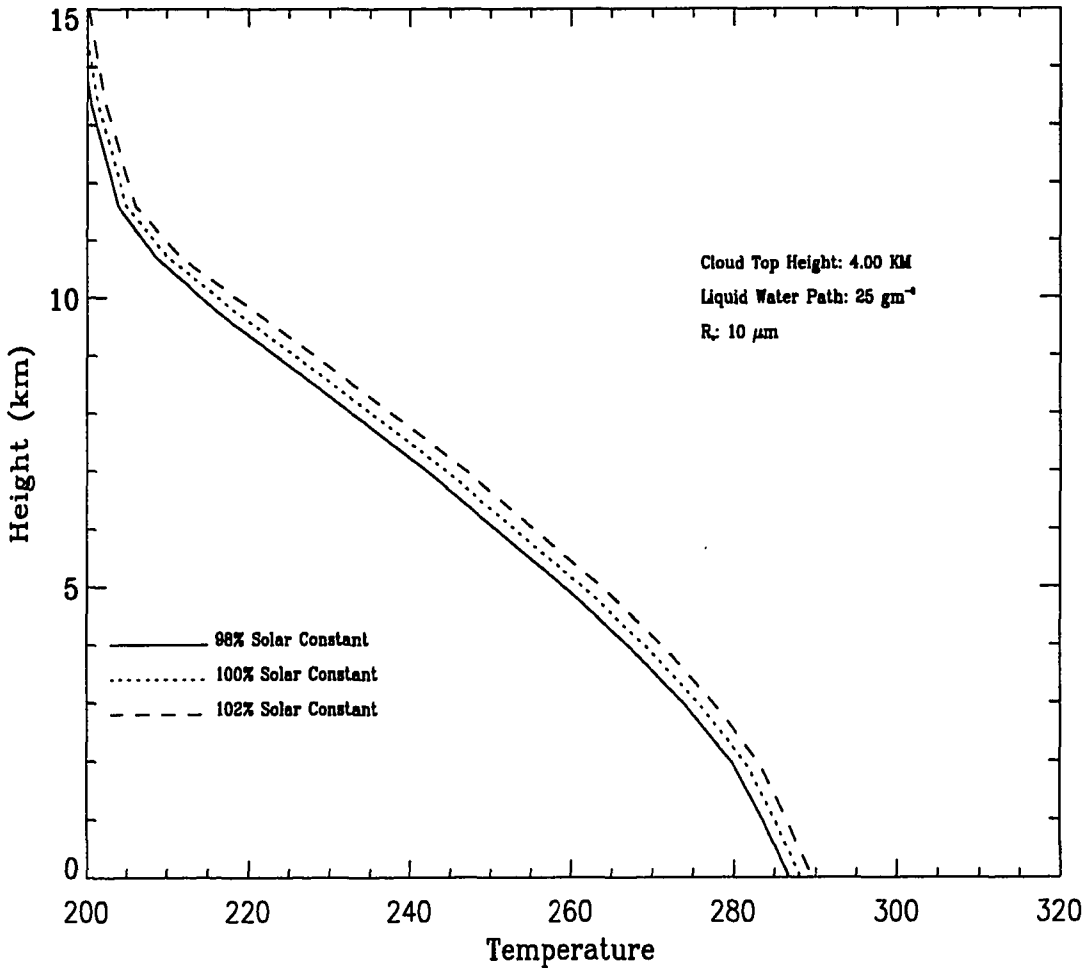

Figure 4.12 The equilibrium of temperature profiles for different solar constant: 98%, 100% and 102%.

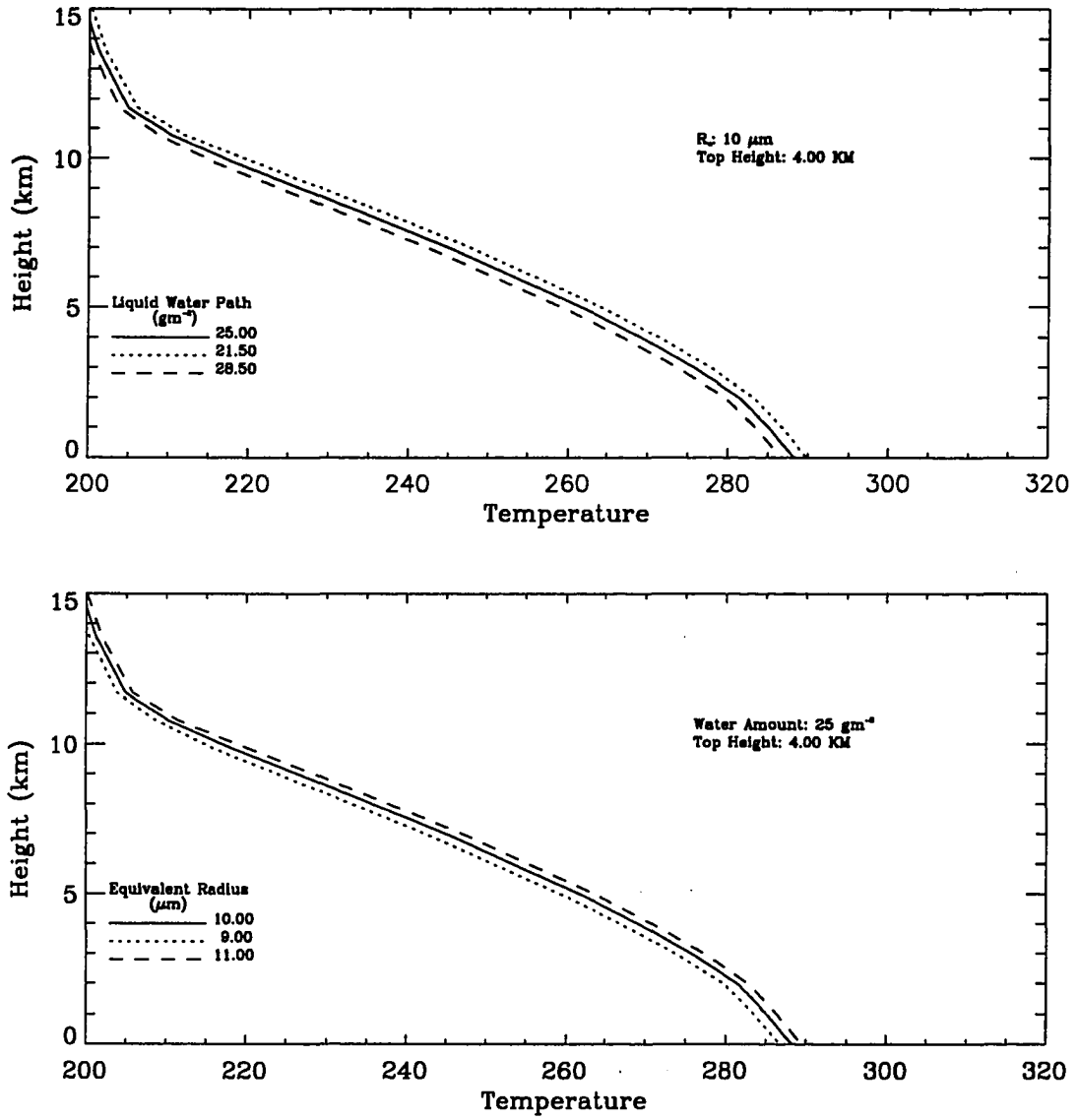

Figure 4.13 The equilibrium of temperature profiles for 15% changes in cloud liquid water path (upper panel) and for 10% changes in cloud equivalent radius (lower panel).

4.3.3 Climate Sensitivity to Cloud Cloud Droplet Size Variation for Fixed Optical Depth

The shortwave cloud absorption from model is significantly smaller than the result of observations. To study the possible impact of an incorrect single scattering albedo in climate models, a sensitivity study is performed with the radiative - convective model. With fixed cloud optical thickness, the variations in the equilibrium temperature profile with different cloud equivalent radii represent the equilibrium temperature response to the differences in the shortwave cloud absorption.

For shortwave radiation, the single scattering albedo changes by an order of magnitude when r_e changes from 7.2 μm to 12.8 μm. The surface temperature difference (Figure 4.14) is bigger than 1.6^0C, the temperature increase due to CO_2 concentration doubling or a 2% increase of the solar constant. The correct understanding of the cloud absorption is important for realistic prediction of the climate change due to CO_2 concentration doubling.

4.4 Summary of the Chapter

The climate sensitivities of the cloud microphysical properties are discussed here. Both cloud radiative forcings and the equilibrium surface temperatures are very sensitive to the variations in cloud equivalent radius. A 10% decrease of cloud equivalent radius or a 15% increase in cloud water amount can compensate the expected warming caused by CO_2 concentration doubling.

The climate impact of the cloud absorption can be isolated by varying the cloud equivalent radii with fixed cloud optical thickness. The shortwave cloud radiative forcing is sensitive to the calculations of cloud absorption. A slight variation of the cloud single scattering albedo can cause a difference in surface temperature as big

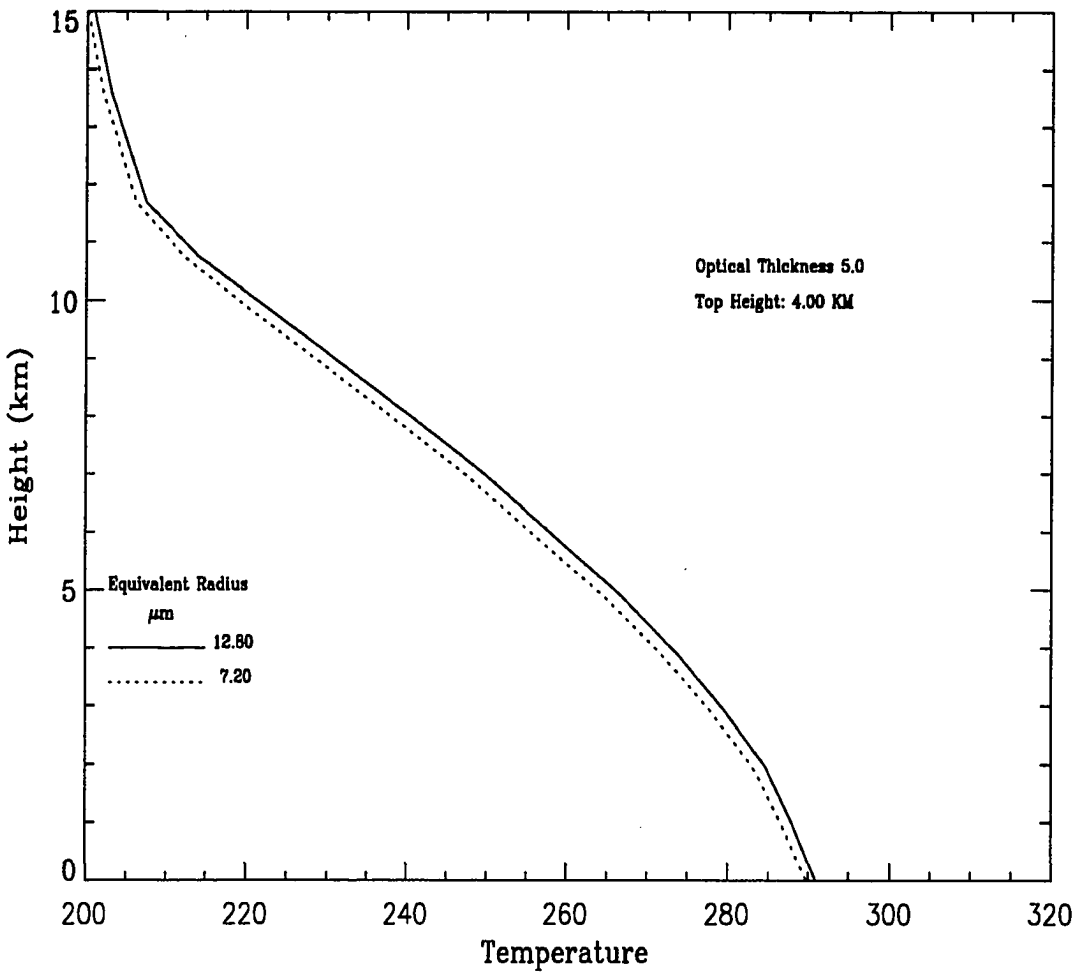

Figure 4.14 The equilibrium of temperature profiles for different cloud equivalent radii with fixed cloud optical thickness: The cloud absorption effect.

as the temperature change due to CO_2 concentration doubling or the 2% increase of solar constant.

Chapter 5

Adjoint Method for Radiative Transfer

5.1 Introduction

Radiative transfer computations are the biggest time comsumers in climate models. Speeding up the radiation computations is crucial to the radiative-convective model. In climate models, the radiative transfer equation has to be solved again and again because the optical properties of the atmosphere vary with time. Using the adjoint method, these repeated computations of the radiative transfer equation can be significantly reduced.

The adjoint method has been widely used in different fields of atmospheric sciences (e. g., Marchuk, G.I., 1958, 1964, 1974, 1992; Cacuci, D.G., 1981, 1988; Gerstl, 1982; Box et al., 1988; Zou, et al., 1993). Unlike the direct equations which describe the meteorological fields forward in time and space, the adjoint equations describe the sensitivity of the system (to different parameters of the equations) backward in time or space direction. The system variables can be calculated through the symmetry equation of inner products in Hilbert space. The

adjoint method is a powerful tool for a linear system. One example of using the adjoint method is the Green's function method. In the atmospheric community, the adjoint method for linearized and full primitive dynamics equations has been developed for long-range weather prediction, parameter estimation for physical parameterization and data assimilation.

The radiative transfer equation for a plane-parrallel atmosphere can be considered as a linear equation over the phase space (τ, θ, ϕ). In this chapter, we will show that the adjoint radiative properties can be easily obtained with the available forward radiative transfer code. The radiative properties such as fluxes, heating rates and their sensitivities to the optical properties (optical depth, single scattering properties, phase function, atmospheric profiles, etc) can be easily obtained from the adjoint radiative intensity.

Using the adjoint method for radiative transfer computations, we can significantly speed up climate models by reducing the time expended on radiative transfer computations. In atmospheric remote sensing, this method will play an important role because it accurately calculates the partial differentials, which are crucial for extracting cloud information from the surface or top of the atmosphere radiative fluxes or intensities.

The concept of the adjoint method for radiative transfer calculation, the scheme of computing adjoint radiative fluxes by using DISORT and the application of this method is discussed in the following sections.

5.2 Adjoint Equation for Radiative Transfer

5.2.1 Adjoint Operator

If L is a linear operator, (x, y) is the inner product of x and y, f and f^* are arbitrary functions, the adjoint operator L^* is a linear operator which satisfies the following equation

$$(f^*, Lf) = (f, L^* f^*). \tag{5.1}$$

The following is an example of how to find the adjoint operator. For $L = \frac{\partial}{\partial x}$ with boundary condition $(f, f^*) = 0$, we have

$$\begin{aligned}
(f^*, Lf) &= \int_a^b f^* \frac{\partial f}{\partial x}\, dx \\
&= (f^*, f)|_a^b - \int_a^b f \frac{\partial f^*}{\partial x}\, dx \\
&= -\int_a^b f \frac{\partial f^*}{\partial x}\, dx \\
&= (f, L^* f^*).
\end{aligned} \tag{5.2}$$

So the adjoint operator is $L^* = \frac{-\partial}{\partial x} = -L$. It is a self-adjoint operator.

The adjoint operator for a constant c is itself, because $(f^*, cf) = (f, cf^*)$.

If the boundary condition is $(f, f^*) = 0$, the adjoint for a linear operator $\frac{\partial^k}{\partial x^k}$ is (the proof for this can be found in standard textbooks such as 'Mathematical Methods for Physicists (Arfken, 1985)):

$$L^* = (-1)^k \frac{\partial^k}{\partial x^k}. \tag{5.3}$$

5.2.2 Adjoint Operator for Differential-Integral Equation

The adjoint operator for $L = aL_1 + bL_2$ is $L^* = aL_1^* + bL_2^*$. Here a and b are constants. For a linear differential-integral equation, we can separate the differential part L_1 and the integral part L_2.

For the integral operator $L = \int_a^b P(\vec{x'} \to \vec{x})\,dx$ where $P(-\vec{x} \to -\vec{x'})\,dx = P(\vec{x'} \to \vec{x})\,dx$ (here P represents the phase function in radiative transfer equation), the inner product of functions f and f^* is

$$\begin{aligned}
(f^*, Lf) &= \int_a^b f^*(x) \int_a^b P(\vec{x'} \to \vec{x}) f(x')\,dx'\,dx \\
&= \int_a^b f^*(x') \int_a^b P(\vec{x} \to \vec{x'}) f(x)\,dx\,dx' \\
&= \int_a^b f^*(x') \int_a^b P(-\vec{x'} \to -\vec{x}) f(x)\,dx\,dx' \\
&= \int_a^b f(x) \int_a^b P(-\vec{x'} \to -\vec{x}) f^*(x')\,dx'\,dx \\
&= (f, L^* f^*). \qquad (5.4)
\end{aligned}$$

So if $P(-\vec{x} \to -\vec{x'})\,dx = P(\vec{x'} \to \vec{x})\,dx$, the adjoint operator of $L = \int_a^b P(\vec{x'} \to \vec{x})\,dx$ is

$$L^* = \int_a^b P(-\vec{x'} \to -\vec{x})\,dx. \qquad (5.5)$$

5.2.3 Adjoint Operator for Radiative Transfer

For the radiative transfer equation

$$\mu \frac{dI}{d\tau} = I - \frac{a}{4\pi} \int_{4\pi} P(\hat{\Omega}' \to \hat{\Omega}) I\,d\omega' + Q \qquad (5.6)$$

where a is the single scattering albedo and Q represents the blackbody emission or incident solar beam. Q is independent of I.

The radiative transfer equation can be written as $LI = Q$, where the linear operator L is

$$L(\hat{\Omega}) = \mu\frac{d}{d\tau} - 1 + \frac{a}{4\pi}\int_{4\pi} P(\hat{\Omega}' \to \hat{\Omega})\, d\omega'. \tag{5.7}$$

The adjoint operator of a constant is itself. From equation 5.3 and equation 5.5, the adjoint operator for equation 5.7 is

$$\begin{aligned} L^* &= -\mu\frac{d}{d\tau} - 1 + \frac{a}{4\pi}\int_{4\pi} P(-\hat{\Omega}' \to -\hat{\Omega})\, d\omega' \\ &= L(-\hat{\Omega}). \end{aligned} \tag{5.8}$$

The computation methods for the regular radiative transfer equation can still be used after we introduce another variable $I'(\hat{\Omega})$, which is

$$I'(\hat{\Omega}) = I^*(-\hat{\Omega}) \tag{5.9}$$

$$\begin{aligned} L^*(\hat{\Omega})I^*(\hat{\Omega}) &= L^*(\hat{\Omega})I'(-\hat{\Omega}) \\ &= L(-\hat{\Omega})I'(-\hat{\Omega}) \\ &= Q'(\hat{\Omega}). \end{aligned} \tag{5.10}$$

Replacing $\hat{\Omega}$ by $-\hat{\Omega}$ in Equation 5.10, then the adjoint radiative transfer equation $L^*I^* = Q'$ is equivalent to

$$L(\hat{\Omega})I'(\hat{\Omega}) = Q'(-\hat{\Omega}). \tag{5.11}$$

Equation 5.11 has the same radiative operator as the regular radiative transfer equation. Thus regular computational routine (with arbitrary intensity-independent source) can be used for solving the adjoint equation.

5.3 Physical Meaning of the Adjoint Intensity

The radiative sources in all the layers of the atmosphere contribute to (or influence) the radiative intensity at any particular level. The adjoint method calculates these contributions (or influences).

The physical meaning of the solution to the adjoint radiative transfer equation is elucidated by looking at the following two equations

$$L^*I^* = \delta(\tau - \tau_i) \tag{5.12}$$

$$LI = \delta(\tau - \tau_j). \tag{5.13}$$

Equation 5.13 is the 'forward' radiative transfer equation for a unit source at level j. Equation 5.12 is the adjoint radiative transfer equation for a unit source at level i.

$$\begin{aligned} (I^*, LI) &= I^*[\tau(j)] \\ (I, L^*I^*) &= I[\tau(i)]. \end{aligned} \tag{5.14}$$

From the definition of the adjoint operator $(I^*, LI) = (I, L^*I^*)$, we have

$$I^*[\tau(j)] = I[\tau(i)]. \tag{5.15}$$

Thus, the solution $I^*(\tau_j)$ of the adjoint equation with a unit source at level I is the same as the solution $I[\tau(i)]$ of the forward equation with a unit source at level j. This implies that the physical meaning of the adjoint radiative intensity $I^*[\tau(j)]$ from the adjoint radiative transfer equation 5.12 is the contribution of the source at each layer j to the radiative intensity of a specific level i.

5.4 Fluxes and Heating Rate Computations

One of the incentives for using the adjoint method to compute fluxes and heating rates is to reduce the burden of radiative transfer computations in climate models. The radiative transfer equation has to be solved for each grid point and time step in the climate models. Because there is no analytical solution for it in general, the radiative transfer equation has to be solved numerically, which is quite time consuming.

Using the adjoint method, we can determine the radiative fluxes and heating rates semi-analytically: the fluxes and heating rates can be expressed analytically as the functions of intensity independent source functions (blackbody emission and incident beam), optical properties (extinction coefficients, phase functions, etc) and adjoint radiative intensities for several typical atmospheric compositions, which can be calculated once and for all. With this method, the radiative fluxes and heating rates of the atmospheric layers can be calculated without repeatedly solving the radiative transfer equation for thousands of grid points, time steps and spectral lines.

In the following subsections, we will first introduce the basic idea of fluxes and heating rates calculation using the adjoint method for constant optical properties and different atmospheric temperature profiles. Then we will introduce the perturbation method for the adjoint radiative transfer problems with perturbations in optical properties.

5.4.1 Basic Idea about the Calculations

First, let's consider the adjoint method for radiative transfer without optical property perturbation. Similar to the idea of solving partial differential equations by using the Green's function method, we can first solve the adjoint radiative transfer

equation with a specific source function $L^*I^* = Q'$. This source function Q' is constructed so that the integration $(I^*, Q) = \int_{-\infty}^{\infty} d\tau \int_{4\pi} I^* Q \, d\omega$ yields the radiative properties we need (here Q represents the actual source function and I^* is the solution of adjoint equation).

We can find Q' from the definition of adjoint $(I^*, LI) = (I, L^*I^*)$.

$$\begin{aligned} (I^*, Q) &= (I^*, LI) \\ &= (I, L^*I^*) \\ &= (I, Q'). \end{aligned} \tag{5.16}$$

As $(I, Q') = \int d\tau \int I \cdot Q' \, d\omega$, we can compare (I, Q') with the radiative properties, such as net fluxes $\int_{4\pi} \mu I \, d\Omega$, to obtain the Q'.

The similiarity of the adjoint radiative transfer method and the Green's function method is: they both simplifies the procedure of solving the whole equation by replacing the real source term with a simple source. The differences is: the Green's function method requires the adjoint equation to have analytical solutions.The adjoint radiative transfer equation does not have an analytical solution in general and has to be solved numerically.

5.4.2 Calculations of Fluxes

5.4.2.1 The Relation of Flux and Adjoint Intensity

The net radiative fluxes at level i is

$$\begin{aligned} F_i &= \int_0^{2\pi} \int_{-1}^{1} \mu I(\tau_i, \mu, \phi) \, d\mu \, d\phi \\ &= (I, \mu\delta(\tau - \tau_i)). \end{aligned} \tag{5.17}$$

The radiative fluxes F_i can be derived (see equation 5.19) by solving the adjoint radiative transfer equation with an adjoint source Q' as

$$\begin{aligned} Q' &= L^* I^* \\ &= \mu\delta(\tau - \tau_i). \end{aligned} \tag{5.18}$$

From equation 5.17, equation 5.18 and the definition of adjoint operator, the flux can be obtained from the solution of adjoint equation $L^* I^* = Q'$ and the source of the regular radiative transfer Q (the incident beam or the thermal emission)

$$\begin{aligned} F_i &= \int_0^{2\pi}\int_{-1}^{1} \mu I(\tau_i, \mu, \phi)\, d\mu\, d\phi \\ &= \int_{-\infty}^{\infty} d\tau \int_0^{2\pi} d\phi \int_{-1}^{1} I(\tau, \mu, \phi) Q'\, d\mu \\ &= (I, Q') \\ &= (I^*, Q) \\ &= \int_{-\infty}^{\infty} d\tau \int_0^{2\pi} d\phi \int_{-1}^{1} I^*(\tau, \mu, \phi) Q\, d\mu. \end{aligned} \tag{5.19}$$

For thermal infrared region, F_i can be calculated from the mean intensity I^* because the thermal emission is independent of μ and ϕ

$$\overline{I^*(\tau)} = \frac{1}{4\pi}\int_0^{2\pi}\int_{-1}^{1} I^*(\tau, \mu, \phi)\, d\mu\, d\phi \tag{5.20}$$

$$F_i = 4\pi \int_{-\infty}^{\infty} \overline{I^*(\tau)} Q(\tau)\, d\tau. \tag{5.21}$$

5.4.2.2 Solving the Adjoint Equation

Refering to equation 5.11, $L^* I^* = Q'$ is equivalent to $LI' = Q'(-\Omega)$. For calculating the terrestrial radiation, $Q' = \mu\delta(\tau - \tau_i)$ (refering to equation 5.18). We can

use the comprehensive discrete ordinate method (Stamnes *et al.*, 1988) to solve the equation.

The source function of the regular equation for terrestrial radiation $(1-a)B(T_i)$ is replaced by $\mu\delta(\tau - \tau_i)$ of the adjoint radiative transfer equation (see equation 5.18). To solve this adjoint radiative transfer equation with the regular radiative transfer model DISORT (Stamnes et al, 1988), we have inserted a very thin emitting layer ($\Delta_a\tau = 10^{-7}$) into level i and changed the thermal source to $\mu/\Delta_a\tau$. It is the only thermal source of the system.

The ground and space are considered as absorbing layers with infinite optical thickness because the adjoint method requires the boundary condition

$$(I, I^*) = 0 \quad for \quad \tau - \tau_i = \pm\infty. \tag{5.22}$$

5.4.2.3 Physical Meaning of $\overline{I^*}$

For the adjoint equation $L^*I^* = \mu\delta(\tau-\tau_i)$, the solution $\overline{I^*}(\tau_j)$ equals the flux $F(\tau_i)$ for the forward radiative problem $LI = \delta(\tau - \tau_j)$

$$\begin{aligned} \overline{I^*}(\tau_j) &= (I^*, \delta(\tau - \tau_j)) \\ &= (I^*, LI) \\ &= (I, L^*I^*) \\ &= (I, \mu\delta(\tau - \tau_i)) \\ &= F(\tau_i). \end{aligned} \tag{5.23}$$

So the physical meaning of the $\overline{I^*}$ at level j for adjoint problem of the terrestrial radiation $L^*I^* = \mu\delta(\tau - \tau_i)$ is the radiative flux at level i contributed by a unit radiative source ar level j. Figure 5.1 shows the changes of such a 'contribution' with the optical thickness.

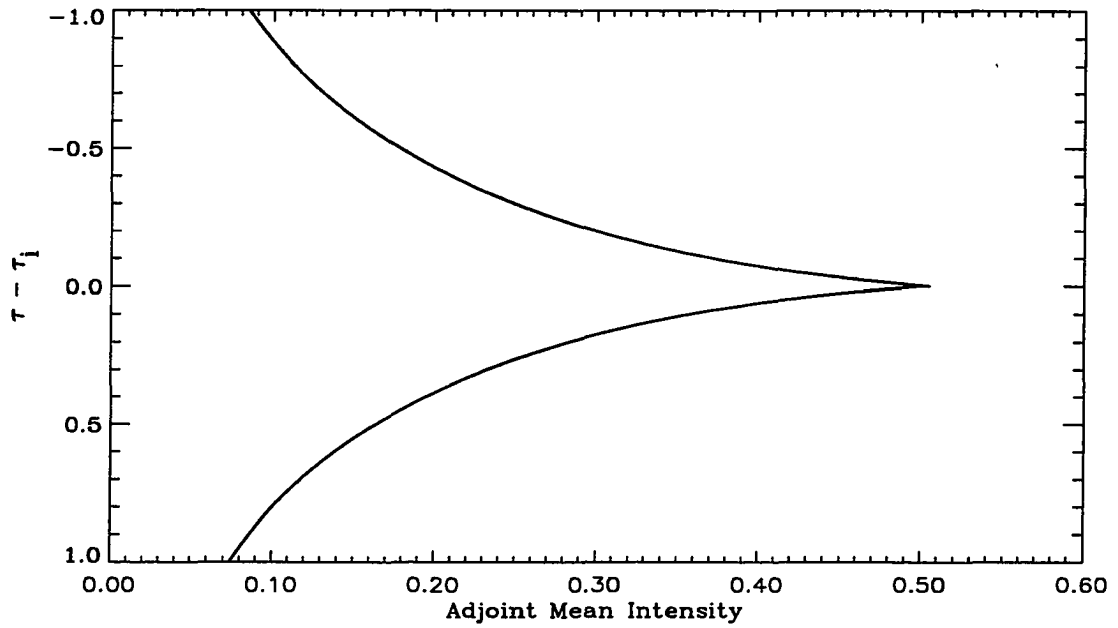

Figure 5.1 The optical depth dependence of the mean intensity for the adjoint equation $L^*I^* = \mu\delta(\tau - \tau_i)$.

5.4.2.4 Results of Flux Calculations

After solving the adjoint radiative transfer equation, the radiative fluxes at each level can be derived by integrating the "contributions" of all the layers (referring to equation 5.21).

As the adjoint mean intensity does not change with optical thickness linearly, we use the Gauss-Laguerre method for the numerical integrations. The fact that the mean intensity attenuates with optical depth has to be considered in the design of the numerical integration.

Figure 5.2 compares the fluxes computed from the adjoint method and fluxes computed from the forward method. The results shows very little difference (less then 0.1% everywhere).

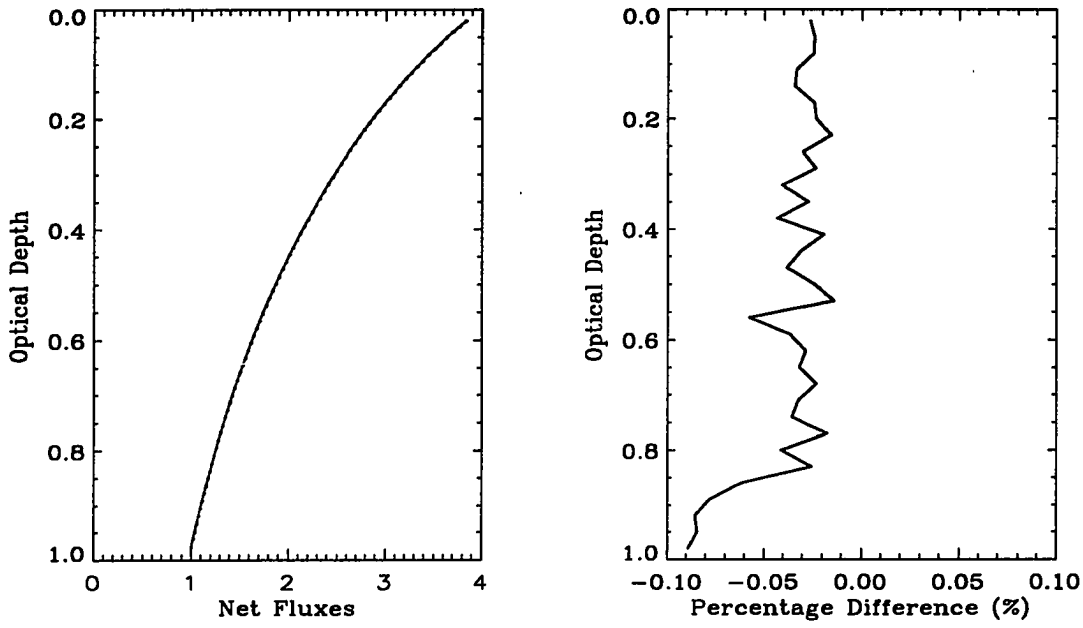

Figure 5.2 The left panel shows the fluxes calculated from the adjoint method F_{adj} (solid line) and from the forward method F_{for} (dotted line). The right panel shows the percentage difference $(100 * F_{adj} - F_{for})/F_{for}$..

5.4.3 Calculations of Heating Rates

The heating rates (warming or cooling rates) of level $\tau = \tau_i$ is:

$$\begin{aligned}
\frac{\Delta T}{\Delta t} &= \frac{1}{c_p \rho \Delta z}\frac{\Delta Q}{\Delta t} \\
&= \frac{1}{c_p \rho}\frac{\partial F}{\partial z} \\
&= \frac{1}{c_p \rho}\int_{2\pi} d\phi \int_{-1}^{1} \mu \frac{\partial I}{\partial z}\, d\mu \\
&= \frac{4\pi}{c_p \rho}\{\overline{I(\tau_i)} - B(T_i)\}. \qquad (5.24)
\end{aligned}$$

The heating rate at level i can be easily derived after $\overline{I(\tau_i)}$ is available.

As $4\pi\overline{I(\tau_i)} = (I, \delta(\tau - \tau_i))$, the adjoint equation for solving $\overline{I(\tau_i)}$ should be $L^* \cdot I^* = \delta(\tau - \tau_i)$. The mean intensity

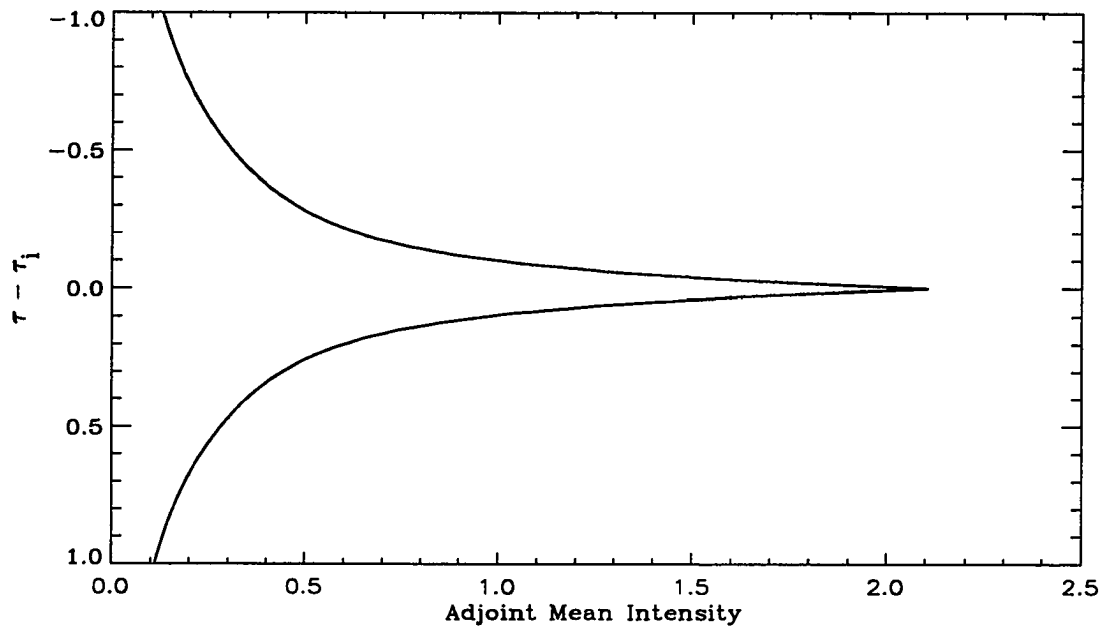

Figure 5.3 The optical depth dependence of mean intensity for adjoint equation $L^*I^* = \delta(\tau - \tau_i)$..

$$
\begin{aligned}
4\pi\overline{I(\tau_i)} &= \int_0^{2\pi} d\phi \int_{-1}^{1} I(\tau_i)\, d\mu \\
&= (I, \delta(\tau - \tau_i)) \\
&= (I, L^*I^*) \\
&= (I^*, LI) \\
&= \int_{-\infty}^{\infty} \int_0^{2\pi} \int_{-1}^{1} I^*(\tau) \cdot (1-a)B(T)\, d\mu\, d\phi\, d\tau. \qquad (5.25)
\end{aligned}
$$

Figure 5.3 shows optical depth dependence of the mean intensity calculated from adjoint equation $L^*I^* = \delta(\tau - \tau_i)$. Figure 5.4 shows that the mean intensities computed from adjoint method are the same as those computed from the forward method.

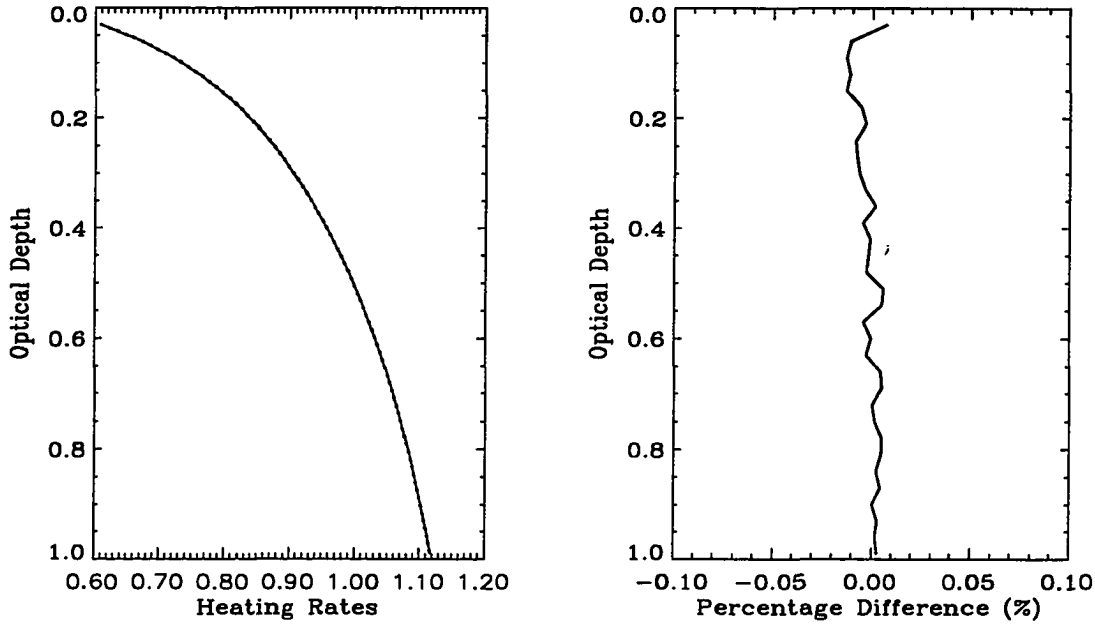

Figure 5.4 The left panel shows the heating rates calculated from the adjoint method H_{adj} (solid line) and from the forward method H_{forw} (dotted line). The right panel shows the percentage difference $(100 * H_{adj} - H_{forw})/H_{forw}$.

5.4.4 Perturbation of Optical Properties

By using the adjoint method, it is easy to calculate $\partial F/\partial\sigma_{ext}$, $\partial F/\partial a$, $\partial F/\partial P(\Theta)$ as well as F (F represents flux, σ represents the extinction cross section, a is the single scattering albedo and $P(\Theta)$ is the phase function). This is also true for other radiative properties such as heating rates and intensity instead of F. These derivatives of F are important for the sensitivity study in climate modeling and remote sensing. We have to solve the radiative transfer equations hundreds of times to compute these derivatives using the regular forward radiative transfer method. The adjoint method will reduce the computations significantly.

For a small perturtation in $L' = L + \delta L$, the flux F' can be calculated from the adjoint method with equation

$$F' = (I'^*, L'I'). \tag{5.26}$$

If L' is very close to L, then $I' \approx I$, $I'^* \approx I^*$. The derivatives $\partial F/\partial L$ is

$$\begin{aligned} \partial F/\partial L &= \lim_{\delta L \to 0} \frac{F' - F}{\delta L} \\ &\approx \lim_{\delta L \to 0} \frac{(I^*, L'I) - (I^*, LI)}{\delta L} \\ &\approx \lim_{\delta L \to 0} \frac{(I^*, \delta LI)}{\delta L}. \end{aligned} \tag{5.27}$$

(5.28)

We can calculate δLI without solving the radiative transfer equation again. So the derivatives of F can be obtained without repeating the solutions of the radiative transfer equation.

These derivatives of the radiative properties are useful for climate modeling and remote sensing. For climate models, the evolution of the climate system possesses slowly varying optical properties (the motion with scale smaller then hundreds of kilometers is nothing but noise in the models and should be parameterized so that only the feature of long time mean value are meaningful). The computations of radiative properties can be significantly simplified through this perturbation procedure.

The perturbation method could also be useful for remote sensing of cloud optical properties because it supplies the derivatives of the radiative flux and intensity with respect to changes in optical properties.

5.5 Summary of the Chapter

The adjoint method for radiative transfer method has been developed and tested by using DISORT (discrete ordinate radiative transfer method). Possible applications

of the method were discussed.

Using the adjoint radiative transfer method, it is possible to reduce the computing time for climate modeling. As we can calculate the derivatives of the radiative properties without having to solve the radiative transfer equation repeatedly, this method offers significant advantages.

Chapter 6

Cloud Microphysics and Climate Macrophysics

6.1 Introduction

The biggest obstacle for understanding cloud - climate interaction is the lack of a connection between cloud microphysics and climate macrophysics.

The energy source of the Earth's climate system is radiation. Clouds play important roles in the climate system by redistributing the radiative energy. Slight perturbations in cloud properties can cause a significant change in climate. Clouds are always changing. The meteorological fields which controls the cloud microphysical structure are always different for different time and space location. The cloud albedo ranges from 0 to 1 within the atmosphere. On the other hand, the macrophysical climate impact of the clouds is very stable from the observations: the planetary albedo of the Earth has been about 0.3 as a global and annual average for solar radiation, which suggests that the climate relevant clouds are very well organized by physical mechanisms that are not yet well understood.

The global climate system is directly affected by planetary scale motions with

space scale of thousands of kilometers. The space scale for cloud systems can be as small as hundred meters. Numerically, it is difficult to include the cloud formation processes in climate models interactively because errors of subscale convective motion will build up in the highly nonlinear atmospheric system. Parameterization schemes which link the cloud microphysical properties to the planetary scale properties are needed.

The existing cloud cumulus parameterization schemes such as the Kuo scheme (Kuo, 1974) and the Arakawa-Schubert scheme (Arakawa and Schubert, 1974) are constructed for numerical weather prediction models, for which the cloud - synoptical scale atmospheric dynamics interaction is the major concern. The synoptical motions (time scale no longer than a week) are very sensitive to the initial conditions (or dynamical effects). The variation of boundary conditions such as the radiative forcing are not as important as the initial conditions. The climate system is not sensitive to initial conditions. The distribution of radiative energy determines the climate state. The physics linking the cloud and climate is through the cloud - radiation interaction, which has been neglected or misrepresented in the current cloud parameterization schemes because the magnitude of cloud - radiation interaction is within the error of the cloud - dynamics interaction with any parameterization scheme.

To understand the role of the clouds in the climate system, the physical principle which governs the variations of the long-term and globally averaged cloud radiative properties is needed. This cloud - climate interaction can be illustrated from a simple one dimensional analysis.

Are the climatic cloud radiative properties deterministic (clouds are determined by deterministic conditions such as incoming solar radiation at the top of the atmosphere, the climate average of compositions of the atmosphere) or chaotic (clouds are sensitive to initial atmospheric conditions)? If the clouds are deterministic,

how are they related to the climate macrophysics?

Most of the theories and observations about clouds are focussed on cloud dynamics which are not relevant to climate (noise to the climate modeling) and with insufficient information about cloud climate interaction. Cloud variability depends on how you look at it (Rossow, 1994). A thermodynamic connection between clouds and climate is needed. Observations relevant to such a connection can be developed based on that.

The aim of this chapter is to study the clouds of the equilibrium state climate system and the link of their radiative properties to the macrophysical properties of the climate system. The physics of the cloud - climate interaction is studied by abstracting it to a simple thermodynamic problem. By studying the stability of the thermodynamic system, a possible rule for cloud - climate interaction is proposed theoretically and partly verified numerically.

6.2 The Thermodynamic Problem

One of the most important aspect of the cloud - radiation - climate interaction can be illustrated by studying the stability of equilibrium states.

6.2.1 Pure Radiative Equilibrium

First we consider a one dimensional atmospheric system with no convection (the "Earth" with no gravity) and no phase change of water. The atmosphere and the ground of the Earth absorb solar radiation and emit infrared radiation. The temperature of each layer will change until the pure radiative equilibrium state is achieved where the energy emitted balances the energy aborbed. A one dimensional radiative model has been developed to achieve such an equilibrium with time stepping of the temperature:

$$T_j^{i+1} = T_j^i + \frac{\partial T_j^i}{\partial t}\Delta t \tag{6.1}$$

where the heating rates of layer j at time step i are calculated from solving the radiative transfer equation. Model study shows that the equilibrium state is not sensitive to the initial temperature profile.

Another way of aproaching the equilibrium state is locating the equilibrium simply from the macrophysical approach, which is the entropy approach.

We will prove that the equilibrium state is the state with the maximum entropy if we consider the Earth, the Sun and the surrounding vacuum as the system.

The system which we are looking at is a "universe" which contains only the Sun, the Earth and the vacuum around them. The entropy flux of blackbody emission is (Planck, 1913):

$$\dot{S} = \frac{4\sigma T^3}{3}. \tag{6.2}$$

If the initial temperature of the Earth is zero (no radiation going out of the Earth or the Earth has no yet been created), the entropy of the solar radiation in the vacuum (per unit time and area) will be the entropy flux of the solar radiation at the surface of the Sun

$$\dot{S}_{Sun} = \frac{4\sigma T_{Sun}^3}{3}. \tag{6.3}$$

To make it simple for demonstration, we consider the Earth as a blackbody with isothermal temperature T_{Earth} at first. The temperature of the Earth will change after it absorbs the solar radiation. The entropy flux of the terrestrial radiation in the vacuum is

$$\dot{S}_{Earth} = \frac{4\sigma T_{Earth}^3}{3}. \tag{6.4}$$

Because of the absorption and emission of the Earth, the change of the entropy in the vacuum per unit time per unit area around the Earth is

$$\begin{aligned}\triangle \dot{S}_{vacuum} &= \dot{S}_{Earth} - \frac{\pi r_{Earth}^2}{4\pi L^2}\dot{S}_{Sun}\frac{\pi r_{Earth}^2}{4\pi r_{Earth}^2} \\ &= \frac{4\sigma T_{Earth}^3}{3} - \frac{r_{Earth}^2}{16L^2}\frac{4\sigma T_{Sun}^3}{3} \end{aligned} \tag{6.5}$$

where L is the distance between the Sun and the Earth.

At the same time, there will be changes within the Earth: The Earth absorbs the solar energy and emits terrestrial radiation. The internal entropy of the Earth itself will change as the temperature changes:

$$\begin{aligned}\triangle \dot{S}_{Earth} &= \frac{Q_{absorb} - Q_{emission}}{T_{Earth}} \\ &= \frac{\frac{\pi r_{Earth}^2}{4\pi L^2}\sigma T_{Sun}^4 \frac{\pi r_{Earth}^2}{4\pi r_{Earth}^2} - \sigma T_{Earth}^4}{T_{Earth}}. \end{aligned} \tag{6.6}$$

The total entropy change because of the Earth's participation will be:

$$\begin{aligned}\triangle \dot{S}_{total} &= \triangle \dot{S}_{Earth} + \triangle \dot{S}_{vacuum} \\ &= \frac{\frac{r_{Earth}^2}{16L^2}\sigma T_{Sun}^4 - \sigma T_{Earth}^4}{T_{Earth}} + \frac{4\sigma T_{Earth}^3}{3} - \frac{r_{Earth}^2}{16L^2}\frac{4\sigma T_{Sun}^3}{3} \\ &> 0 \ (for\ all\ values\ of\ T_{Earth}\ and\ T_{Sun}). \end{aligned} \tag{6.7}$$

No matter what T_{Earth} and T_{Sun} is, it is not difficult to prove that the above $\triangle \dot{S}_{total}$ is always bigger than 0 (simple algebra: from $y' = 0$, we can find the extrema of the function y. For the $y = \triangle \dot{S}$, there is only one solution of $y' = 0$ at which y is minimum). The minimum value of $\triangle \dot{S}_{total}$ is achieved (very close to but greater than 0) when the incoming solar radiation energy is balanced by the outgoing terrestrial energy

$$\frac{d\triangle\dot{S}_{total}}{dT_{Earth}} = \frac{\sigma}{4T_{Earth}^2}[T_{Earth}^4 - \frac{r_{Earth}^2}{16L^2}T_{Sun}^4] = 0 \tag{6.8}$$

$$T_{Earth} = \{\frac{r_{Earth}^2}{16L^2}T_{Sun}^2\}^{\frac{1}{4}}. \tag{6.9}$$

The physical meaning of this is: for this isolated "universe" (the Sun + the Earth + vacuum), $\triangle S_{total} \geq 0$ as the evolution proceeds, until the final state is achieved when $\triangle\dot{S}$ reaches minimum. If the minimum go to zero, then the entropy will be maximum. If the minimum is larger than zero, the the entropy will always increase but the final state has the smallest value of entropy change per unit time per unit area.

Until now, we have proved that the irreversibility of the "universe" requires that the blackbody temperature of the Earth will change until the energy balance is achieved. The equilibrium temperature is determined by the incoming solar radiation no matter what the initial temperature of the Earth is. The characteristic function for this problem is the entropy change, which is the minimum at the final state. The role of entropy change in this problem is similar to the role of the Gibbs function in the equilibrium phase change problem. It tells the time direction.

If the surface temperature of the Earth is larger than the temperature at the top of the atmosphere, then there will be some irreversible processes from the absorptions between the different layers. Numerical simulation of the evolution of the system shows that the final state is not sensitive to the initial temperature profiles, which implies that the final state follows the same rule above: The entropy of the whole system will increase until the entropy change reaches minimum when the absorption balances the emission for every layer at the final state (pure equilibrium).

6.2.2 The Extrema of the Dry Earth

Now we can take a look at the Earth with gravity but without the phase change of water. The gravitational instability prevents the pure radiative equilibrium: the temperature lapse rate $\partial T/\partial z$ for the pure radiative equilibrium state is bigger than g/C_p. Convective motion will be generated and maintained by the net radiative heating through abosorption of the radiation at the surface of the Earth and the net radiative cooling of the atmosphere.

The evolution of temperature for each layer can be simulated with a simple one dimensional radiative - convective model. An interesting result from the numerical simulation is: the equilibrium state temperature profile is not sensitive to the initial temperature profiles again, which suggests that there is an attractor of this nonlinear thermodynamic system. It is not difficult to verify that the characteristic function of the system (which characterizes the final state) is the entropy change of the whole system (the Sun, the Earth and the vacuum) under the constraint of convective adjustment. The theoretical interpretation is provided in the next section.

6.2.3 The Irrevesibility Problem of the Earth with Water

Without water, there will be no problem about the modeling of the climate. With the participation of the water, the previous extrema do not apply any more. The climate simulation will be questionable because the results are very sensitive to the cloud - radiation - climate interaction, which is not yet properly understood.

As we mentioned in the previous section, the gravitational instability prevents the pure radiative equilibrium and the resulting imbalance of radiative energy generates and maintains the continuous convection in the atmosphere. With the participation of the water phase change along with the convection, the instability

is strengthened (CISK: conditional instability of second type) by the latent heat release. On the other hand, clouds redistribute the radiative energy by absorption, scattering and thermal emission. Like the gravitational instability constraint, the phase changes of water put additional constraints on the minimum increase of the entropy of the whole system.

Satellite observations show that the average albedo of the Earth, which is very sensitive to the cloud radiative properties, is always around 0.3 from year to year. This suggests that there exists a thermodynamic certainty about globally and annually averaged clouds from a one dimensional point of view.

The cloud - climate interaction can be defined as a nonequilibrium (entropy is always changing) nonlinear (convective processes) phase change problem. The climatic state is the equilibrium state of the system, which is strongly dependent on the cloud radiative properties. For most cloud radiative properties the equilibrium is not thermodynamically stable (otherwise the climate is not predictable). If we believe that there exists a stable climate state which is determined by the solar radiation at the top of the atmosphere and the compositions of the atmosphere and the Earth (water is allowed to change phase continuously), there will be only one kind of cloud radiative properties which is most likely to be selected.

The cloud climate feedback process can be studied after we find the connection between the climate and the corresponding cloud radiative properties.

6.3 Stability of Nonlinear Thermodynamic State and Entropy Production

For an isolated system, the entropy always increase. At the equilibrium, the entropy reaches maximum, which can be characterized as

$$\frac{dS}{dt} = 0 \quad and \quad \frac{d^2S}{dt^2} < 0. \tag{6.10}$$

For a closed (not isolated) system (the Earth's atmosphere), the changes of the entropy can be separated to two part: entropy exchange with the surroundings d_eS and internal entropy production d_iS (Prigogine, 1969; Peixoto et al., 1991). If the system is not far from equilibrium, the equilibrium (or steady state) can be characterized by the so-called "minimum entropy production principle" (Prigogine, 1969)

$$\frac{d_iS}{dt} \geq 0 \quad and \quad \frac{d_i^2S}{dt^2} \leq 0. \tag{6.11}$$

Thermodynamic characteristic functions such as entropy and the Gibbs function exists for the above two kinds of systems because the equilibrium is an "extremum" condition. All cloud physics knowledge is based on that.

For systems with large perturbations (such as our atmospheric system in three dimensional point of view), the above two "extrema" do not apply. The evolution of these systems generally follows the so called "general evolution criterion"

$$\frac{d_iS}{dt} \geq 0 \quad and \quad \frac{d_x}{dt}\{\frac{d_iS}{dt}\} \leq 0 \tag{6.12}$$

where d_x means the change caused by the variation of the distribution of internal thermodynamic forces such as the temperature distribution of the system. There are no "extrema" for these systems in general as d_x is not a total differential. But if the system is far from equilibrium because of convective instability (such as the atmopheric general circulation), there does exist a stability criterion (Glansdorff and Prigogine, 1971) which acts like the thermodynamic characteristic function for determining the system macrophysical properties (such as temperature distribution). The Criterion is a conditional variational principle (Glansdorff and Prigogine, 1971): the changes of the entropy generated by a fluctuation of the internal

variable (such as temperature distribution or phase change) will be minimum if all the thermal energy is balanced and all the dynamic instability requirement is satisfied.

For the globally and yearly averaged one dimensional radiative-convective climate system, the incoming solar radiation is balanced by the outgoing terrestrial radiation and the equilibrium state is in convectively stable condition. The radiative - convective model has considered all the irreversible processes other than those related to the internal thermodynamic processes. The entropy production will be a minimum positive value, if not zero, as a result of the internal irreversible processes.

There are two main kinds of internal irreversible processes which will influence the entropy production: i. the evaporation at higher temperature and the condensation at lower temperature; ii. the inhomogenity of radiative energy absorption and emission.

For the processes of evaporation at higher temperature and the condensation at lower temperature, the entropy increases.

$$\triangle_{e,c}S = \sum \frac{Q_{j,latent}}{T_j} > 0 \tag{6.13}$$

where T_j is the temperature of atmospheric layer j, $Q_{j,latent}$ is the heat absorbed through phase change ($Q < 0$ for evaporation).

The solar energy absorbed by the Earth is balanced by the outgoing terrestrial radiation. Satellite observations show that the Earth is in radiative equilibrium in general. The radiative energy inside the atmosphere is always imbalanced because the convective instability prevents it from happening. The net radiative energy absorption and emission by clouds, water vapor and other greenhouse gases are different in different layers and at the surface of the Earth. The higher temperature surface gains radiative energy (the total absorption is greater than the total

emission) while the lower temperature atmosphere loses radiative energy. This is one of the most interesting thermodynamic processes because it decreases entropy and thus drives the atmospheric engine.

$$\triangle_{rad}S = \sum \frac{Q_{j,rad}}{T_j} < 0 \tag{6.14}$$

where $Q_{j,rad}$ is the net gain of solar energy ($Q_{j,rad} < 0$ for the atmosphere and $Q_{j,rad} > 0$ for the surface).

At the radiative - convective equilibrium, the total change in entropy per unit time is a locally minimum non-negative value the system can have through its internal processes (such as cloud formation). This requires that

$$\triangle_{total}S = \triangle_{e,c}S + \triangle_{rad}S \geq 0 \tag{6.15}$$

and

$$\delta(\triangle_{total}S) > 0 \tag{6.16}$$

where $\delta(\triangle_{total}S)$ is the change of the $\triangle_{total}S$ with any perturbation in the internal thermodynamic properties.

6.4 A Theoretical Study of the Size Distribution of Radiatively Stable Clouds

6.4.1 The Most Probable Distribution Function

Basic assumption: the distribution functions $f(x)$ are equally partitioned over phase space X.

Question: If the second moment of a distribution is given,

$$\int_0^\infty f(x)x^2\,dx = A. \tag{6.17}$$

What is the most probable distribution $f(x)$?

Answer: the equilibrium distribution is:

$$f(x)dx = \frac{cx}{A}exp[-\frac{\pi x^2}{A}]dx \tag{6.18}$$

where c is a constant.

Why: From the Boltzmann H theorem, the H function decreases monotonously

$$\frac{dH}{dt} = \frac{d}{dt}\int f(x)lnf(x)\,dx \leq 0. \tag{6.19}$$

The H is minimum for the equilibrium size distribution under the constraint equation 6.17. This equilibrium function can be derived by using the variational method with the constraint (Eqn. 6.17)

$$\frac{\partial}{\partial f}[flnf - \lambda x^2 f] = 0. \tag{6.20}$$

The solution is the $f(x) = \frac{cx}{A}exp[-\frac{x^2}{A}]$. (See Reza, 1961 and Guiasu, 1977).

6.4.2 The Size Distribution of Stable Clouds

The clouds of the equilibrium state climate have to be thermodynamically stable. The physics of the cloud -climate interaction might be revealed from the studies of the radiation - stable clouds interaction.

The radiative effect is indispensable for the energy balance, thus the maintenance of the stable water clouds (Telford et al., 1993; Shen and Moeng, 1993; Nicholls, 1989; Nicholls and Leighton, 1986). The radiative properties must be stable. The total surface area and the total liquid water of a stable cloud (such

as a stable stratus cloud) are fixed at a certain height (the bulk optical properties are stable). Thus, the most probable size distribution is:

$$n(r^2)dr = crexp[\frac{-r^2}{A}]dr. \tag{6.21}$$

Observations of the extinction cross section and the cloud droplet size distribution are required for testing the theory.

The implied physics is that if the total cross sectional area and the total liquid water content (thus the radiative properties) are fixed for the clouds with the same temperature and pressure (because of the requirement of the radiative properties), the mean surface area of the final state is the maximum and thus the total number of droplets is minimum.

6.5 Stability Analysis of the Clouds in Climate System

A three dimensional model is not suitable to answer the simple question: is the climate deterministic? The reason is the small scale energy processes such as cloud radiative heating is related to the large scale motion variables of the nonlinear atmospheric equations and the nonlinear atmospheric system might not have a attractor, which represents the long term behaviour of the system, from a three dimensional point of view, unless some simple physics connecting the different scale motions are discovered.

It is more feasible to study the deterministic feature of the cloud - climate interaction from a one dimensional point of view. In this section, we will look at the cloud structure which is thermodynamically stable from a one dimensional point of view and study the possible rules the clouds have to follow.

6.5.1 Phase Equilibrium of Water

As a globally averaged one dimensional climate system, the surface of the Earth gains energy from radiative process (Solar + Terrestrial) and the lower atmosphere (troposphere) loses energy from radiative processes. Convective motion tranports latent heat and sensible heat from the surface to the atmosphere to balance the energy both at the surface and the atmophere until the radiative-convective equilibrium is achieved (temperature of each layer does not vary any more).

This equilibrium climate system can be treated as a closed thermodynamic system with a fixed temperature profile. There is plenty of water in this system. The climate equilibrium is not stable unless the phase equilibrium of water is achieved. The phase equilibrium is another requirement in addition to the radiative energy balance at the top of the atmosphere and the convective stable state of the lower atmosphere.

6.5.1.1 Equal Opportunity for Condensation

A water molecule is evaporated from the surface of the Earth (atmospheric pressure P_0). What is the probability X that this water molecule appears at an atmospheric level with pressure and temperature (P, T) ?

For the equilibrium state, every water vapor molecule is thermodynamically the same. So, the probability X is:

$$X = \frac{E(P)}{\frac{1}{P_0}\int_0^{P_0} E(P)\,dP} \tag{6.22}$$

where $E(P)$ is the water vapor pressure of the atmospheric level with pressure and temperature (P, T) at the radiative-convective equilibrium.

At the radiative-convective equilibrium state, the water vapor pressure of each level $E(P)$ is not varying with time. Every molecule evaporated from the sur-

face of the Earth must condense somewhere. Every water vapor molecule in the radiative-convective equilibrium has the equal chance of condensing. The long time averaged condensation at any particular atmospheric layer will be proportional to the number of water vapor molecules within that layer.

6.5.1.2 Thermodynamic Explanation

In radiative - convective equilibrium climate state, water keeps evaporating at the Earth's surface and condensing in the atmosphere so as to transport energy from the surface to the air as a result of radiative energy imbalance. In this natural process, the entropy always increases if we take the atmosphere and the ocean (the Earth) as the system because the temperature of the surface is higher than the temperature of the air

$$\triangle S_{j,latent} = -\frac{Q_{Evap}}{T_{surf}} + \sum \frac{Q_{j,cond}}{T_j} > 0. \tag{6.23}$$

Even in the equilibrium state (or steady state), there will still be an increase of the entropy ($\triangle S_{j,latent} > 0$).

Considering the atmosphere without water as the system, the system is at equilibrium when the net heating is zero everywhere. So the entropy does not change

$$\frac{dS}{dt} = \frac{d_i S}{dt} + \frac{d_e S}{dt} = 0 \tag{6.24}$$

where

$$\frac{d_e S}{dt} = \frac{dQ_{j,latent}}{T_j} \tag{6.25}$$

$$d_i S = \sum \{C_p \delta \frac{1}{T_k} + \delta \frac{R}{p_k}\}$$

$$
\begin{aligned}
&= \sum\{\delta\theta_{se,k} - \frac{L_v \delta E(p_k)}{T_k}\} \\
&= -\sum \frac{L_v \delta E(p_k)}{T_k} \\
&= -\frac{d_e S}{dt} \qquad (6.26)
\end{aligned}
$$

where $\frac{d_i S}{dt}$ is the so-called "entropy production". $\frac{d_i S}{dt}$, which is not directly relevant to the external heat fluxes, is the entropy change generated from the internal irreversible processes such as changing the temperature and the pressure gradients, which should be zero for equilibrium state of an isolated system. p_k is the pressure at level k. θ_{se} is the pseudo-adiabatic potential temperature, which is constant with height in the one dimensional radiative - convective model. $E(p_k)$ is the water vapor amount at level k.

From Equations 6.25 and 6.26, we can find that the moist convective instability ($\delta\theta_{se} = 0$) requires the net heating of the atmosphere by latent heat be proportional to the equilibrium water vapor amount of the steady state. The latent heat released in layer j will be proportional to the amount of the water vapor within the layer so as to be consistent with the constant pseudo-adiabatic lapse rate for the radiative - convective model.

6.5.2 The Role of Clouds in the Equilibrium Climate State

The net radiative cooling of the troposphere is mainly balanced by the condensation of water vapor (sensible heat is less than 10% of the latent heat on average), which transports energy from the Earth's surface to the atmosphere. If there are no clouds, the distribution of the net radiative cooling depends only on the radiative properties of the gases. The distribution of the latent heat with height depends on the equilibrium temperature profile and the net radiative forcing at the surface. The net radiative cooling and the latent heat transport are not balanced within

the troposphere if there is no cloud. Thus the globally and annually averaged atmospheric temperature keeps changing because of the radiative and latent heat energy imbalance.

The one dimensional climatology of averaged temperature in the real atmosphere is very stable. Thus the energy imbalance does not exist. Clouds are the only substances available for the adjustment of the net radiative cooling.

From Equation 6.22, the latent heat release is determined by the net radiative heating of the surface and the total net radiative cooling of the whole atmosphere, which determines the temperature profile and thus the water vapor profile $E(P)$. The clouds, which is the major adjustment of the system, affect the $\triangle_{rad}S$ by redistributing the net radiative cooling of different layers of the atmosphere. The clouds also affect the $\triangle_{e,c}S$ indirectly by changing the equilibrium temperature profile through the net radiative heating of the Earth's surface and the total net radiative cooling of the atmosphere.

So, the role of the clouds in the 1-D climate system is to balance the latent heat release for each individual layer. On the other hand, the variation of the clouds changes the magnitudes of the net radiative heating of the Earth's surface and the net radiative cooling of the atmosphere and provide a feeback to the convective motion. This process continues until the radiative - convective equilibrium is achieved. The balance of the net radiative cooling and the latent heat release in each layer is a new requirement in addition to all the other requirements of the previous radiative - convective models.

$\triangle_{total}S$ will be zero by the end of the iteration of the cloud adjustments and the feedback processes

$$\triangle_{total}S = \sum\{\frac{Q_{j,rad}}{T_j} + \frac{Q_{j,latent}}{T_j}\} = 0. \qquad (6.27)$$

Most previous radiative - convective models did not achieve a real equilibrium

because the latent heat release was not balanced by the radiative cooling for each layer inside the troposphere.

6.6 Approaching the Correct Equilibrium State

Is there a radiative-convective equilibrium which satisfies the above cloud requirement? Is the equilibrium unique? Is the result reasonable compared with the one dimensional climatology of the Earth?

To answer these questions, the one dimensional radiative-convective model has been modified to include the variation of cloud radiative properties. The equilibrium state of one dimensional radiative - convective models has the properties (cf. Chapter 3):

- $\frac{\partial T}{\partial t} = 0$ for every layer above the tropopause;
- the net radiative flux is zero at the top of the atmosphere;
- the net radiative cooling of the entire troposphere is balanced by the net radiative heating of the Earth's surface.

The equilibrium state temperature profile depends on the cloud properties. At equilibrium, the net radiative cooling of each layer in the atmosphere is constrained to balance the latent heat release in the same layer.

The energy exchange processes within the troposphere have been neglected in all the previous radiative - convective models. The clouds in the previous models were not adjusted to change the radiative cooling rates of the atmosphere so as to balance the latent heat release of every layer in the troposphere.

The new radiative - convective model presented here adjusts the clouds until the net radiative cooling balances the latent heat release in each layer in the troposphere.

To evaluate the cloud adjustment, a new computational technique is required.

The energy balance of net radiative cooling and latent heat release requires that at each time step, the cloud optical thickness is adjusted

$$A(i,j)\triangle\tau_j = Q_{latent}(i) - Q_{rad}(i) \tag{6.28}$$

where τ_j is the cloud optical thickness of atmospheric layer j, $Q_{latent}(i)$ is the latent heat release in layer i, $Q_{rad}(i)$ is the net radiative cooling of layer i, the element a_{ij} of matrix $A(i,j)$ is the changes of the net radiative cooling in layer i as a result of an infinitely small change in cloud optical thickness τ_j, which is easy to derive by using the adjoint radiative transfer method (cf. Chapter 5). At the equilibrium state

$$Q_{latent}(i) = Q_{rad}(i) \qquad A(i,j)\triangle\tau_j = 0. \tag{6.29}$$

This model experiment is still in progress.

6.7 Indirect Proof: Maximum Power of Atmospheric Steam Engine

Another simple way to look at the role of clouds in the climate system is to study the power of the atmospheric steam engine for radiative - convective equilibrium states with different cloud optical properties.

6.7.1 Maximum Power of the Atmospheric Engine

The clouds and water vapor profile of the climate equilibrium state are related. The water vapor is also the most important and the most variable greenhouse gas in the atmosphere. In this section, we will discuss the whole hydrological cycle from an irreversibility point of view.

6.7.1.1 The Efficiency of a Steam Engine and Time Arrow of Irreversibility

Considering the following thermodymical processes:

- M kg of Water is evaporated at temperature T and pressure and P;
- the water vapor adiabatically moves to the phase space $T-\triangle T$ and $P-\triangle P$;
- the water vapor condenses at $T-\triangle T$ and $P-\triangle P$;
- the liquid water adiabatically moves to T and P.

This process is the most simplified atmospheric engine: water evaporates because of the strong absorption of shortwave radiation at the surface, then condense at the lower temperatured atmosphere. The total work performed in the cycle is $A = M(v_{vapor} - v_{liquid})\triangle P$. The total heat absorbed is $Q = ML_v$. The efficiency of the cycle η is

$$\eta = \frac{A}{Q} = \frac{(v_{vapor} - v_{liquid})\triangle P}{L_v}. \tag{6.30}$$

The carnot cycle has the maximum efficiency

$$\eta = \frac{\triangle T}{T} \tag{6.31}$$

$$\frac{\triangle T}{T} = \frac{(v_{vapor} - v_{liquid})\triangle P}{L_v}. \tag{6.32}$$

When $\triangle T$ and $\triangle P$ is very small, we have

$$\frac{dP}{dT} = \frac{L_v}{T(v_{vapor} - v_{liquid})}. \tag{6.33}$$

Equation 6.33 is the so-called Clausius-Claperon equation.

So, the steam engine has the maximum efficiency when these thermodynamic processes eventually reach equilibrium. At the equilibrium state, the temperatures

of both layer do not vary and the water vapor for both layers is saturated. If there is air in the system (water is a small part of the system), the relative humidity should be the same for both layers. The irreversible phase change processes for such a system have a time arrow which is increasing the efficiency (or the power of the engine).

The above thermodynamic processes is similar to the convective processes in the atmosphere. If the temperature profile is determined (radiative - convective equilibrium state is achieved when the net atmospheric radiative cooling is balanced by the net radiative heating at the surface), the water cycle (evaporation and condensation) will proceed until the efficiency of the engine reaches a maximum.

For the one dimensional radiative - convective climate equilibrium, the efficiency of the atmospheric "engine" is

$$\eta = \frac{1}{\sum Q_{j,latent}} \sum Q_{j,latent} \frac{T_{surface} - T_j}{T_{surface}} \tag{6.34}$$

where $Q_{j,latent}$ is the latent heat release per unit time at layer j. The higher the surface temperature, the lower the efficiency. The hydrological cycle acts to decrease the surface temperature if the surface heating does not change.

6.7.1.2 Cloud Radiative Effect and the Final State

It is important to point out that the time arrow for systems with different constraints are different. The general circulation of the Earth's atmosphere is similar to the above steam engine system. The only difference is that the radiative heating at the surface changes with the clouds.

To find the proper cloud properties of the one dimensional radiative - convective system, the irreversibility involving the cloud - climate feedback has to be studied.

The clouds change the net radiative heating of the Earth's surface and thus

provide a feedback into the climate system. The clouds vary in response to the need to balance the latent heat release in every layer with radiative cooling.

Comparing the equilibrium states for different clouds in a one dimensional radiative - convective model, we find that the surface temperature and variations in net radiative heating at the surface are always negatively correlated: the higher the surface temperature, the smaller the net surface radiative heating; the lower the surface temperature, the bigger the surface radiative heating.

Model studies show that the Earth's surface is much warmer if there is no water (vapor and clouds) on the planet. Clouds generally cools the atmosphere and the Earth's surface (Ramanathan, 1989). The decrease of the temperature because of the hydrological cycle (including precipitation and the cloud radiative effects) will increase the efficiency of the atmospheric steam engine and the surface radiative heating should increase with the participation of the water. The increase in the surface radiative heating prevents the temperature from dropping continiously. This cloud - climate interaction process will proceed until the surface heating is so big that the temperature can not drop any more as a result of the hydrological cycle, at which point the power of the atmospheric engine goes to maximum: starting with a radiative - convective equilibrium without water; then, water comes in, $\sum Q_{j,latent}$ always increase, T_j decreases until the equilibrium is achieved. The observation that downward radiative fluxes is at a local maximum (Curry, 1993) can be explained by this mechanism. As the summer Arctic has similar thermodynamic conditions as that for the one dimensional climate system, the role of arctic stratus clouds in the summer arctic climate will be similar to the role of clouds in the global climate. The data from the North Slope of Alaska ARM site will provide a good opportunity for a detailed study of this mechanism.

For the radiative - convective climate processes, the increase of the engine power is the time arrow which controls the evolution of the phase change including the

equilibrium state cloud properties.

If the power of the atmospheric engine is the highest one, any perturbation of the processes involved with the phase change of water will attenuate with time because the irreversible phase change processes pull the system toward the maximum power state.

This theory can be partly verified with a simple radiative - convective model study.

6.7.2 Results from Modeling

The one dimensional radiative - convective model has been used for the testing of the theory. The idea is to compare the "engine power" of the equilibrium states with hundreds of different clouds.

The equilibrium states with different cloud equivalent radii but the same cloud liquid water amount are compared. Figure 6.1 shows that the "engine power" goes to maximum for a system albedo (cloud optical thickness is the major component) of 0.3, which matches the climate states exactly.

Figure 6.2 compares the "engine power" of the equilibrium states with the same equivalent radius but with different cloud liquid water paths. Again, the power of the engine reaches a maximum when the planetary albedo equals 0.3.

Figure 6.3 compares the "engine power" of the equilibrium states with the same cloud optical thickness but with different cloud height. The higher the clouds, the higher the surface temperature. The results show that the surface temperature is the best when the "engine power" reaches a maximum.

All the computations show that looking at the climate system as a one dimensional radiative - convective equilibrium state, the current climate system including the water cycle, is the most powerful steam engine it might have, with the help of

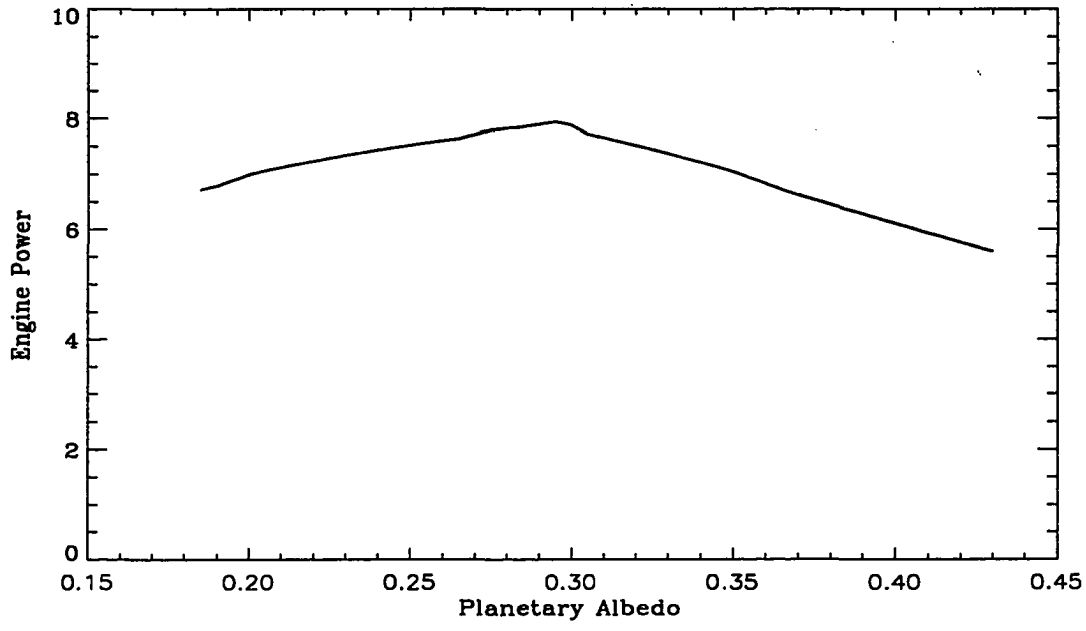

Figure 6.1 The power of the atmospheic steam engine for the radiative - convective equilibrium state with the variation of the planetary albedoes (fixed cloud R_e, varying liquid water path)..

the cloud - climate interaction.

6.8 Summary of the Chapter

A theoretical analysis of the possible connection between cloud microphysical structure and the climate macrophysical characteristics has been discussed here.

The role of the clouds is to balance the latent heat release in the troposphere as a climate scale average. The role of the clouds in the climate system is to balance the latent heat release of each atmospheric layer in troposphere. The irreversibility of the atmosphere - water system governs the cloud - radiation - climate interaction and the power of the atmospheric stem engine is the biggest one for all the possible radiative - convective equilibrium states distribution of water (clouds, water vapor and liquid water at the ground).

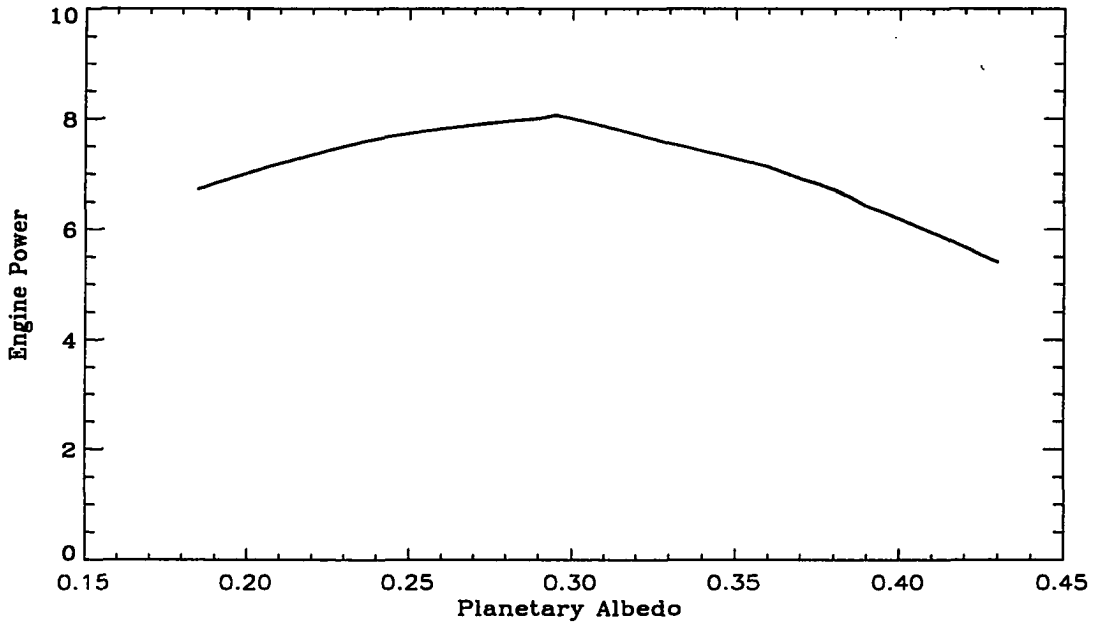

Figure 6.2 The power of the atmospheic steam engine for the radiative - convective equilibrium state with the variation of the planetary albedo (varying cloud R_e, fixed liquid water path)..

Simple model studies show that the current climate system is indeed in such a radiative - convective equilibrium with the highest steam engine power for its water cycle.

Simple experiments which simulate the phase change processes of the climate system will be helpful for validating the theory.

The summer arctic stratus clouds at are the best natural examples for the study of the irreversibility which exhibits similar physics to the one dimensional cloud - radiation - climate interaction. ARM data will be crucial for such a study. The radiative forcing at the surface and its correlation with the atmospheric temperature profile for different cloud conditions are important quantities for validating the theory.

The radiative - convective model with the adjoint method for deriving the

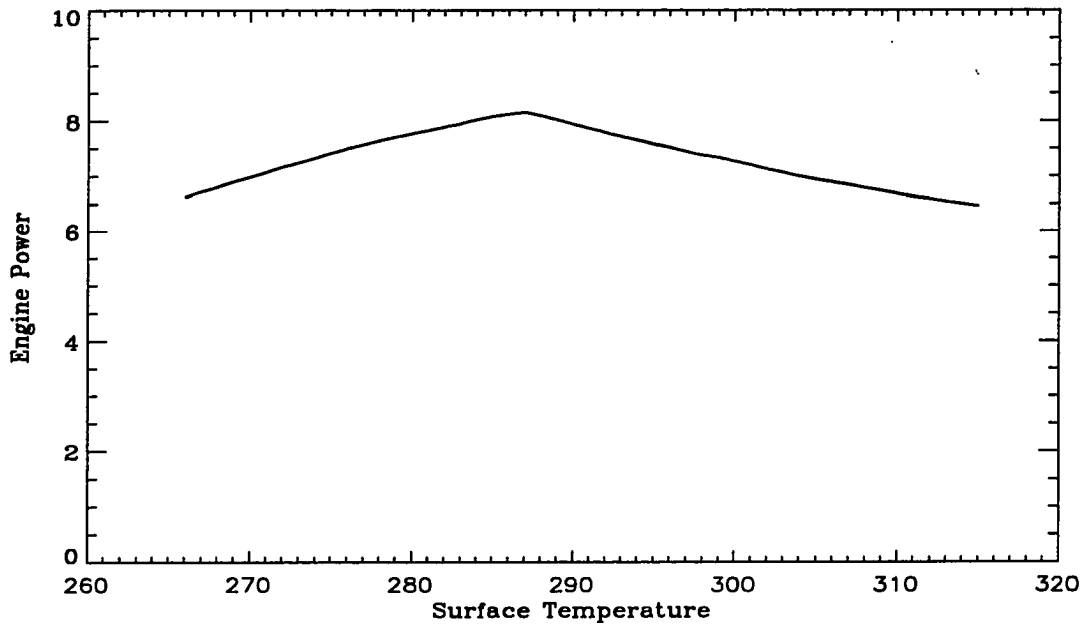

Figure 6.3 The power of the atmospheric steam engine for the radiative - convective equilibrium state with the variation of the surface temperature (fixed cloud R_e and liquid water path, varying cloud height)..

variation of cloud optical thickness can be used to study how the cloud - climate feedbacks take place.

Cloud climatological data which has information about the radiative fluxes both at the top of the atmosphere and the surface in a globally averaged sense will be most helpful.

Chapter 7

Summary and Future Studies

The major contributions of this thesis are:

• The climate related cloud radiative properties (fluxes and heating rates) are found to be determined by the second and the third moments of the cloud droplet size distribution. The detailed distribution of the cloud droplet size is difficult to observe and unneccessary to obtain for climate purposes.

• An accurate parameterization of cloud optical properties suitable for climate models is developed. This parameterization has been widely adopted in the atmospheric modeling community.

• An new radiative-convective model has been developed and used for studying cloud-climate interactions. The radiative transfer method adopted in the model is accurate and numerically stable. The energy balance at the earth-atmosphere interface is treated in a self-consistent manner which avoids artificial tuning. The energy exchange processes at the lower boundary are physically sound. The cloud radiative properties are accurately incorporated and are suitable for sensitivity studies of cloud-radiation-climate interactions.

• A sensitivity study of role of the cloud microphysical properties in the climate system is performed by studying the impact of cloud radiative forcing on

the equilibrium state temperature. The cloud equivalent radius is found to be a very important variable in the climate system. There is big discrepancy between modeling and observations of cloud shortwave absorption. A climate sensitivity study is performed to highlight the important role of the cloud absorption.

• An adjoint radiative transfer method is developed for use in cloudy and aerosol-loaded atmospheres. The physical meaning of the adjoint radiative properties is discussed. This adjoint method allows for rapid computation of the impact of the changes in atmospheric state (including cloud properties, aerosol properties and temperature profile) on the radiative energy budget and the radiative heating rates of the atmosphere. It is therefore expected to be useful in global climate modeling and the remote sensing of the atmosphere and the Earth from space.

• Based on the above studies, a preliminary study of the atmospheric irreversibility is performed to elucidate the connection between cloud microphysical properties and the macrophysical direction of global climate. The globally averaged climate processes is irreveresible: the long-term variation of the atmospheric motion tends to approach the radiative energy balance; the convective instability prevents the pure radiative equilibrium in the troposphere; the latent heat release enhances the convective motion. The conditionally variational principle (the climate version of Glansdorff - Prigogine universal criteria for convective instability) which describes the macrophysical character of the climate system is established.

• The radiative properties of the clouds in the climate system are governed by the irreversibility of the global atmosphere as a whole. The role of clouds in the climate system is to change the distribution of the net radiative cooling of the atmosphere so that the heat released in each layer by the moist convective motion are balanced by the net radiative cooling.

More observational and the global climate modeling research is required:

• Finding out a right concept to study from the available cloud climate data sets. As the cloud variability depends on how you look at it (Rossow, 1994), a new concept about cloud which is climatically meaningful and radiatively related has to be developed so that the certainty about the cloud - climate interaction can be studied.

• Impoving the cloud and radiation parameterization scheme in the current CCM2 (the community climate model of NCAR) with the parameterization of cloud radiative properties and the adjoint radiative transfer method.

Appendix A

Flow Chart of RCM

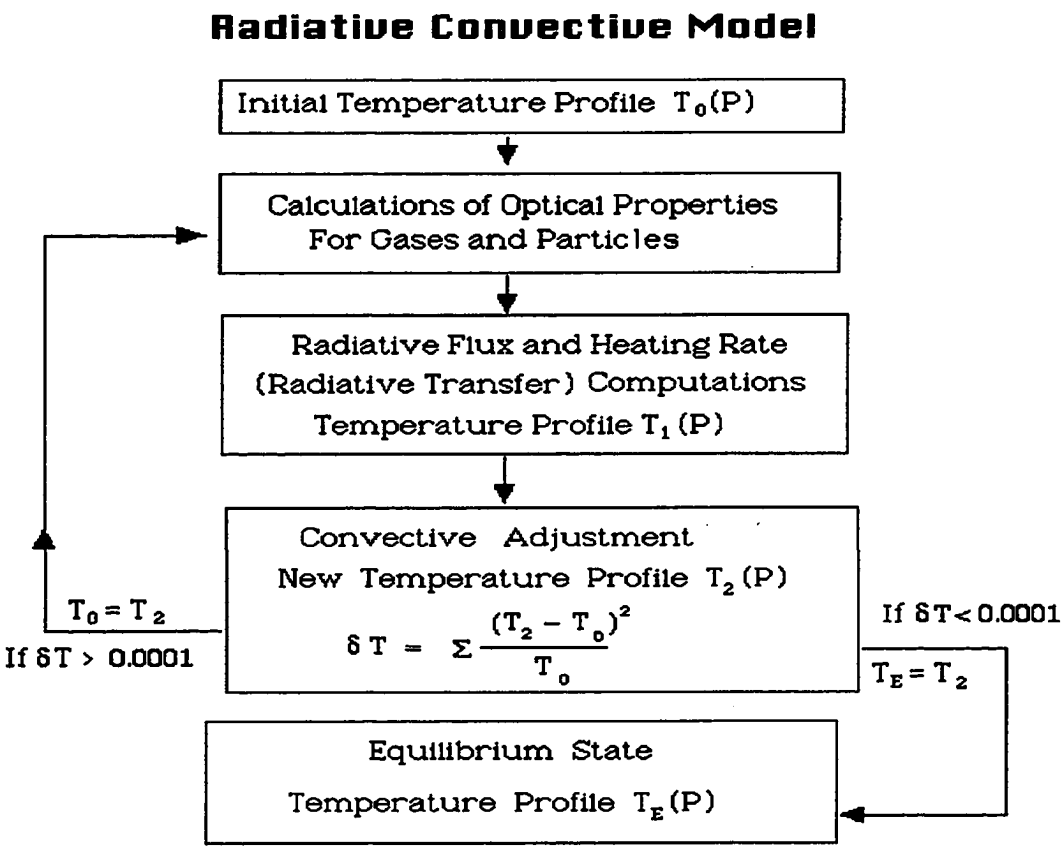

References

Ackerman, S.A. and G.L. Stephens, 1987: The Absorption of Solar Radiation by Cloud Droplets: An Application of Anomalous Diffraction Theory, *J. Atm. Sci.*, *44*, 1574-1588.

Albrecht, B. and S. K. Cox, 1975: The Large-scale Response of the Tropical Atmosphere to Cloud Modulating Infrared Heating, *J. Atm. Sci.*, *32*, 16-24.

Albrecht, B.A., 1989: Aerosols, Cloud Microphysics and Fractional Cloudiness, *Science*, *245*, 1227-1230.

Arakawa, A. and W.H. Schubert, 1974: Interaction of a Cumulus Cloud Ensemble with the Large-Scale Environment, *J. Atm. Sci.*, *31*, 674-701.

Arfkan, G, 1985: *Mathematical Metheds for Physisists*, *Academic Press*, pp985.

Betts, A.K. and Harshvardhan, 1987: Thermodynamic Constraint on the Cloud Liquid Water Feedback in Climate Models, *J. Geophys. Res.*, *92*, 8483-8485.

Blyth, A. M. and J. Latham, 1991: A Climatological Parameterization for Cumulus Clouds, *J. Atm. Sci.*, *48*, 2367-2371.

Bohren, C.F. and D.R. Huffman, 1983: *Absorption and Scattering of Light by Small Particles*, *Wiley & Sons*, New York, 530pp.

Bower, K.N. and T.W. Choularton, 1988: The Effects of Entrainment on the Growth of Droplets in Continental Cumulus Clouds, *Qaurt. J. Roy. Meteor. Soc.*, *114*, 1411-1434.

Box, M.A., S.A.W. Gerstl and C. Simmer, 1988: Application of Adjoint Formulation to the Calculation of Atmospheric Radiative Effects, *Beitr. Phys. Atmosph.*, *61*, 303-311.

Cacuci, D.G., 1981a: Sensitivity Theory for Nonlinear Systems. I. Nonliear Functional Analysis Approach, *J. Math. Phys.*, *22*, 2794-2802.

Cacuci, D.G., 1981b: Sensitivity Theory for Nonlinear Systems. II. Extensions to Additional Classes of Responses, *J. Math. Phys.*, *22*, 2803-2812.

Cacuci, D.G., 1988: The Forward and the Adjoint Methods of Sensitivity Analysis, In *Uncertainty Analysis.*, *CRC Press*, 71-144.

Callies, U. and Herbert F., 1988: Radiative Processes and Non-Equilibrium Thermodynamics, *Appl. Math. Phys.*, *39*, 242-266.

Cess, R. D. and G. L. Potter, 1987: Exploratory Studies of Cloud Radiative Forcing with a GCM, *Tellus*, *39A*, 460-473.

Cess, R.D., et al., 1989: Interpretation of Cloud-Climate Feedback as Produced by 14 GCMs, *Science*, *245*, 513-516.

Cess, R.D. and I.L. Vulis, 1989: Inferring Surface Solar Absorption from Broadband Satellite Measurements, *J. Climate*, *2*, 974-985.

Cess, R.D., et al., 1990: Intercomparison and Interpretation of Climate Feedback Processes in 19 Atmospheric GCMs, *J. Geophys. Res.*, *95*, 16601-16615.

Cess, R.D., E.G. Dutton, J.J. Deluisi and F. Jiang, 1991: Determining Surface Solar Absorption from Broadband Satellite Measurements for Clear Skies: Comparison with Surface Measurements, *J. Climate*, *4*, 236-247.

Cess, R.D., E.F. Harrison, P. Minnis, B. R. Barkstrom, V. Ramanathan and T. Y. Kwon, 1992: Interpretation of Seasonal Cloud-Climate Interactions Using ERBE Data, *J. Geophys. Res.*, *97*, 7613-7617.

Charlock, T.P., 1982: Cloud Optical Feedback and Climate Stability in a Radiative-Convective Model. , *Tellus*, *34*, 245-254.

Charlock, T.P. and V. Ramanathan, 1985: The Albedo Field and Cloud Radiative Forcing Produced by a General Circulation Model with Internally Generated Cloud Optics, *J. Atmos. Sci.*, *42*, 408-1429.

Charlson, R.J., J.E. Lovelock, M.O. Andreae and S.G. Warren, 1987: Oceanic Phytoplankton, Atmospheric Sulfer, Cloud Albedo and Climate, *Nature*, *326*, 655-661.

Charlson, R.J., S. E. Schwartz, J. M. Hales, R.D. Cess, J.A. Coakley, J.E. Hansen and D.J. Hofmann, 1992: Climate Forcing by Anthropogenic Aerosols, *Science*, *255*, 423-430.

Chertock, B., R. Frouin and R.C.J. Somerville, 1991: Global Monitoring of Net Solar Irradiance at the Ocean Surface, *J. Climate.*, *4*, 639-650.

Chou, M.-D., 1991: The Derivation of Cloud Parameters from Satellite Measured Radiances for Use in Surface Radiation Calculation, *J. Atm. Sci.*, *48*, 1549-1559.

Coakley, J.A., R.L. Bernstein, P.A. Durkee,1987: Effect of Ship-Stack Effluents on Cloud Reflectivity, *Science*, *237*, 1020-1022.

Curry, J.A., E.E. Ebert and J.L. Schramm, 1993: Impact of Clouds on the Surface Radiation Balance of the Arctic Ocean, *Meteor. Atmos. Phys.*, *51*, 197-217.

de Groot, S.R. and Mazur, P, 1984: *Non-Equilibrium Thermodynamics*, *Dover*, New York.

Downing, H.D. and D. Williams, 1975: Optical constants of Water in the Infrared, *J. Geo-*

phys. Res., *80*, 1656-1661.

Dowling, D.R. and L.F. Radke, 1990: A Summary of the Physical Properties of Cirrus Clouds, *J. Appl. Meteor.*, *29*, 970-978.

Dutton, J.A., 1973: The Global Thermodynamics of Atmospheric Motion, *Tellus*, *25*, 89-110.

Emanual, K.A., 1991: A Scheme for Representing Cumulus Convection in Large-Scale Models, *J. Atm. Sci.*, *48*, 2313-2335.

Essex, C., 1984: Radiation and the Violation of Bilinearity in the Thermodynamics of Irreversible Processes, *Planet. Space. Sci.*, *32*, 1035-1043.

Essex, C., 1987: Global Thermodynamics, the Clausius Inequality and Entropy Radiation, *Geophys. Astrophy. Fluid Dyn.*, *38*, 1-13.

Foot, J.S., 1988: Some Observations of the Optical Properties of Clouds, *Qaurt. J. Roy. Meteor. Soc.*, *114*, 145-164.

Fu, Q. and K.-L. Liou, 1993: Parameterization of the Radiative Properties of Cirrus Clouds, *J. Atm. Sci.*, *50*, 2008-2025.

Gerstl, S.A.W., 1982: Application of the Adjoint Method in Atmospheric Radiative Transfer Calculations., *Atmospheric Aerosols: Their Formation, Optical Properties and Effects*, *Spectrum Press*, 241-254.

Glansdorff, P. and Prigogine, I., 1971: *Thermodynamic Theory of Structure Stability and Fluctuations*, *J. Wiley and Sons*, London.

Golitsyn G.S. and Mokhov, I.I., 1978: Stability and External Properties of Climate Models,, *Izv. Atmos. Oceanic. Phys.*, *14*, 271-277.

Grassl, H., 1981: The Climate at Maximum Entropy Production by Meridional Atmospheric and Oceanic Heat Fluxes, *Qaurt. J. Roy. Meteor. Soc.*, *107*, 153-206.

Guiasu, S., 1977: *Information Theory with Application*, *McGraw Hill*, p298.

Hale, G.M. and M.R. Querry, 1973: Optical Constants of Water in the 200nm to 200μm Wavelength Region, *Appl. Opt.*, *12*, 555-563.

Hansen, J., 1984: *Climate Process and Climate Sensitivity*, *AGU Series*, 130-163.

Harrison, E.F., et al., 1990: Seasonal Variation of Cloud Radiative Forcing Derived from the ERBE, *J. Geophys. Res.*, *95*, 18687-18703.

Harshvardhan, D.A. Randall, T.G. Corsetti and D. A. Dazlich, 1989: Earth Radiation Budget and Cloudness Simulations with a GCM, *J. Atm. Sci.*, *46*, 1922-1942.

Herman, G., M.-L. Wu and W. Johnson, 1980: The Effects of Clouds on the Solar and Infrared Radiation Budget, *J. Atm. Sci.*, *37*, 1251-1261.

Hu, Y.-X. and K. Stamnes, 1993: An Accurate Parameterization of Cloud Radiative Properties Suitable for Climate Modeling, *J. Climate.*, *6*, 728-742.

Hummel, J.R. and W.R. Kuhn, 1981: Comparison of Radiative-Convective Models with Lapse Rates, *Tellus*, *33*, 254-261.

Jonas, P., 1990: On the Parameterization of Clouds Containing Water Droplets, *Qaurt. J. Roy. Meteor. Soc.*, *117*, 257-263.

Johnson, D. B., 1980: The Influence of Cloud-Base Temperature and Pressure on Droplet Concentration, *J. Atm. Sci.*, *37*, 2079-2085.

Kiehl, J.T. and B.P. Briegleb, 1992: Comparison of the Observed and Calculated Clear Sky Greenhouse Effect: Implications for Climate Studies, *J. Geophys. Res.*, *97*, 10037-10049.

Kiehl, J.T. and V. Ramanathan, 1990: Comparison of Cloud Forcing Derived from the ERBE with that Simulated by the NCAR CCM, *J. Geophys. Res.*, *95*, 11679-11698.

Kroll, W., 1967: Properties of the Entropy Production Due to Radiative Transfer, *Qaurt. J. Roy. Meteor. Soc.*, *7*, 715-723.

Kuo, H.-L., 1965: On Formation and Intensification of Tropical Cyclones Through Latent Heat Release by Cumulus Convection, *J. Atm. Sci.*, *22*, 40-63.

Kuo, H.-L., 1974: Further Studies of the parameterization of the Influence of Cumulus Convection on Large-Scale Flow, *J. Atm. Sci.*, *31*, 1232-1240.

Lesins, G.B., 1990: On the Relationship between Radiative Entropy and the Temperature Distribution, *J. Atm. Sci.*, *47*, 795-803.

Leaitch W.R., G.A. Isaac, J.W. Strapp, C.M. Banic and H.A. Wiebe, 1992: The Relationship between Cloud Droplet Number Concentrations and Anthropogenic Pollution: Observations and Climatic Implications, *J. Geophys. Res.*, *97*, 2463-2474.

Li, Z. and H.G. Leighton, 1993: Global Climatologies of Solar Radiation Budgets at the Surface and in the Atmosphere from 5 Years of ERBE Data, *J. Geophys. Res.*, *98*, 4919-4930.

Lindzen, R.S., A.Y. Hou and B.F. Farrell, 1982: The Role of Convective Model Choice in Calculating the Climate Impact of Doubling CO_2, *J. Atm. Sci.*, *39*, 1189-1205.

Liou, K.-N., S.C.S. Ou and P.J. Lu, 1985: Interactive Cloud Formation and Climatic Temperature Perturbation, *J. Atm. Sci.*, *42*, 1969-1981.

Manabe, S. and R.F. Strickler, 1964: Thermal Equilibrium of the Atmosphere with a Convective Adjustment, *J. Atm. Sci.*, *21*, 361-385.

Manabe, S. and R.T. Wetherald, 1967: Thermal Equilibrium of the Atmosphere with a Given Distribution of Relative Humidity, *J. Atm. Sci.*, *24*, 241-259.

Marchuk, G.I., 1958: *Numerical Methods of Nuclear Reactor Design*, *Atomizdat*, Moscow.

Marchuk, G.I., 1964: Equation for the Value of Information from Weather Satellites and Formulation of Inverse Problems, *Kosmicheskie Issledovaniya*, Vol. 2, No.3, 462-477.

Marchuk, G.I., 1974: Methods of Long-Range Weather Forcast on a Basis of Solving the Main and Adjoint Problems, *Meteorologia Gidrologia*, 3, 17-34.

Marchuk, G.I., 1992: Adjoint Equations and Analysis of Complex Systems, Nauka, pp. 1-335.

Mitchell, J.F.B., C.A. Senior and W.J. Ingram, 1989: CO_2 and Climate: A Missing Feedback?, *Nature*, *341*, 132-134.

Mitchell, J.F.B. and W. J. Ingram, 1992: Carbon Dioxide and Climate: Mechanisms of Changes in Cloud, *J. Climate.*, *5*, 5-21.

Molnar, G., W.-C. Wang, 1992: Effects of Cloud Optical Property Feedbacks on the Greenhouse Warming, *J. Climate.*, *5*, 814-821.

Nicolis, G. and C. Nicolis, 1980: On the Entropy Balance of the Earth-Atmospheric System, *Qaurt. J. Roy. Meteor. Soc.*, *106*, 691-706.

Nicolis, C. and G. Nicolis, 1981: Stochastic Aspect of Climatic Transition, *Tellus*, *33*, 225-234.

Nicholls, S and J. R. Leighton, 1986: A Observational Study of the Structure of Stratiform Cloud Sheets, *Qaurt. J. Roy. Meteor. Soc.*, *112*, 431-460.

Nicolls, S., 1989: The Structure of Radiatively Driven Convection in Stratocumulus, *Qaurt. J. Roy. Meteor. Soc.*, *115*, 487-511.

Palmer, K.F. and D. Williams, 1974: Optical Properties of Water in the Near Infrared, *J. Opt. Soc. Am.*, *64*, 1107-1110.

Paltridge, G.W., 1974: Infrared Emissivity, Short-wave Albedo and the Microphysics of Stratiform Water Clouds, *J. Geophys. Res.*, *79*, 4053-4058.

Paltridge, G.W. and C.M.R. Platt, 1976: *Radiative Processes in Meteorology and Climatology*, Elsevier.

Paltridge, G. W., 1980: Maximum Entropy and Climate, *Qaurt. J. Roy. Meteor. Soc.*, *106*, 895-899.

Peixoto, J.P. and A.H. Oort, 1992: *Physics of Climate*, *American Insititute of Physics*, 520pp.

Peixoto, J.P., A.H. Oort and M. deAlmeida, 1991: Entropy Budget of the Atmosphere, *J. Geophys. Res.*, *96*, 10981-10988.

Penner, J. E., R. E. Dickinson and C. A. O'Neil, 1992: Effects of Aerosol from Biomass Burning on the Global Radiation Budget, *Science*, *256*, 1432-1434.

Pinker, R.T. and J.D. Tarpley, 1988: The Relationship between the Planetary and Surface Net Radiation: An Update, *J. Appl. Meteor.*, *27*, 957-964.

Planck, M, 1913: *Theory of Heat Radiation*, *Translated and Published by Dover*, 1959.

Platt, C.M.R., 1976: Infrared Absorption and Liquid Water Content in Stratocumulus

Clouds, *Qaurt. J. Roy. Meteor. Soc.*, *102*, 553-561.

Platt, C.M.R. and Harshvardhan, 1988: Temperature Dependence of Cirrus Extinction: Implications for Climate Feedback, *J. Geophys. Res.*, *93*, 11051-11058.

Platt, C.M.R., 1989: The Role of Cloud Mircophysics in High-cloud Feedback Effects on Climate Change, *Nature*, *341*, 428-429.

Prigogine, I., 1947: *Etude Thermodynamique des phenomenes irreversibles*, *Desoer*, Liege.

Prigogine, I., 1969: *Introduction to Thermodynamics of Irreversible Processes*, *Interscience*, New York.

Ramanathan, V and J. Coakley, 1978: Climate Modeling through Radiative-Convective Models, *Rev. Geophys. Space Physics*, *16*, 465-489.

Ramanathan, V., E. J. Pitcher, R. C. Malone and M. L. Blackmon, 1983: The Response of a Spectral General Circulation Model to Refinements in Radiative Processes, *J. Atm. Sci.*, *40*, 605-630.

Ramanathan, V., 1987: The Role of Earth Radiation Budget Studies in Climate and General Circulation Research, *J. Geophys. Res.*, *92*, 4075-4095.

Ramanathan, V., R. D. Cess, E. F. Harrison, P. Minnis, B. R. Barkstrom, E. Ahmad and D. Hartmann, 1989: Cloud Radiative Forcing and Climate: Results from the ERBE, *Science*, *243*, 57-63.

Ramanathan, V. and W. Collins, 1991: Thermodynamic Regulation of Ocean Warming by Cirrus Clouds Deduced from Observations of the 1987 EL Nino, *Nature*, *351*, 27-32.

Ramanathan, V. and W. Collins, 1992: Thermostat and Global Warming, *Nature*, *357*, 649.

Randall, D. A., J. A. Abeles and T. G. Corsetti, 1985: Seasonal Simulations of the Planetary Boundary Layer and Boundary-layer Stratocumulus Clouds with a GCM, *J. Atm. Sci.*, *42*, 641-676.

Raval, A. and V. Ramanathan, 1989: Observational Determination of the Greenhouse Effect, *Nature*, *342*, 758-736.

Reza, F.M., 1961: *An Introduction to Information Theory*, *McGraw Hill*, 279-282.

Roeckner, E., U. Schlese, J. Biecamp and P. Loewe, 1987: Cloud Optical Depth Feedbacks and the Climate Modeling, *Nature*, *329*, 138-140.

Robock, M., 1978: Internally and Externally Caused Climate Change, *J. Atm. Sci.*, *35*, 1111-1122.

Rossow, 1994: Cloud Variability Depends on How You Look at It, *Reprint of the Eighth Conference on Atmospheric Radiation*, *Joint Session*, J2.

Schmetz, J., 1993: Relationship between Solar Net Radiative Fluxes at the Top of the

Atmosphere and at the Surface, *J. Atm. Sci.*, *50*, 1122-1132.

Schneider, S.H., 1972: Cloud and Climate, *J. Atm. Sci.*, *29*, 1413-1422.

Schlesinger, M.E., 1988: Negative or Positive Cloud Optical Depth Feedback?, *Nature*, *335*, 303-304.

Shaw, G.E., 1983: Bio-controlled Thermostasis involving the sulfur cycle, *Climate Change*, *5*, 297-303.

Shaw, G.E., G.N. Slinn andO. Preining, 1992: Climate Cooled by Particles and Clouds?, *Atmos. Environ.*, *26*, 522-523.

Shaw, G.E., K. Stamnes and Y.X. Hu, 1993: Arctic Haze: Perturbation to the Radiation Field, *Meteor. and Atmosph. Phys.*, *51*, 227-235.

Shen, S. and C.-H. Moeng, 1993: Comparison of a Computer-Simulated Stratus-Topped Boundary Layer with Aircraft Observations, *Bound.-Lay. Meteor.*, *65*, 29-53.

Slingo, A., and H.M. Schrecker, 1982: On the Shortwave Radiative Properties of Stratiform Water Clouds, *Qaurt. J. Roy. Meteor. Soc.*, *108*, 407-426.

Slingo, A, 1985: Simulations of the Earth's Radiation Budget with the 11-layer General Circulation Model, *Meteor. Mag.*, *114*, 121-141.

Slingo, A. and J. M. Slingo, 1988: The Response of a GCM to Cloud Longwave Radiative Forcing, *Qaurt. J. Roy. Meteor. Soc.*, *114*, 1027-1062.

Slingo, A., 1989: A GCM Parameterization for the Shortwave Radiative Properties of Water Clouds, *J. Atm. Sci.*, *46*, 1419-1427.

Slingo, A., 1990: Sensitivity of the Earth's Radiation Budget to Changes in Low Clouds, *Nature*, *343*, 49-51.

Smith, R. N. B., 1990: A Scheme for Predicting Layer Clouds and Their Water Content in a GCM, *Qaurt. J. Roy. Meteor. Soc.*, *116*, 435-460.

Somerville, R.C. and L.A. Remer, 1984: Cloud Optical thickness feedbacks in the CO_2 Climate Problem, *J. Geophys. Res.*, *89*, 9668-9672.

Stamnes, K., S.-C. Tsay, W. Wiscombe and K. Jayaweera, 1988a: Numerically Stable Algorithm For Discrete-Ordinate-Method Radiative Transfer In Multiple Scattering and Emitting Layered Media, *Appl. Opt.*, *27*, 2502-2509.

Stephens, G.L, 1978: Radiation Profiles in Extended Water Clouds. II: Parameterization Schemes, *J. Atm. Sci.*, *35*, 2123-2332.

Stephens, G.L., 1979: Optical Properties of Eight Water Cloud Types. ,*CSRIO*, *Aust. Div. Atmos. Phys. Tech. Pap.*, *36*, 35pp.

Stephens, G. L. and P. J. Webster, 1979: Sensitivity of Radiative Forcing to Variable Cloud and Moisture, *J. Atmos. Sci.*, *36*, 1542-1556.

Stephens, G.L., 1984: The Parameterization of Radiation for Numerical Weather

Prediction and Climate Models, *Mon. Wea. Rev.*, *112*, 826-867.

Stephens, G.L. and S.-C. Tsay,1990: On the Cloud Absorption Anomaly, *Qaurt. J. Roy. Meteor. Soc.*, *116*, 671-704.

Stephens, G.L., S.-C. Tsay, P.W. Stackhouse and P.J. Flatau, 1990: The Relevence of the Microphysical and Radiative Properties of Cirrus Clouds to Climate and Climatic Feedback, *J. Atmos. Sci.*, *47*, 1742-1753.

Stephens, G.L. and D.M. O'Brien, 1993: Entropy and Climate. I: ERBE Observations of the Entropy Production of the Earth, *Qaurt. J. Roy. Meteor. Soc.*, *119*, 121-152.

Stephens, G. L., D. A. Randall, I. L. Wittmeyer, D. A. Dazlich, S. Tjemkes, 1993: The Earth's Radiation Budget and Its Relation to Atmospheric Hydrology. 3: Comparison of Observations over the Oceans with a GCM *J. Geophys. Res.*, *98*, 8683-8693.

Suzuki, T, M. Tanaka, T. Nakajima, 1993: The Microphysical Feedback of Cirrus Cloud in Climate Change, *J. Meteor. Soc. Japan*, *71*, 701-713.

Sundqvist, H., 1978: A Parameterization Scheme for Non-convective Condensation including Prediction of Cloud Water Content, *Qaurt. J. Roy. Meteor. Soc.*, *104*, 677-690.

Sundqvist, H., 1981: Prediction of Stratiform Clouds: Results from a 5 Day Forcast with a Global Model, *Tellus*, *33*, 242-253.

Telford, J.W. and S.K. Chai, 1993: Marine Fog and its Dissipation over Warm Water, *J. Atm. Sci.*, *50*, 3336-3349.

Tsay, S.-C., K. Stamnes and K. Jayaweera, 1989: Radiative Energy Budget In The Cloudy and Hazy Arctic, *J. Atm. Sci.*, *46*, 1002-1018.

Tsay, S.-C. and G.L. Stephens, 1990: *A Physical/Optical Model For Atmospheric Aerosols with Application to visibility problems*, CIRA 0737-5352-16.

Tsay, S.C., K. Stamnes, and K. Jayaweera, 1990: Radiative Transfer in Stratified Atmospheres: Development and Verification of a Unified Model, *J. Quant. Spectrosc. Radiat. Transfer*, *43*, 133-148.

Twomey, S. A., 1978: *Atmospheric Aerosols*, *Elsevier*, North Holland.

Twomey, S. A., M. Piepgrass and T. L. Wolfe, 1984: An Assessment of the Impact of Pollution on Global Cloud Albedo, *Tellus*, *36B*, 356.

van de Hulst H.C., 1957: *Light Scattering by Small Particles*, *Dover*, New York, 470pp.

Wang, W.-C., W.B. Rossow, M.-S. Yao and M. Wolfson, 1981: Climate Sensitivity of a One-Dimensional Radiative-Convective Model with Cloud Feedback, *J. Atm. Sci.*, *38*, 1167-1178.

Wallace, J. M.m 1992: Effect of Deep Convection on the Regulation of Tropical Sea Surface Temperature, *Nature*, *357*, 230-231.

Wetherald, R. T. and Manabe, S., 1988: Cloud Feedback Processes in a general circula-

tion model, *J. Atm. Sci.*, *45*, 1397-1415.

Wigley, T. M. L., 1991: Cloud Microphysics and the Climate Effect, *Nature*, *349*, 503-506.

Wildt, R., 1972: Thermodynamics of the Gray Atmosphere. IV. Entropy Transfer and Production, *Astrophys. J.*, *174*, 69-77.

Wiscombe, W.J., R.M. Welch and W.D. Hall, 1984: The Effects of Very Large Drops on Cloud Absorption, *J. Atm. Sci.*, *41*, 1336-1355.

Wyant, P.H., A. Mongroo and S. Hameed, 1988: Determination of the Heat-Transfer Coefficients in Energy-Balance Climate Models by Extremization of Entropy Production, *J. Atm. Sci.*, *45*, 189-193.

Zou, X., A. Barcilon, I.M. Navon, J. Whitaker and D.G. Cacuci, 1993: An adjoint Sensitivity Study of Blocking in a Two-Layer Isentropic Model, *Mon. Wea. Rev.*, *121*, 2833-2857.